ALMA MATER STUDIORUM - UNIVERSITÀ DI BOLOGNA

DOTTORATO DI RICERCA IN MECCANICA E SCIENZE AVANZATE DELL'INGEGNERIA: DISEGNO E METODI DELL'INGEGNERIA INDUSTRIALE E SCIENZE AEROSPAZIALI

Ciclo XXIII

ING-IND/06

Statistical analysis and simulation techniques in wall-bounded turbulence

Andrea Cimarelli

Coordinatore Dottorato:
Prof. Franco Persiani

Relatore:
Prof. Elisabetta De Angelis

Esame finale Anno 2011

Dedicato ai nonni
Antonia,
Erino,
Gianna.

Abstract

The present work is devoted to the assessment of the energy fluxes physics in the space of scales and physical space of wall-turbulent flows. The generalized Kolmogorov equation will be applied to DNS data of a turbulent channel flow in order to describe the energy fluxes paths from production to dissipation in the augmented space of wall-turbulent flows. This multidimensional description will be shown to be crucial to understand the formation and sustainment of the turbulent fluctuations fed by the energy fluxes coming from the near-wall production region. An unexpected behavior of the energy fluxes comes out from this analysis consisting of spiral-like paths in the combined physical/scale space where the controversial reverse energy cascade plays a central role. The observed behavior conflicts with the classical notion of the Richardson/Kolmogorov energy cascade and may have strong repercussions on both theoretical and modeling approaches to wall-turbulence. To this aim a new relation stating the leading physical processes governing the energy transfer in wall-turbulence is suggested and shown able to capture most of the rich dynamics of the shear dominated region of the flow. Two dynamical processes are identified as driving mechanisms for the fluxes, one in the near wall region and a second one further away from the wall. The former, stronger one is related to the dynamics involved in the near-wall turbulence regeneration cycle. The second suggests an outer self-sustaining mechanism which is asymptotically expected to take place in the log-layer and could explain the debated mixed inner/outer scaling of the near-wall statistics.

The same approach is applied for the first time to a filtered velocity field. A generalized Kolmogorov equation specialized for filtered velocity field is derived and discussed. The results will show what effects the subgrid scales have on the resolved motion in both physical and scale space, singling out the prominent role of the filter length compared to the cross-over scale between production dominated scales and inertial range, l_c, and the reverse energy cascade region Ω_B. The systematic characterization of the resolved and subgrid physics as function of the filter scale and of the wall-distance will be shown instrumental for a correct use of LES models in the simula-

tion of wall turbulent flows. Taking inspiration from the new relation for the energy transfer in wall turbulence, a new class of LES models will be also proposed. Finally, the generalized Kolmogorov equation specialized for filtered velocity fields will be shown to be an helpful statistical tool for the assessment of LES models and for the development of new ones. As example, some classical purely dissipative eddy viscosity models are analyzed via an *a priori* procedure.

Contents

I have sometimes thought that what makes a man's work classic is often just this multiplicity (of interpretations), which invites and at the same time resists our craving for a clear understanding.

Wright (1982, p. 34), on Wittgenstein's philosophy

Chapter 1

Introduction

Although the equations governing the turbulent motion are well known since the nineteenth century, Navier-Stokes (1822-1845), we are still not able to understand the overall rich physics of turbulence which remains one of the grand challenges of physics and engineering. Indeed, turbulent flows are one of the most ubiquitous phenomena in nature and applications. A particular feature of most of these turbulent flows is that are bounded, at least in part, by one or more solid surfaces. This aspect makes wall-turbulence one of the most interesting phenomena in fluid dynamics and of great relevance for the applications. Problems involving wall turbulent flows can be found in aerospace engineering, ground transportation systems, flow machinery, energy production (turbines), as well as in nature such as the atmospheric boundary layer and the flow of rivers. One of the effects of turbulence in wall bounded flows is the enhancement of the momentum exchange between the solid surface and the external stream. Just to mention a few examples, the viscous resistance encountered by fast objects moving through air (e.g. airplanes, cars, trains) or water (e.g. ships, sailing boats) is largely enhanced by turbulence, which is able to dissipate most of the power needed to maintain the speed of the body. Analogous considerations concern pressure losses along pipelines, where turbulence, by increasing the skin friction, leads to a substantial increase in the power needed for pumping a given flow rate through the piping system. Another important effect of turbulence is that turbulent fluctuations greatly enhance also mixing. Therefore turbulence-wall interactions are also crucial for the heat exchange capability of a given system.

Despite the obvious differences between the different flow configurations, the basic physics of wall-bounded turbulence is substantially identical meaning that the identification and physical comprehension of the mechanisms responsible for the generation and sustainment of turbulence in a fluid stream

near a solid wall would have a general validity. The lack in the physical knowledge of these kind of flows reflects in poor predictive capability of system, configurations and environmental phenomena involving wall-turbulence. Even if the ever increasing performance of super-computers, the direct numerical computation of the Navier-Stokes equations at the Reynolds number usually encountered in the applications is still not feasible. For this reason, the computational fluid dynamics applies averaging (RANS) or filtering (LES) operator to the Navier-Stokes equations in order to reach the Reynolds number of the applications. The resulting approach and the success of the simulation is entirely demanded to the turbulence models quality which, however, is very poor. In this context, a better understanding of the wall turbulent physics could be used immediately for a correct turbulence modeling as the proper tool to achieve numerical simulation and predictions of large Reynolds number flows.

Despite its crucial importance, the dynamics of wall turbulence is still a matter of scientific debate and, as a consequence, turbulence models are not able to account for the physical processes of the flow. Most of turbulence models use in more or less explicit form, two basic theories of turbulence. The first one is the phenomenology of the turbulent cascade of energy from the large production scales towards the small dissipative scales. This concept is based on ideas developed in the context of homogeneous isotropic turbulence. The second phenomenology is the universal law of the wall, which dictates the shape of the mean velocity profile in the near wall region. This law derives from the classical division of wall-bounded turbulent flows in a near-wall, inner region, and an outer region populated by large turbulent fluctuations. These two distinct regions are present in all wall-bounded flows and are coupled through the overlap region. The velocity profile in this region appears to exhibit a large degree of universality between different flows and can be described by a logarithmic function (to a certain degree of accuracy).

While there is no doubt that these two ideas raised interesting scientific results, they still present unsolved physical problems and most efforts are actually devoted to the study of these concepts and also other physical aspects here not mentioned. The unsolved physical problems of wall-turbulence has been adressed from different points of view by the research community and some of them have been listed in [78][56].

Apart from the turbulence modeling and the related predictive capability, a better understanding of the wall turbulent physics could be also used in the field of turbulence control and drag reduction with immediately strong repercussions for the applications. Indeed, the control of wall-bounded turbulent flows with the aim of reducing the wall-shear stress has enormous beneficial effects for engineering flow systems, such as less consumed fuel

in aeronautical applications or for propelling gas and oil along pipelines. Control techniques, whether active or passive, have been studied for a long time, [64][16], highlighting that the mechanisms responsible for drag reduction can be summarized as the suppression of the self-sustaining mechanisms of wall-turbulence. Hence, in order to achieve optimal control techniques, an assessment of the physics of the turbulent fluctuations involved in these turbulent regeneration cycle is needed.

Given the variety of key issues concerning the wall-turbulent physics, purpose of the present work is the investigation of the alterations taking place in the theoretical results raised from the study of homogeneous isotropic turbulent flows when applied to wall turbulence. As will be shown in the next section, this is a very important topic for the understanding of some unsolved physical problems of wall-turbulence, such as the the controversial reverse energy cascade, and could have repercussions for turbulence modeling.

1.1 Wall-turbulent physics and its modeling

Real turbulent flows are difficult to classify as either spatially homogeneous or isotropic. Nonetheless, these idealizations allow the identification of certain universal features associated with the small-scales motion almost invariably observed in a variety of different conditions. The single most significant aspect is an energy flux through the spectrum of scales commonly related to the phenomenology of the Richardson energy cascade (1922). Referring to this phenomenology, Kolmogorov (1941) developped one of the most famous and important theory for the description of the turbulent physics. In particular, he obtained an exact quantitative relation for the energy cascade under the specific statistical assumption of local small scale isotropy. This relation, called 4/5ths law, states that turbulent energy, extracted from the mean motion at large scale fluctuations, flow down to small inertial scales with a constant rate proportional to the viscous energy dissipation rate. This picture is claimed to be highly universal. No matter what the large scale processes which feed turbulence are, the small scales of every turbulent flows at sufficiently high Reynolds number are believed to behave according to this picture.

Beside the deep impact in the context of theoretical understanding of the physics of turbulent flows, the Kolmogorov theory and its universality and scale-invariance assumptions has been widely used in the field of turbulence modeling. The most evident example is given by the Large Eddy Simulation (LES) approach for the numerical solution of the filtered Navier-Stokes equations. The Large Eddy Simulation is a technique intermediate between

the Direct Numerical Simulation (DNS) and the solution of the Reynolds Averaged Navier-Stokes (RANS) equations. The LES approach took inspiration from the Kolmogorov's assumption of the local small scale statistical isotropy. Indeed, the basic idea of LES simulation is to compute explicitly the large, energy-carrying, turbulent structures which are directly affected by the boundary conditions while the small scales which tend to be more homogeneous and isotropic that the large ones are modeled. Therefore, it is thought that relatively simple and universal models can be used to describe them. For that reason LES represents the most promising technique for the simulation of high Reynolds number flows.[1]

The most important feature of LES models should be their ability to accurately reproduce the energy transfer between large resolved scales and small subgrid scales, e.g. see [67]. In this context, most of the commonly used LES models assume that the main role of the subgrid scales is to drain energy from the large resolved scales accordingly to the idea of an inertial range in the spectrum of scales where the Kolmogorov's 4/5ths law holds. Indeed, the phenomenology associated with this law is claimed to be highly universal and many LES models take inspiration from it. The most prominent example is the widely used concept of eddy viscosity. In this kind of turbulence modeling, the Kolmogorov energy cascade was used to define a suitable eddy viscosity able to reproduce the inertial range effects, [74] and [51].

This kind of turbulence physics and the related modeling have given good results in homogeneous and in unbounded shear flows but less in wall-turbulence. In fact, in proximity of a solid wall the anisotropic dynamics related with turbulent production affect most of the turbulent eddies. The shear is sufficiently strong to hinder the isotropic recovery even at very small scales, see e.g. [1], [7] and [30]. But, the single most striking phenomenon observed in wall bounded flows is the complete modification of the Richardson scenario up to a reverse energy flux from small to large scales in the buffer layer. Even if it is well known that turbulent flows are characterized by events of energy back-scatter also in globally isotropic and homogeneous conditions, [46] [36] [49], in the production region of wall turbulent flows these phenomena result in a net reverse energy flux from small to large scales. Evidence of reverse energy fluxes in the buffer layer was provided in [54] based on the balance equation for the second order structure function, which can

[1]Beside the expected higher accuracy of the numerical solution obtained by an LES with respect a RANS approach, it is important to note that the direct solution of the large turbulent fluctuations in LES simulations allows to improve the physical description of different physical aspects of interest for the application. As an example, spectra and two-point correlation can be used for broadband noise simulation of major importance to study nuisance from turbo-engines.

be understood as a scale-energy. The strong back-scatter events at the base of this reverse energy cascade have been attributed to the dynamics of the near-wall turbulent fluctuations involved in the self-sustaining mechanisms of wall-turbulence, [62]. Whereas, the complex interactions between anisotropic turbulence production processes and inhomogeneous spatial fluxes have been conjectured in [32] as possible sources of a sort of *spatially evolving reverse cascade* between different wall-distances.

These observations have a huge repercussions in a context of turbulence modeling. In fact, in a context of filtered dynamics, this phenomena result in an energy flux from small subgrid to large resolved scales in the buffer layer for certain value of the filter lenght as highlighted in [24]. This behaviour cannot be reproduced with LES models based on the classical Kolmogorov inertial range concept.

1.2 Objectives and data sets

Starting from the idea that wall turbulent flows show different aspects where the classical concepts of the Richardson cascade and the theories of Kolmogorov fail, the main goal of the present work is the investigation of these phenomena and of their repercussions in the turbulence modeling and simulation. To this aim a generalization of the Kolmogorov approach to wall-turbulence will be adopt in terms of the analysis of a balance equation for the second order structure function in fully inhomogenous and anisotropic conditions, see [26] for the derivation of the equation and [54] for the application to a turbulent channel flow. The generalization of the Kolmogorov approach will be instrumental for the identification of the basic mechanisms responsible for the breakdown of the Kolmogorov's theory. These results will be shown relevant for the correct modeling of wall-turbulence. Furthermore, the informations about the scales where these relevant processes occur at different geometrical location will be used for the comprhension of the filtered wall turbulent dynamics. Indeed, in a context of LES simulations, the same approach will be again generalized in order to account for the filtered dynamics composed by a resolved velocity field affected by subgrid scale stresses. The main goal of this part of the work is the assessment of the capability of a filtered velocity field to correctly reproduce the wall-turbulent dynamics as a function of the filter scale used. In particular, the balance equation for the filtered second order structure function and the related informations achievable as function of the scale and physical location will be instrumental for the assessment of the filtered physics when the filter length change. Whereas, the application of LES models for the subgrid stresses to this equation will

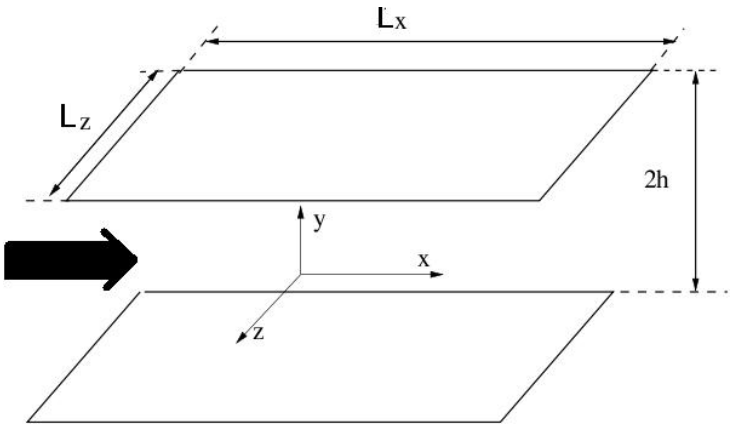

Figure 1.1: Channel flow configuration and nomenclature. The mean flow $U(y)$ goes in the streamwise direction x while the spanwise and wall-normal directions are z and y, respectively. The fluctuating velocity components are u, v and w in the x, y and z directions, respectively.

allow a detailed description of the limit and merit of these models.

The analysis of the generalized Kolmogorov equation and of its extension to filtered velocity fields will be performed using direct numerical simulation (DNS) data of a turbulent channel flow [2]. The computational domain, shown in figure 1.1, is a channel flow with infinite extension in the streamwise and spanwise direction. Periodic boundary conditions are applied in the homogeneous directions x and z and impermeability and no-slip are imposed on the solid walls. The simulations have been carried out with an highly accurate numerical formulation based on a pseudo-spectral code [53] where the spatial discretization in the homogeneous directions is performed with a Fourier expansion while in the wall-normal direction a Chebyshev expansion is used, see [27] for an overview of the spectral methods. The time advancement is performed using a mixed Crank-Nicholson/Runge-Kutta scheme.

In what follow two numerical data sets will be considered corresponding to two turbulent channel flow simulations at a friction Reynolds number $Re_\tau = 298$ and $Re_\tau = 545$, respectively. The friction Reynolds number is defined as $Re_\tau = u_\tau h/\nu$, where ν is the kinematic viscosity, h is half the channel height and u_τ is the friction velocity evaluated as $u_\tau = \sqrt{\tau_w/\rho}$ where τ_w is the average viscous stress at the wall and ρ the constant density of the

[2]Earlier, this energy budget was studied also experimentally using high resolution dual plane Particle Image Velocimetry (PIV), [70], but the measurements were conducted only in two locations of the logarithmic layer of a turbulent boundary layer over a flat plate due to resolution requirements unfeasible in the near-wall regions.

fluid. All throughout this work, the so-called inner variable will be denoted by a superscript + which imply a normalization of lengths with the friction scale ν/u_τ and velocities with u_τ. The parameter of the two simulations considered in this work are reported in table 1.1. The channel flow case at $Re_\tau = 550$

Re_τ	L_x	L_y	L_z	N_x	N_y	N_z	Δx^+	Δz^+
300	2π	2	π	512	193	256	3.7	3.7
550	8π	2	4π	1024	257	1024	13.3	6.6

Table 1.1: Parameters of the simulations. Re_τ is the nominal friction Reynolds number. L_x, L_y and L_z are the size of the flow domain in the streamwise, wall-normal and spanwise directions, respectively. N_x, N_y and N_z are the grid points used in each direction and Δx^+, Δz^+ are the resolutions in wall units in the homogeneous directions.

will be used for the analysis of the generalized Kolmogorov equation while the case at $Re_\tau = 300$ will be used for the analysis of the filtered dynamics. The first simulation at $Re_\tau = 550$ has been performed in order to analyse a wall turbulent flow with a Reynolds number large enough to begin to appreciate some asymptotic behaviours with a flow domain sufficiently large to capture the long and wide scale features of the wall-turbulent fluctuations. Whereas, the very high resolution of the second simulation at $Re_\tau = 300$, quite unique for a turbulent channel flow, has been chosen, at the expense of the Reynolds number achievable, to capture the phenomena occurring in the dynamics of the velocity field up to the dissipative scales and to better appreciate the alterations taking place in the statistics when the small scales effects are removed by an explicit filtering. A detailed analysis of these two simulations can be found in [71][73].

The material is organized as follow. Chapter 2 is a description of the Kolmogorov theory and of the Richardson energy cascade for isotropic and homogeneous turbulence. The generalization of the Kolmogorov approach to wall-turbulence is introduced and a description of the generalized Kolmogorov equation is given. The analysis of this equation with the channel flow data at $Re_\tau = 550$ is performed in chapter 3. The extension of the Kolmogorov equation to filtered wall turbulence is introduced in chapter 4. In the same chapter the analysis of this equation performed with the channel flow data at $Re_\tau = 300$ and filtered in the homogenous directions is reported. The conclusions and the appendices will conclude the work.

Some results of the present work of thesis have been published and other are in preparation for publication. In particular, some of the results reported

in chapter 3 have been published in [11] while those in chapter 4 in [13] [12] and [10].

Chapter 2

The Kolmogorov's approach generalized to wall-turbulence

One of the most important aspect of wall-turbulent flows is the anisotropy induced by the mean gradient. This anisotropy is reflected by the presence of a turbulent energy production process embedded in the system. Moreover, the presence of the wall induces inhomogeneity which leads to a spatial redistribution of turbulent kinetic energy. Thanks to the inhomogenity of the flow, the problem of wall-turbulent flows has been classically studied by dividing the flow domain into well characterized regions depending on wall-distance. In this context, the classical view of wall bounded flows is based on a production region close to the wall (buffer layer) and two energy sink regions one at the wall and another one in the core flow which is eventually anticipated by an equilibrium layer for large Reynolds number flows. However, the description in physical space alone is insufficient to capture the complete dynamics of wall-turbulence since the turbulent processes take place into an hierarchy of scales of motion. Indeed, it is well known that turbulent flows are characterized by fluctuations which range in size from the characteristic width of the flow, L, to much smaller scales, which become progressively smaller as the Reynolds number increases. In this view, turbulent flows are characterized by different dynamics distributed among the various scales of motion. The classical idea regarding the physical processes occurring on these scales concerns the scale-space distribution of the turbulent kinetic energy. In particular, for homogeneous turbulence, Richardson (1922) introduced the idea that kinetic energy enters the turbulence through a production mechanism at the largest scales of motion. This energy is then transferred by inviscid processes to smaller scales until, at the smallest one, the energy is dissipated by viscous action.

Actual turbulent flows have a much richer physics which involves, in addi-

tion to turbulent energy production, cascade and dissipation, the spatial flux of energy induced by inhomogeneity. In wall-turbulent flow, such as channel flow, two energy transfer take place, one in the wall-normal direction due to inhomogeneity and one through eddies of different size. In this scenario, it is, therefore, necessary to consider a general approach, able to analyze the scale-dependent dynamics in inhomogeneous conditions. The proper quantities to consider for a simultaneous description of the turbulent dynamics in physical and scale space, are the two-point statistical observables such as second order structure function, velocity correlation and energy spectrum. In particular, the present work of thesis will focus on the second order structure function $\delta u^2 = \delta u_i \delta u_i$ where $\delta u_i = u_i(x_s + r_s) - u_i(x_s)$ denotes the fluctuating velocity increments between points x_i' and x_i. This quantity can be thought as a measure of the amount of fluctuating energy at scale $r = \sqrt{r_s r_s}$ and depends both on the separation vector r_i and the spatial location of the mid-point $X_{c_i} = 1/2(x_i' + x_i)$. The balance equation for the second order structure function for anisotropic inhomogeneous wall-flows is a generalization of the balance equation used by Kolmogorov in its famous works in 1941. Looking at wall-turbulence with the same point of view of Kolmogorov will be foundamental to understand the breaking of the Kolmogorov's universality and the physical ingredients responsible of it, [77].

In the first part of this chapter the phenomenology of the fully developed turbulence and, in particular, of the energy cascade proposed by Richardson (1922) will be treated. The Kolmogorov's works which took inspiration from the concept of the Richardson energy cascade, will be described in the next section. These two parts of the chapter will follow the discussion of these topics given in [20] and [55]. Finally, the generalization of the Kolmogorov's approach to wall-turbulence will be treated in the last section.

2.1 The phenomenology of the Richardson energy cascade

In fully developed turbulence it is possible to establish scaling laws by starting from unproven but plausible hypothesis and then proceeding in a systematic fashion following a certain phenomenolgy. By phenomenology of fully developed turbulence one understands a kind of shorthands system whereby the same results can be recovered in a much simpler way, although, at the price of less systematic arguments. In some case, with phenomenology it becomes possible to grasp intuitively some of the shortcomings which are present in turbulence. As described in [20], with phenomenology it is pos-

sible for example to count the degrees of freedom of a turbulent flow, to compare macroscopic and microscopic scales, to find the probabiblity distribution function of the velocity gradients and to find the law of decay of turbulent energy.

A considerable part of existing works on turbulence are associated to the phenomenological concepts and images of the Richardson energy cascade which had a very important role in the history of turbulence and in particular in applied areas such as turbulence modeling. Richardson observed that turbulent flows are composed by eddies[1] of different size, l and different characteristic velocity, u_l and time scales, τ_l. In the Richardson's view of turbulence these eddies are superimposed, i.e. large eddies contain smaller eddies. The largest eddies are characterized by a lenght scale l_0 which is comparable to the lenght of the domain embedding the fluid. Their characteristic velocity is comparable to the root mean square velocity fluctuations, $u_0 = \sqrt{\langle u^2 \rangle}$. To note that in homogeneous and isotropic turbulence $\langle u^2 \rangle = \langle v^2 \rangle = \langle w^2 \rangle$. The Reynolds number associate to these eddies, $Re_0 = u_0 l_0/\nu$, is large and the effects of viscosity are negligible. According to Richardson's intuition (1922), [65], these eddies are unstable and break down, transferring their energy by nonlinear interactions towards smaller eddies. These smaller eddies experience a similar break down process and transfer their energy towards much smaller eddies. This process continues until the lenght scales involved are associated with velocity gradients sufficiently large to give an appreciable viscous dissipation of energy into heat. In other words, this mechanism continues until the Reynolds number associated to the smallest eddies, $Re_l = u_l l_l/\nu$, reaches the unity. This phenomenological description of turbulence is usually referred to as *energy cascade*.

As done in [20], it is usefull to recast this phenomenology with images. The eddies of various size can be imaged as blobs stacked in decreasing sizes. The larger eddies have scale l_0, while the successive generations of eddies have scales, $l_n = l_0 r^n$, with $n = (0, 1, 2, ...)$ and $0 < r < 1$ whose common choice is $r = 1/2$ but the exact value has no meaning. Assuming that the small eddies are space-filling as the large ones, the number of eddies per unit volume grows with n as r^{-3n}. In this spectrum of eddies, the turbulent energy, introduced at the top at a rate $\langle \epsilon \rangle$, is cascading down this hierarchy of eddies at the same rate $\langle \epsilon \rangle$ and is removed at the bottom by dissipation still at the rate $\langle \epsilon \rangle$. As we shall see, the rate $\langle \epsilon \rangle$ is exactly the viscous dissipation of turbulent energy into heat. In this picture two basic assumptions are made.

[1]The eddy is a loose phenomenological concept and eludes a precise definition, but it can be interpreted as a turbulent motion localized within a region of defined size wherein shows at least a moderate coherence.

The first one is *scale-invariance*. This would be violated if, for example, small eddies were less and less space-filling. The second assumption is the *localness* of the interactions at the base of the energy flux. This means that the energy cascade at scales l involves predominantly scales of comparable size, for example from rl to $r^{-1}l$.

One of the most important insight of Richardson, is that turbulent fluctuations at large scales receive their energy directly from the mean motion and thus are inhomogeneous and anisotropic. Their characteristics are directly affected by the boundary conditions of the flow which determine the mechanisms of generation of the turbulence. Hence, the large scales features cannot be universal but are related to the particular kind of flow. But Richardson argued that due the chaotic transfer of energy towards small scales, the orienting effects of the mean motion and of the geometry should became negligibly small for sufficiently small eddies. Hence, the statistical characteristics of the small scales of sufficiently large Reynolds number flows should be homogeneous, isotropic and steady. Even if in the Kolmogorov's 1941 papers no explicit reference to Richardson is made, the basic assumptions of his works are physically based on "Richardson's idea of the existence in turbulent flows of vortices of all possible scales" as he wrote in [41] and on the statistical small scale isotropic recovery assumption.

Apart the idea that the energy flux is initialized at the largest eddies[2], the most relevant assumption made in the Richardson cascade concept is that the energy dissipation is placed at the end of the cascade process. A relevant consequence is that the rate of dissipation $\langle\epsilon\rangle$ is determined by the first process in the sequence which is the transfer of energy from the largest eddies. These eddies have energy of the order u_0^2 and time scale $\tau_0 = l_0/u_0$, so the rate of transfer can be supposed to scale as $u_0^2/\tau_0 = u_0^3/l_0$. Consequently, consitent with experimental observations, this picture of energy cascade indicates that $\langle\epsilon\rangle$ scales as u_0^3/l_0 indipendently of ν.

As concluding note about the energy cascade some historical and poetical note are reported. It is thought that Richardson (1922) took inspiration from observations of clouds and from Jonathan Swift's verse:

> So, nat'ralists observe, a flea
> Hath smaller fleas that on him prey;
> And these have smaller yet to bite 'em,
> And so proceed *ad infinitum*.
> Thus every poet, in his kind,
> Is bit by him that comes behind.

[2]As we shall see in chapter 3, this paradigm fails in wall turbulence with turbulent energy generated amid the spectrum.

While, Richardson, in his work (1922), succinctly summarized the energy cascade concept as:

> Big whorls have little whorls,
> Which feed on their velocity;
> And little whorls have lesser whorls,
> And so on to viscosity
> (in the molecular sense).

Although the great contribution given by the energy cascade concept to the understanding of the turbulent physics, several questions remain unanswered some of these are adressed by the Kolmogorov theory reported in the following section.

2.2 The Kolmogorov theory

Still most of the research in turbulence and most of the new developments in this field take inspiration from the Kolmogorov's work in 1941, [38, 39, 40]. His works contain one of the very few exact and nontrivial results in the field of turbulence, as well as very modern ideas on scaling, and most of the current turbulent theories and models try to reproduce, [42, 43, 44, 46]. In the present section a revisitation of the Kolmogorov's results will be presented. This review will be instrumental for the generalization to wall-turbulent flows of the Kolmogorov's statistical tools and for the understanding of the departure of such a flows from the expected Kolmogorov universal phenomenology.

2.2.1 Homogeneous and isotropic turbulence

The Kolmogorov's groundbreaking intuition was reducing the complex problem of turbulence to its essential features, by assuming homogeneity and isotropy. In these conditions, the main process governing turbulence is the energy transfer among scales which is described by a single scalar parameter, the averaged dissipation rate. The concept of homogeneous isotropic turbulence was introduced by Taylor (1935) and since then it has played a major role in the analysis of the structures of turbulent flows as in the Kolmogorov's works. Let us recall that statistical homogeneity means that all the multidimensional probability densities of the velocity components are invariants with respect to translations and statistical isotropy means that the statistical characteristics of the field are invariant under rotations and reflections with respect to the coordinate axis.

It is important to note that the concept homogeneous isotropic turbulence is a mathematical idealization since this hypothesis could be fulfilled only if the fluid domain is infinite in space. However, it is possible to suppose that these hypothesis could be partially satisfied in small regions away from the boundaries of the flow. Alternatively, as proposed by Kolmogorov, it is possible to suppose a local homogeneity and isotropy of the small scales of any turbulent flows. The large eddies are directly affected by the boundary conditions of the flow and, therefore, are highly anisotropic. On the contrary, Kolmogorov argued that this directional bias of the large scales is lost in the chaotic scale-reduction process expected to occurs according to the phenomenology of the energy cascade towards smaller and smaller scales. Hence,

Kolmogorov's hypothesis of local isotropy. At sufficiently high Reynolds number, the small-scale turbulent motions ($l \ll l_0$) are homogeneous, isotropic and steady.

As a consequence, the statistics of the small-scale motions are in a sense universal (similar in every high Reynolds number flows) since they loose the informations about the mean flow and the boundary conditions. According again to the concept of the energy cascade, if the Reynolds number is sufficiently large so that the energy containing range of scales and the dissipation range do not overlap, the energy injeced into the large eddies should be equal to the amount of energy transfer and finally to the energy dissipated to heat. Consequently, as shown in the previous section, the rate of energy dissipation can be estimated as $\langle\epsilon\rangle \approx u_0^3/l_0$ which does not involves viscosity. In this context Kolmogorov stated:

Kolmogorov's first similarity assumption. In every turbulent flows at sufficiently high Reynolds number, the small scale statistical properties are uniquely and universally determined by the scale l, the mean energy dissipation rate $\langle\epsilon\rangle$ and the viscosity ν.

Given the two parameter $\langle\epsilon\rangle$ and ν, there are unique lenght, velocity and time scales that can be formed. These are the Kolmogorov scales:

$$\eta = \left(\frac{\nu^3}{\langle\epsilon\rangle}\right)^{1/4}, \tag{2.1}$$

$$u_\eta = \left(\langle\epsilon\rangle\nu\right)^{1/4}, \tag{2.2}$$

$$\tau_\eta = \left(\frac{\nu}{\langle\epsilon\rangle}\right)^{1/2}. \tag{2.3}$$

The Reynolds number based on the Kolmogorov scales is unity, i.e. $u_\eta\eta/\nu = 1$, clearly indicating that the Kolmogorov scales characterize the very small,

dissipative, scales. According to the first similarity assumption the small scales of large Reynolds number are statistically similar meaning that these statistics once scaled with the Kolmogorov scales are identical. The ratio of the smallest scale to the largest scale is easily determined from the definition of η and from the scaling $\langle\epsilon\rangle \approx u_0^3/l_0$. The results are

$$\frac{l_0}{\eta} = Re^{3/4}, \tag{2.4}$$

$$\frac{u_0}{u_\eta} = Re^{1/4}, \tag{2.5}$$

$$\frac{\tau_0}{\tau_\eta} = Re^{1/2}. \tag{2.6}$$

Evidently, at high Reynolds number, the velocity scales and timescales of the smallest eddies are small compared with those of the largest eddies. As a consequence, there is a range of scales, very small compared with l_0 but very large compared with η, which is not affected viscous effects. Therefore, we can introduce:

Kolmogorov's second similarity assumption. In every turbulent flow, in the limit of infinite Reynolds number, all the small scales statistical properties are uniquely and universally determined by $\langle\epsilon\rangle$ and l indipendent by ν.

Clearly, we have to assume that in the limit of vanishing viscosity, $Re \to \infty$, the rate of energy dissipation is finite and equal to the energy flux, $\lim_{\nu\to 0}\langle\epsilon(\nu)\rangle = \langle\epsilon\rangle$ which is confirmed by experimental evidence [76] and by the energy dissipation law, $\langle\epsilon\rangle \approx u_0^3/l_0$, since it does not involve viscosity. For large, but finite Reynolds number all the statistics are determined by $\langle\epsilon\rangle$ in the *inertial range*, $\eta \ll l \ll l_0$, where the main physical effect is the inertial transfer of energy towards smaller scales without any appreciable dissipation. In conclusion, for small scales compared to the large energy containing eddies, an universal equilibrium range exists where the first similarity assumption holds. In this range the eddies can adapt quickly, since their small time scales, to mantain an equilibrium with the energy transfer rate imposed by the largest eddies. For finite Reynolds number, this equilibrium range can be divided into two subrange: the inertial range where the second similarity assumption holds being the viscous effects negligible and the dissipation range at the smallest scales where viscosity dominates and so is responsible for essentially all the dissipation.

2.2.2 The 4/5 law

Kolmogorov in his third 1941's paper, [40], derived an exact relation for the third order longitudinal structure function. This equation follows from the Karman-Howarth equation, [35], by re-expressing the correlation function in terms of velocity differences. Starting from the Navier-Stokes equations in homogeneous isotropic condidtions, it is possible to derive the evolution equation for the correlation tensor. It is possible to consider a globally isotropic field since the statistical state of the small scales is universal and the resulting relations should be valid for any locally isotropic field, whether or not the turbulence is globally isotropic.

Since isotropic turbulence is not self-sustained, we are dealing with a problem of freely decaying turbulence. The evolution equation for the second order two-point correlation tensor, defined as

$$R_{ij}(\mathbf{X}_c, \mathbf{r}, t) = \langle u_i(\mathbf{x}, t) u_j(\mathbf{x} + \mathbf{r}, t) \rangle \tag{2.7}$$

where for homogeneity R_{ij} does not vary with the absolute position, $R_{ij}(\mathbf{X}_c, \mathbf{r}, t) = R_{ij}(\mathbf{r}, t)$, can be derived if we write the Navier-Stokes equations for u_i at point x_i and for u'_i at point x'_i then we multiply the first equation by u'_j and the second equation by u_j. After adding the two equations and averaging we obtain,

$$\frac{\partial \langle u_i u'_j \rangle}{\partial t} = \frac{\partial}{\partial r_k}(\langle u_i u_k u'_i \rangle - \langle u_i u'_j u'_k \rangle) + \frac{1}{\rho}\left[\frac{\partial \langle p u'_j \rangle}{\partial r_i} + \frac{\partial \langle p' u_i \rangle}{\partial r_j}\right] + 2\nu \frac{\partial^2 \langle u_i u'_j \rangle}{\partial r_k^2} \tag{2.8}$$

which is valid for an homogeneous field, not necessarily isotropic. It is useful now to introduce the third order two-point correlation tensor,

$$S_{ij,k} = \langle u_i(\mathbf{x}) u_j(\mathbf{x}) u_k(\mathbf{x} + \mathbf{r}) \rangle$$

where the subscript after the comma denotes the variables evaluated at point x'_i. If we compute the trace of equation 2.8 we obtain

$$\frac{\partial R_{ii}}{\partial t} = 2\frac{\partial S_{ik,i}}{\partial r_k} + 2\nu \frac{R_{ii}}{\partial r_k^2} \tag{2.9}$$

where the term containing pressure disappears for homogeneity while for isotropy $S_{i,ik} = -S_{ik,i}$.

Karman and Howarth in their work (1938), more details can be found in [58], considering a globally isotropic field, re-expressed the tensors R_{ii} and $S_{ik,i}$ in terms of two scalar functions,

$$R_{ii} = \langle u^2 \rangle \left[3 + r\frac{d}{dr}\right] \langle u_{||} u'_{||} \rangle \qquad S_{ik,i} = \langle u^3 \rangle \frac{r_k}{2} \left[\frac{4}{r} + \frac{d}{dr}\right] \langle u_{||} u_{||} u'_{||} \rangle,$$

where $\mathbf{u}_{||} = (u_i r_i / r^2)\mathbf{r}$, $\langle u^2 \rangle$ and $\langle u^3 \rangle$ are the variance and the skewness of the velocity field, respectively. Substituting these expressions in equation 2.9 one obtains,

$$\left[3 + r\frac{d}{dr}\right] \frac{\partial \langle u_{||} u'_{||} \rangle}{\partial t} =$$

$$\left[3 + r\frac{d}{dr}\right] \left(\frac{4}{r} + \frac{d}{dr}\right) \langle u_{||} u_{||} u'_{||} \rangle + 2\nu \left[3 + r\frac{d}{dr}\right] \left(\frac{d^2}{dr^2} + \frac{4}{r}\frac{d}{dr}\right) \langle u_{||} u'_{||} \rangle.$$

Since the application of $(3 + rd/dr)$ to a generic function of r admits only the zero solution which is not singular at the origin, we have

$$\frac{\partial \langle u_{||} u'_{||} \rangle}{\partial t} = \left(\frac{4}{r} + \frac{d}{dr}\right) \langle u_{||} u_{||} u'_{||} \rangle + 2\nu \left(\frac{d^2}{dr^2} + \frac{4}{r}\frac{d}{dr}\right) \langle u_{||} u'_{||} \rangle \tag{2.10}$$

which is the Karman-Howarth equation (1938).

Let us now derive the Kolmogorov's 4/5ths law by re-expressing the terms of the Karman-Howarth equation 2.10 in terms of longitudinal structure functions, $\delta u_{||}^2$ and $\delta u_{||}^3$. These quantities are related to $\langle u_{||} u'_{||} \rangle$ and $\langle u_{||} u_{||} u'_{||} \rangle$ through the relations,

$$\langle u_{||} u'_{||} \rangle = \langle u^2 \rangle - \frac{1}{2}\langle \delta u_{||}^2 \rangle \qquad \langle u_{||} u_{||} u'_{||} \rangle = -\frac{1}{6}\langle \delta u_{||}^3 \rangle,$$

so that the equation reads

$$\frac{\partial}{\partial t}\left(\langle u^2 \rangle - \frac{1}{2}\langle \delta u_{||}^2 \rangle\right) =$$

$$-\left(\frac{4}{r} + \frac{d}{dr}\right) \frac{1}{6}\langle \delta u_{||}^3 \rangle + 2\nu \left(\frac{d^2}{dr^2} + \frac{4}{r}\frac{d}{dr}\right) \left(\langle u^2 \rangle - \frac{1}{2}\langle \delta u_{||}^2 \rangle\right) \tag{2.11}$$

Since for $r \ll l_0$ the small scale statistical properties should not depend on time and for globally isotropic turbulence $\partial \langle u^2 \rangle / \partial t = -2/3 \langle \epsilon \rangle$ [3], we have

$$-\frac{2}{3}\langle \epsilon \rangle = -\frac{1}{6}\left[\frac{d\langle \delta u_{||}^3 \rangle}{dr} + \frac{4}{r}\langle \delta u_{||}^3 \rangle\right] - \nu \left[\frac{d^2\langle \delta u_{||}^2 \rangle}{dr^2} + \frac{4}{r}\frac{d\langle \delta u_{||}^2 \rangle}{dr}\right]$$

[3]The evolution equation of the turbulent kinetic energy $q = 1/2\langle u_i u_i \rangle$ in homogeneous conditions takes the simple form

$$\frac{\partial q}{\partial t} = -\nu \langle \frac{\partial u_i}{\partial x_j}\frac{\partial u_i}{\partial x_j} \rangle = -\langle \epsilon \rangle.$$

For isotropic turbulence, $u^2 = v^2 = w^2$, hence $\partial \langle u^2 \rangle / \partial t = -2/3 \langle \epsilon \rangle$

which integrated over r leads to

$$\langle \delta u_{||}^3 \rangle - 6\nu \frac{d\langle \delta u_{||}^2 \rangle}{dr} = -\frac{4}{5}\langle \epsilon \rangle r. \tag{2.12}$$

Equation 2.12 is of foundamental interest, since it is an equilibrium equation between second and third order longitudinal structure function and represents a mean turbulent energy balance for each scale r. Equation 2.12 gives the exact relation governing the third order longitudinal structure function in terms of the separation r. Indeed, in the inertial range where the viscous effects are negligible or equivalently in the limit $\nu \to 0$ which eliminates any residual viscous diffusion at every finite scale, equation 2.12 leads to the Kolomogorov 4/5ths law,

$$\langle \delta u_{||}^3 \rangle = -\frac{4}{5}\langle \epsilon \rangle r. \tag{2.13}$$

This is one of the most important results in turbulence since it is exact and it is a sort of boundary condition for the theories of turbulence which must satisfy this law or must violate the assumptions on which it is based. This relation allows to identify $\langle \delta u_{||}^3 \rangle / r$ as the energy flux among eddies of different sizes quantitatively assessing the phenomenological concept of the energy cascade. At the moment, the experimental evidence confirms the 4/5ths law. This relation is quite general and since involves only velocity differences it is though to be exact for all tipe of flows, provided that local homogeneity and local isotropy hold.

In the absence of intermittency, equation 2.13 suggests that the main parameter involved in any inertial range scaling should be $\langle \epsilon \rangle$ which is equal to the energy flux through scales. In this context the scaling behaviour of the p-order structure function is assumed to be, on dimensional ground,

$$\langle \delta u_{||}^p \rangle \propto \langle \epsilon \rangle^{\frac{p}{3}} r^{\frac{p}{3}}$$

which means that the flow is expected to be scale invariant in the inertial range with a unique scaling exponent $h = p/3$, [20]. However, experimental results have shown that the scaling laws present exponent $\zeta(p)$ substantially different from the dimensional prediction for large p. This behaviour is essentially related to the intermittent nature of the dissipation field ϵ, as raised by [48] (1944) and remarked in [45] (1974). The Landau's objection asserted that the intermittent variation of ϵ is driven by the large eddies and, therefore, is different for different flows. Consequentely, the result of the averaging of ϵ cannot be universal for the scaling of the different p-order structure function but only for $p = 3$. For this reason, intermittency corrections have been applied, following for instance the refined Kolmogorov's hypothesis [41] where

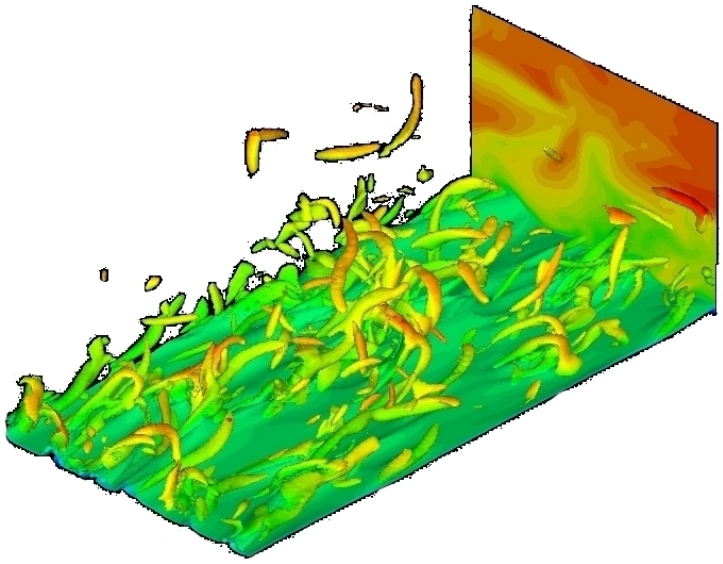

Figure 2.1: Istantaneous vortical structures in a turbulent channel flow visualized by mean of isosurface of λ_2, [31].

the scaling exponents are related to the statistics of the dissipation field. Another phenomenological model, proposed by Parisi and Frisch in [20], assumed that the velocity increments possess a continuous range of scaling exponents related to the multi fractal structure of the turbulent field. While a processing technique which greatly improve the accuracy of the exponents has been proposed in [4], called *extended self-similarity* (ESS), and is based on the observation that the functional forms of the structure function at the beginning of the dissipative range are the same.

2.3 Anisotropic and inhomogeneous wall turbulent flows

Actual turbulent flows have a much richer physics than those described for globally isotropic homogeneous turbulence. Beyond energy transfer, anisotropic turbulent production and inhomogenous spatial fluxes occur. The turbulent self-sustaining mechanisms and energy redistribution embedded in the flow domain modify the phenomenological picture of globally homogeneous isotropic turbulence adding anisotropic effects which change appreciably in the different flow region due to inhomogeneity (see the inhomogeneous distribution and the directionality of the istantaneous vortical structures in a

turbulent channel flow shown in figure 2.1). A detailed understanding of these interacting phenomena requires a description of the physical processes occurring simultaneously in physical space and in the space of turbulent scales. This multidimensional description is the only one approach which allows to verify if the classical picture of turbulence as described by Richardson holds, if the assumption of the small scales statistical properties universality and the assumption of local homogeneity and isotropy are verified. To deal with these more general conditions, the 4/5ths law has been extended [26] in the form of a balance equation for the second order structure function $\langle \delta u^2 \rangle = \langle \delta u_i \delta u_i \rangle$, where the fluctuating velocity increments at position X_{c_s} and vector separation r_s are $\delta u_i = u_i(X_{c_s} + r_s/2) - u_i(X_{c_s} - r_s/2)$. This equation, specialized for the symmetries of the channel flow, will be analyzed in the present work and introduced in this section.

2.3.1 Inhomogeneity and spatial fluxes

Wall-bounded turbulent flows such as boundary layers, pipe flows and channel flows are characterized by a mean velocity gradient which is caused by the shearing effect of the flow over a rigid wall. This mean gradient varies with the distance from the wall producing a strong inhomogeneity in the wall-normal direction. This inhomogeneity leads to a spatial redistribution of energy and to a strong position-dependence of the turbulent dynamics. For that reason, wall turbulence has been classically studied through the balance equation for the turbulent kinetic energy, $q = \langle u_i u_i \rangle / 2$. Indeed, this equation allows to characterize wall-turbulence in well defined layers where different turbulent phenomena dominate. The clear description of the dynamics of energy between these regions of the flow is crucial to the understanding of wall-bounded turbulent flows.

The turbulent kinetic energy balance for a turbulent channel flow reads,

$$\frac{d\phi(y)}{dy} = s(y), \tag{2.14}$$

where the spatial flux $\phi = (\langle qv \rangle + \langle pv \rangle / \rho - \nu d\langle q \rangle / dy)$, due to the symmetries of the flow domain, is a scalar flux in the wall-normal direction, y, due to inertial fluctuations, pressure-velocity correlation and viscous diffusion, respectively. The term in the right hand side, $s(y) = -(\langle uv \rangle dU/dy + \langle \epsilon \rangle)$ describes the turbulent energy source/sink given by the balance between production and dissipation at given wall-normal location. The production term, $-\langle uv \rangle dU/dy$, occurs also in the balance equation for the mean kinetic energy with opposite sign and describes the energy exchange between the mean and fluctuating motion. This term is positive at all wall-distances

and, consequentely, the wall-turbulent motion is self-sustained. The wall-turbulent fluctuations does not need an external mechanisms to replenish the turbulent energy dissipated by viscous forces. The dissipation term, $-\langle\epsilon\rangle$ represents the mean rate of viscous dissipation of turbulent kinetic energy into heat. As a consequence, equation 2.14 states that the divergence of the spatial fluxes balances the y-behaviour of the energy source/sink given by the difference between production and dissipation.

The y-distribution of the terms in equation 2.14 has been used for the classification of the wall-turbulent region into well defined layers. The first one close to the wall, dominated by dissipation, is normally referred to as viscous sublayer. In turn, the intermediate region where production is predominant is generally called buffer layer. Above this region there is a zone, traditionally called logarithmic layer, where for very high Reynolds number flows an overlap between an inner and an outer scaling appears and production and dissipation balance, [63], see also [25] and [72] for the largest Reynolds number simulations carried out in wall turbulence. This asymptotic state is not reached at the Reynolds number of the simulations preformed in this thesis, however in the rest of the work we will conventionally refer to the logarithmic layer as the region where production approximatively balances with dissipation, see figure 2.2 for the channel flow case at $Re_\tau = 550$, and the rate of spatial energy flux is nearly zero. This results in a constant spatial flux of energy which crosses this equilibrium layer feeding the fluctuations in the bulk central region of the channel where production vanishes. In conclusion, wall bounded flows are charaterized by an energy source region, the buffer layer, and two energy sink regions, one in the proximity of the walls and another one in the core flow which may be preceded by an equilibrium layer.

2.3.2 The generalized Kolmogorov equation

Clearly, a detailed assessment of the dynamics of energy between different regions in physical space is crucial to the understanding of wall-turbulent flows. However, a view based on spatial energy transfer alone is insufficient to completely describe the wall-turbulent dynamics. A parallel view based on the decomposition of the flow field into an hierarchy of scales is required in order to appreciate the behaviour of production, dissipation and energy transfer for different ranges of scales and wall-distances. The conceptual picture is that of a double flux of energy both in physical and scale space. Indeed, the simultaneous analysis of the energy processes through the space of scales and wall-distances adds the phenomenon of the energy cascade to the spatial flux accountable for with equation 2.14.

According to Kolmogorov's four-fifths law [40], equation 2.13, the promi-

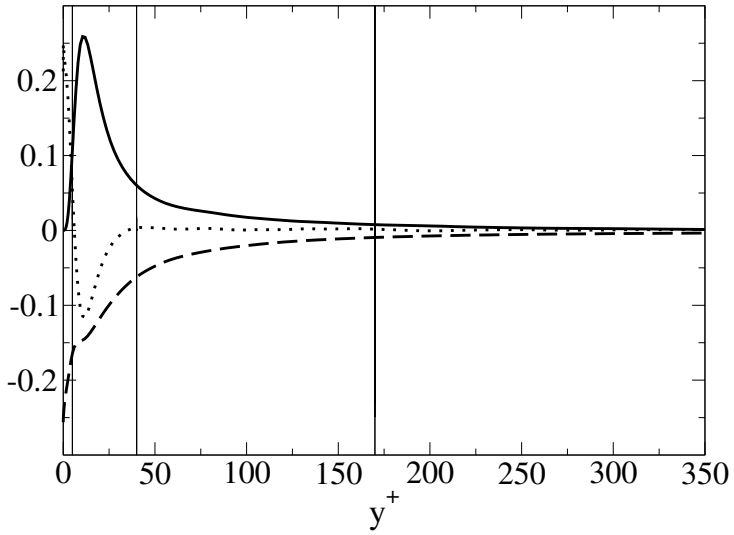

Figure 2.2: Turbulent kinetic energy budget, equation 2.14, for the channel flow simulation at $Re_\tau = 550$. Turbulent production (solid line), dissipation (dashed line) and the rate of spatial flux (dotted line). The three vertical lines identify the viscous sublayer, the buffer layer, the putative logarithmic layer and the bulk flow.

nent feature of high Reynolds number turbulent flows is the energy transfer from large to small scales believed to universally occur in the inertial range of turbulence. In this view the velocity increment between two points is a central object. Energy balance prescribes its third order moment to be linear in the separation r and proportional to the average dissipation rate $\langle\epsilon\rangle$. Since, it is thought that all the possible symmetries of the Navier-Stokes equations, usually broken by the mechanisms producing turbulence, are restored in a statistical sense at small scales (the local isotropy assumption), it is important to verify these assertions in more realistic conditions of globally anisotropic and inhomogeneous flows. To deal with these more general conditions, the generalization of the Kolmogorov's approach to turbulence in the form of a balance equation for the second order structure function, $\langle\delta u^2\rangle$, can be used. Following the procedure described in [26], it is possible to derive from the Navier-Stokes equations the generalized form of the Kolmogorov equation for globally anisotropic and inhomogeneous conditions,

$$\frac{\partial\langle\delta u^2\rangle}{\partial t} + \frac{\partial\langle\delta u^2\delta u_j\rangle}{\partial r_j} + \frac{\partial\langle\delta u^2\delta U_j\rangle}{\partial r_j} + 2\langle\delta u_i\delta u_j\rangle\frac{\partial\delta U_i}{\partial r_j} + \frac{\partial\langle u_j^*\delta u^2\rangle}{\partial X_{cj}} + \frac{\partial\langle\delta u^2 U_j^*\rangle}{\partial X_{cj}} +$$

$$2\langle u_j^* \delta u_i \rangle \frac{\partial \delta U_i}{\partial X_{cj}} = -4\langle \epsilon^* \rangle + 2\nu \frac{\partial \langle \delta u^2 \rangle}{\partial r_i \partial r_i} - \frac{2}{\rho} \frac{\partial \langle \delta p \delta u_i \rangle}{\partial X_{ci}} + \frac{\nu}{2} \frac{\partial^2 \langle \delta u^2 \rangle}{\partial X_{cj}^2} \ . \quad (2.15)$$

This evolution equation allows to identify all the processes which characterize the dynamics of inhomogeneous anisotropic flows both in the space of scales and in physical space. In particular, the terms with r-derivatives describe physical processes which transfer energy through scales while those with X_{c_j}-derivatives arise due to inhomogeneity and describe physical processes which transfer energy through different regions of the flow. When homogeneous and isotropic conditions are reached, the generalized Kolmogorov equation reduces to the classical Kolmogorov equation 2.12. Hence, the potential breakdown of the small scales universality and of the related phenomenology of the energy cascade can be directly adressed via a scale by scale analysis of equation 2.15 in the different regions of the flow.

Homogeneous isotropic turbulence

Assuming that the local isotropy homogeneous assumption holds the X_{c_j}-derivatives and the contributions of the mean velocity vanish and equation 2.15 reduces to

$$\frac{\partial \langle \delta u^2 \delta u_i \rangle}{\partial r_i} = -4\langle \epsilon \rangle + 2\nu \frac{\partial \langle \delta u^2 \rangle}{\partial r_i r_i}, \quad (2.16)$$

which is a balance equation analogous to the Kolmogorov equation 2.12. In the limit of vanishing viscosity, $\nu \to 0$, or equivalently at inertial scales, this equation expressed in terms of the longitudinal velocity increments reduces to the 4/5ths law, equation 2.13. In the same conditions, equation 2.16 leads to a relation analogous to the 4/5ths law derived by [60] without any assumptions about the isotropy of the flow structure. Considering the integration of equation 2.16 over a sphere B of radius $|\mathbf{r}|$ centered at $\mathbf{r} = 0$ for fixed small scale, equation 2.16 leads to,

$$\int_{\partial B} \langle \delta u^2 \delta u_i \rangle \cdot \mathbf{n_r} dS = -\frac{4}{3} \langle \epsilon \rangle r \quad (2.17)$$

where $\mathbf{n_r}$ is the outward normal to the ball and it is used the divergence theorem on the resulting volume integrals and it is divided by $2\pi r^2$. Since the flow considered here is isotropic the integration over the ball is redundant and relation 2.17 reduces to,

$$\frac{\langle \delta u^2 \delta u_i \rangle r_i}{r} = -\frac{4}{3} \langle \epsilon \rangle r \quad (2.18)$$

which is the analogous of the 4/5ths law but involving both longitudinal and transversal velocity increments. In the same limits, another relation analogous to the 4/5ths law can be obtained from equation 2.16 simply neglecting the viscous diffusion mechanisms,

$$\frac{\partial \langle \delta u^2 \delta u_i \rangle}{\partial r_i} = -4\langle \epsilon \rangle \ , \tag{2.19}$$

which again holds without the assumptions of isotropy but only for $\nu \to 0$ or small r.

Equations 2.17, 2.18 and 2.19, as the 4/5ths law, establish that in the spectrum of turbulent scales an inertial range exists where the turbulent energy is transfered through the scales of motion from large to small scales indipendently on the scale under consideration and with a constant flux proportional to the energy input/dissipation, $\langle \epsilon \rangle$. There is not direct energy injection and not direct energy extraction. These results are commonly associated to the phenomenology of the Richardson energy cascade. This picture is claimed to be highly universal, in the sense that, no matter what the details of the flows are at large scales, the small scales of large Reynolds number flows are believed to behave according to the balance established by equation 2.19. In its universality, equation 2.19 neglects the details of the processes which feed the turbulence to provide the constant energy flux through the inertial range.

Homogenous shear flow

In turbulent flows such as the homogeneous shear flow with a mean velocity $U = Sy$ in the x direction where $S = dU/dy$ is the shear in the y direction, the generalized Kolmogorov equation reduces to

$$\frac{\partial \langle \delta u^2 \delta u_i \rangle}{\partial r_i} + \frac{\partial \left(\langle \delta u^2 \rangle S r_y \right)}{\partial r_x} + 2S\langle \delta u \delta v \rangle = -4\langle \epsilon \rangle + 2\nu \frac{\partial \langle \delta u^2 \rangle}{\partial r_i \partial r_i}. \tag{2.20}$$

This is the simplest non-trivial flow which fully retains the basic anisotropic mechanism of turbulent kinetic energy production typical of any shear flow [6]. Besides energy transfer, viscous diffusion and dissipation the additional anisotropic energy injection alters the balance modifying the energy cascade process. In this flow, due to the presence of a mean velocity the inertial flux of turbulent kinetic energy in the space of scales is due to both the mean flow and the turbulent fluctuations, the firts two terms on the left hand side of equation 2.20.

The homogeneity of the flow implies that the process of energy production, $2S\langle \delta u \delta v \rangle$, inject energy at a given range of scales at rate $-4\langle \epsilon \rangle$. The

range of scales affected by this anisotropic action could be rationalized introducing a new characteristic quantity, the cross-over scale l_c. By comparing the magnitude of the energy processes of equation 2.20, the cross-over scale can be identifed as the scale where production and inertial energy transfer balance. Therefore, the scale l_c splits the range of scales affected by the anisotropic energy production from those which follow the classical Kolmogorov equation 2.16. This scale is closely related to the shear scale, L_s, whose magnitude can be evaluated with dimensional analysis[4] as

$$L_s = \sqrt{\frac{\langle \epsilon \rangle}{S^3}} \, . \tag{2.21}$$

One of the advantage related to the study of homogeneous shear flows is that spatial homogeneity implies a well defined value of the shear scale L_s and, therefore, also of the cross-over scale, l_c. The production mechanisms are active at scales larger than l_c, while for smaller scales there is a classical inertial range dominated by a Richardson energy cascade. In this range the Kolmogorov equation 2.16 can be used to model the turbulent dynamics using as boundary condition an incoming energy flux at scales of order l_c. Therefore, the cross-over scale is crucial for the small-scale isotropic recovery as shown in [7][8]. In conclusion, for Reynolds number sufficiently large so that l_c and the viscous diffusion scales are well separated, an inertial range where the Komogorov's hypothesis and the associated Richardson energy cascade can be found in shear flows.

Wall-turbulence: channel flow

When dealing with wall-flows, the statistical inhomogeneous condition and not only anisotropy has to be considered. Inhomogeneity increases the complexity of the turbulent physics spatially modulating the scale energy balance, [54, 14]. The additional spatial energy flux and turbulent production modify the energy cascade through the spectrum of scales in a different manner depending on the spatial position. In turbulent wall-flows, such as channel flow with a longitudinal mean velocity $U(y)$, the generalized Kolmogorov equation specializes,

$$\frac{\partial \langle \delta u^2 \delta u_i \rangle}{\partial r_i} + \frac{\partial \langle \delta u^2 \delta U \rangle}{\partial r_x} + 2 \langle \delta u \delta v \rangle \left(\frac{dU}{dy} \right)^* + \frac{\partial \langle v^* \delta u^2 \rangle}{\partial Y_c} =$$

[4] By comparing the estimate of the velocity fluctuations induced at a given scale r by the mean shear, $\delta u_S(r) \propto Sr$, with the estimate given in the inertial range by the Kolmogorov scaling $\delta u_K(r) \propto \epsilon^{1/3} r^{1/3}$, it is possible to dimensionally identify the lenght scale which splits production dominated scales from cascade dominated scales as $L_s = \sqrt{\langle \epsilon \rangle / S^3}$

$$-4\langle\epsilon^*\rangle + 2\nu\frac{\partial^2\langle\delta u^2\rangle}{\partial r_i\partial r_i} - \frac{2}{\rho}\frac{\partial\langle\delta p\delta v\rangle}{\partial Y_c} + \frac{\nu}{2}\frac{\partial^2\langle\delta u^2\rangle}{\partial {Y_c}^2} \tag{2.22}$$

where * denotes a mid-point average, i.e. $u_i^* = (u_i(x_s') + u_i(x_s))/2$, $\epsilon = \nu(\partial u_i/\partial x_j)(\partial u_i/\partial x_j)$ is the viscous pseudo-dissipation, $\langle\cdot\rangle$ denotes now average in the homogeneous directions and the Y_c dependence is associated with inhomogeneity. For a detailed derivation see Hill [26] and also [83] and [76] for an alternative approach. In this flow the second order structure function is a function not only of the separation vector r_i but also of the mid-point $Y_c = 1/2(y' + y)$. Compared to the turbulent kinetic energy balance equation which describes the turbulent phenomena varying through different wall-distances, equation 2.22 is written in a four-dimensional space, (r_x, r_y, r_z, Y_c), which will be hereafter referred to as *augmented space*. Namely, we can account for the different behaviour of the turbulent dynamics in the three-dimensional space of scales for different wall-distances. In particular, equation 2.22 allows to analyze the two energy fluxes simultaneously occurring in wall-flows, namely the spatial flux through different Y_c and the energy transfer through different r_i. The terms with r-derivatives describe the rate of energy flux in the space of scales. In this context, equation 2.22 distinguishes three different contributions due to fluctuating turbulence, mean motion and viscous diffusion,

$$\frac{\partial\langle\delta u^2\delta u_i\rangle}{\partial r_i}\ , \qquad \frac{\partial\langle\delta u^2\delta U\rangle}{\partial r_x} \qquad \text{and} \qquad 2\nu\frac{\partial^2\langle\delta u^2\rangle}{\partial r_i\partial r_i}\ ,$$

respectively. While, the terms with Y_c-derivatives describe the additional rate of spatial fluxes due to the inhomogeneity of wall-turbulence. These energy fluxes are due to fluctuating turbulence, pressure-velocity correlation and viscous diffusion,

$$\frac{\partial\langle v^*\delta u^2\rangle}{\partial Y_c}\ , \qquad \frac{2}{\rho}\frac{\partial\langle\delta p\delta v\rangle}{\partial Y_c} \qquad \text{and} \qquad \frac{\nu}{2}\frac{\partial^2\langle\delta u^2\rangle}{\partial {Y_c}^2}\ ,$$

respectively. This double energy flux balance with the behaviour in the augmented space of the energy source due to the anisotropic production by mean shear,

$$2\langle\delta u\delta v\rangle\left(\frac{dU}{dy}\right)^*$$

and of the energy sink due to viscous dissipation,

$$4\langle\epsilon^*\rangle\ .$$

For large separations, equation 2.22 approaches an asymptotic behavior given by four-times the single point turbulent kinetic energy budget, equation

2.14, which can be understood as the large scale boundary condition for the energy processes of the balance of the second order structure function. For example, the large scale limit of the divergence of the inertial energy flux among scales is

$$\lim_{r\to\infty} \frac{\partial\langle \delta u^2 \delta u_i\rangle}{\partial r_i} = \frac{1}{2}\left(\frac{\partial\langle u^2 u_i\rangle}{\partial x_i} + \frac{\partial\langle u'^2 u_i'\rangle}{\partial x_i'}\right) = \frac{\partial\langle u^2 u_i\rangle^*}{\partial X_{c_i}} \tag{2.23}$$

where the following rules for the transformation of the derivatives have been used,

$$\frac{\partial}{\partial r_i} = \frac{1}{2}\left(\frac{\partial}{\partial x_i'} - \frac{\partial}{\partial x_i}\right) \qquad \text{and} \qquad \frac{\partial}{\partial X_{c_i}} = \frac{1}{2}\left(\frac{\partial}{\partial x_i'} + \frac{\partial}{\partial x_i}\right) .$$

The limit 2.23 suggests that the only one non vanishing term at large separations is in the wall-normal direction,

$$\lim_{r\to\infty} \frac{\partial\langle \delta u^2 \delta u_i\rangle}{\partial r_y} = \frac{1}{2}\left(\frac{\partial\langle u^2 u_i\rangle}{\partial y} + \frac{\partial\langle u'^2 u_i'\rangle}{\partial y'}\right) = \frac{\partial\langle u^2 u_i\rangle^*}{\partial Y_c} . \tag{2.24}$$

Whereas, the large scale limit of the divergence of the inertial energy flux in physical space is

$$\lim_{r\to\infty} \frac{\partial\langle \delta u^2 v^*\rangle}{\partial Y_c} = \frac{\partial\langle u^2 u_i\rangle^*}{\partial Y_c} . \tag{2.25}$$

Relation 2.24 and 2.25 reveal that both the contributions, in the space of scales and physical space, of the turbulent energy flux are present with the same value in the turbulent kinetic energy balance. The single-point divergence of the turbulent spatial flux represents the large scale boundary condition for the corresponding terms in the augmented space.

In homogeneous flows, the turbulent energy fluxes take place only in the space of scales and the large scale limit of the divergence, equation 2.23, is zero. In this condition the turbulent flux

$$\lim_{r\to\infty} \langle \delta u^2 \delta u_i\rangle = \delta\langle u^2 u_i\rangle \tag{2.26}$$

also vanishes suggesting that in homogeneous turbulence the energy cascade is initialized at finite scales by the displacement towards small scales of the energy provided at the largest scales by the production term or equivalently by the forcing term in isotropic turbulence. This is a distinguish feature of homogeneous flows with respect actual turbulent flows where inhomogeneity is present. As we shall see in chapter 3 these boundary conditions have strong repercussions on the observed behaviour of the energy fluxes.

As for homogeneous shear flows, in addition to the two lenght-scales typical of homogenous isotropic turbulence, namely the dissipative and the integral scales, the anisotropic turbulent production introduces a further characteristic quantity, the cross-over scale l_c, which splits the range of scales affected by the anisotropic production of energy from those which are not influenced by the mean shear. The main difference compared to homogenous shear flows is that the cross-over scale has not a well defined value but varies for different wall distances, i.e. $l_c = l_c(y)$, and the same applies to the dissipative scales, i.e. $\eta = \eta(y)$. Classically, the y-behaviour of these quantity has been adressed through dimensional analysis. According to the classical equilibrium theory for the logarithmic layer, turbulent production and dissipation balance. With this assumption and since the mean shear S can be written as $S \approx u_\tau/(\kappa y)$, [63], it is possible to find that the local dissipation $\langle\epsilon\rangle$ can be estimated as $\langle\epsilon\rangle = u_\tau^3/(\kappa y)$, where κ is the Kármán constant and u_τ is the friction velocity. Assuming this scaling for dissipation, the Kolmogorov scale $\eta = (\nu^3/\langle\epsilon\rangle)^{1/4}$ is expected to scale with the wall-distance as $\eta^+ \propto (\kappa y^+)^{1/4}$, while the shear scale $L_s = (\langle\epsilon\rangle/S^3)^{1/2}$, is expected to scale with the wall-distance as $L_s^+ \propto (\kappa y^+)$, [52], where the superscripts + denote viscous units. Since the cross-over scale l_c is dimensionally related to the shear scale, it is expected that the same y-behaviour applies, i.e. $l_c(y) \propto \kappa y^+$. To note that, due to the assumption of isotropy, the dimensional behaviour of the cross-over scale does not take into account the different values this scale could assume in the three dimensional scale-space due to anisotroy.

Differently from homogeneous shear flows, scales smaller than the cross-over scale l_c do not necessarily follow the classical Kolmogorov equation 2.16 due to the presence of inhomogeneous spatial fluxes which could modify the picture of the energy cascade adding/subtracting energy at a given scale for different wall distances. In order to verify the assumption of the universal small scales isotropic recovery, an extended cross-over scale $\mathbf{l_{ce}}$ defined by the condition

$$\left(\frac{\partial\langle\delta u^2\delta u_i\rangle}{\partial r_i} + \frac{\partial\langle\delta u^2\delta U\rangle}{\partial r_x}\right)(\mathbf{l_{ce}}, Y_c) =$$

$$-\left(2\langle\delta u\delta v\rangle\left(\frac{dU}{dy}\right)^* + \frac{\partial\langle v^*\delta u^2\rangle}{\partial Y_c} + \frac{2}{\rho}\frac{\partial\langle\delta p\delta v\rangle}{\partial Y_c}\right)(\mathbf{l_{ce}}, Y_c)$$

should be considered. To note that the scale $\mathbf{l_{ce}}$ is considered now as a vector quantity since the turbulent processes of production and spatial flux could exhibit different behaviours in the three directions of the r-space due to anisotropy. The viscous diffusion cutoff scale should be also extended to

account for viscous diffusion both in scale and physical space, namely

$$\left(\frac{\partial\langle\delta u^2\delta u_i\rangle}{\partial r_i}+\frac{\partial\langle\delta u^2\delta U\rangle}{\partial r_x}\right)(\mathbf{l_{de}},Y_c)=\left(2\nu\frac{\partial^2\langle\delta u^2\rangle}{\partial r_i\partial r_i}+\frac{\nu}{2}\frac{\partial^2\langle\delta u^2\rangle}{\partial {Y_c}^2}\right)(\mathbf{l_{de}},Y_c)$$

where $\mathbf{l_{de}}$ is the extended viscous scale. Therefore, considering increments r_i smaller than the extended cross-over scale, $|\mathbf{r}|<|\mathbf{l_{ce}}|$ and sufficiently large so that the viscous diffusion can be negletted, $|\mathbf{r}|>|\mathbf{l_{de}}|$, a Kolmogorov inertial range could be found also in wall flows where equation 2.16, i.e.

$$\frac{\partial\langle\delta u^2\delta u_i\rangle}{\partial r_i}=-4\langle\epsilon\rangle,$$

holds. Indeed, in such an ideal range there is not energy injection and extraction via anisotropic turbulent production and inhomogeneous spatial fluxes. The turbulent energy freely flows down to small scales whitout interferences and, hence, with a constant rate until the viscous diffusion scales are reached. This picture holds only when a large separation between $|\mathbf{l_{ce}}|$ and $|\mathbf{l_d}|$ occurs. In spite of shear flows where the shear scale L_s and equivalently l_c have a well-defined value corresponding to large scales, in wall-flows expecially in the near-wall region there is no reason to assert that the anisotropic and inhomogeneous phenomena which locate $\mathbf{l_{ce}}$ are confined at larger scales.

Chapter 3

The energy fluxes paths and their origin

The present study is devoted to the description of the energy fluxes from production to dissipation in the augmented space of wall-turbulent flows. The multidimensional description will be shown crucial to understand the formation and sustainment of the turbulent fluctuations fed by the energy fluxes coming from the near-wall production region, see figure 3.1. An unexpected behavior of the energy fluxes comes out from this analysis consisting of spiral-like paths in the combined physical/scale space where the controversial reverse energy cascade plays a central role. The observed behavior conflicts with the classical notion of the Richardson/Kolmogorov energy cascade and may have strong repercussions on both theoretical and modeling approaches to wall-turbulence. To this aim a new relation stating the leading physical processes governing the energy transfer in wall-turbulence is suggested and shown able to capture most of the rich dynamics of the shear dominated region of the flow. Two dynamical processes are identified as driving mechanisms for the fluxes, one in the near wall region and a second one further away from the wall. The former, stronger one is related to the dynamics involved in the near-wall turbulence regeneration cycle. The second suggests an outer self-sustaining mechanism which is asymptotically expected to take place in the log-layer and could explain the debated mixed inner/outer scaling of the near-wall statistics.

3.1 The flow of energy in the augmented space

Wall-bounded turbulence is characterized by several processes which maybe thought as belonging to two different classes: phenomena which occur in

physical space and phenomena which take place in the space of scales. The most significant aspect of the former is the spatial flux of turbulent kinetic energy and of the latter is the energy transfer among scales due to the coupling between eddies of different size. As a consequence, a full understanding of these phenomena requires a detailed description of the processes occurring simultaneously in physical and scale space. In this context, the present section provides a description of the paths the energy takes from the production to the dissipation regions of the augmented space, (r_x, r_y, r_z, Y_c). To this aim, the generalized Kolmogorov equation is used. Formally, the scale-energy budget, 2.22, can be recast in a conservative form as

$$\nabla \cdot \mathbf{\Phi}(\mathbf{r}, Y_c) = \xi(\mathbf{r}, Y_c) \tag{3.1}$$

where $\nabla\cdot$ is the four-dimensional divergence and

$$\xi = 2\langle \delta u \delta v \rangle \left(dU/dy\right)^* - 4\langle \epsilon^* \rangle$$

is the scale-energy source/sink. Equation 3.1 is written in a four dimensional space (r_x, r_y, r_z, Y_c) and involves a four-dimensional vector field,

$$\mathbf{\Phi} = (\Phi_{r_x}, \Phi_{r_y}, \Phi_{r_z}, \Phi_c) \ ,$$

hereafter called the scale-energy hyper-flux. The projection of the hyper-flux in the three-dimensional space of scales will be called the three-dimensional energy transfer vector,

$$\mathbf{\Phi}_r = (\Phi_{r_x}, \Phi_{r_y}, \Phi_{r_z}) = \langle \delta u^2 \delta \mathbf{u} \rangle - 2\nu \nabla_r \langle \delta u^2 \rangle \ .$$

The projection in physical space, a pseudo-scalar for the symmetries of the channel flow, is the spatial energy flux

$$\Phi_c = \langle v^* \delta u^2 \rangle + 2\langle \delta p \delta v \rangle / \rho - \nu / 2 \partial \langle \delta u^2 \rangle / \partial Y_c \ .$$

The conservative form, equation 3.1, allows to appreciate the two kinds of scale-energy fluxes occuring in wall-flows, namely $\mathbf{\Phi}_r$ through the scales of motion and Φ_c in physical space. In classical homogeneous isotropic turbulence, the flux occurs only in the space of scales, is radial and, at inertial separations, quantified by $\Phi_r = -5\langle \delta u_\parallel^3 \rangle / (4r)$. In homogeneous conditions, the source is always negative, $\xi_{hom}(\mathbf{r}) \leq 0$, actually a sink, consistently with the classical notion of Richardson cascade [65]. The energy cascade is initialized at the largest scales by the displacement towards small scales of the energy provided at the largest scales by production at a rate equal to the energy dissipation, i.e. $\xi_{hom}(\mathbf{r}) = 0$ for $r \to \infty$. Then, out of the limit of large

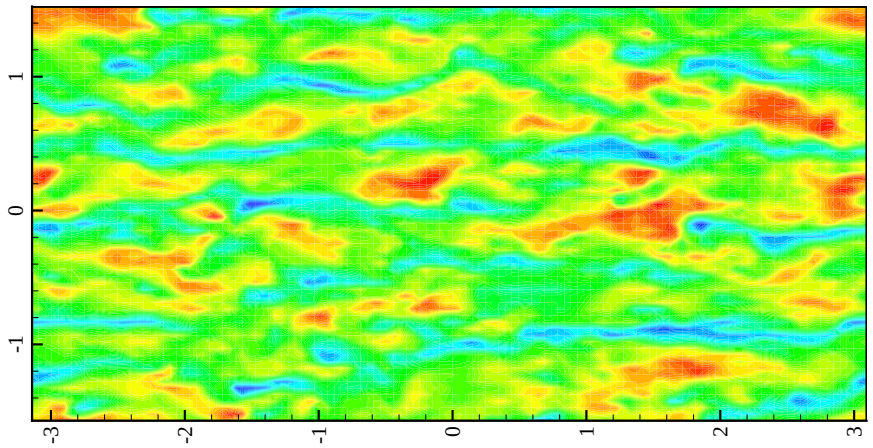

Figure 3.1: Isocontour of the fluctuating streamwise velocity in an horizontal plane parallel to the walls at $Y_c^+ = 60$.

scales, the source term becomes negative, $\xi_{hom}(\mathbf{r}) < 0$, due to the monotonic decrease of the scale-energy production moving to small scales, [6].

In more general cases, when the scale-energy source is positive, production exceeds the energy dissipation rate. As a consequence of the form in divergence of equation 3.1, the regions of the $(\mathbf{r}, Y_c)$-space where $\xi(\mathbf{r}, Y_c) > 0$ can be thought of as the origin of the scale-energy fluxes. This is a distinguishing feature of realistic inhomogeneous flows, where energy production is embedded in the system rather than being provided by an external agent. Indeed, it is well known that, in wall flows, turbulent production exceeds dissipation in the buffer layer leading to an excess of energy, $\langle 1/2u^2 \rangle$, and a spatial energy flux towards both the bulk of the flow and the viscous sub-layer [79]. As we shall see, wall bounded flows are peculiar, since the source is not located at the largest scales, as the paradigm of homogeneous isotropic turbulence leads to believe. This is a very important phenomenon which strongly modifies the scale-energy fluxes pattern of wall-turbulence from those usually observed in homogeneous flows. Equation 3.1 describes an energy fluxes vector field $\mathbf{\Phi}(\mathbf{r}, Y_c)$ where are present both energy source $(\xi(\mathbf{r}, Y_c) > 0)$ and sink $(\xi(\mathbf{r}, Y_c) < 0)$ regions and not only regions of energy sink as in homogeneous flows.

Purpose of the present section is to describe the unexpected paths the scale-energy takes from production to dissipation in the augmented space by

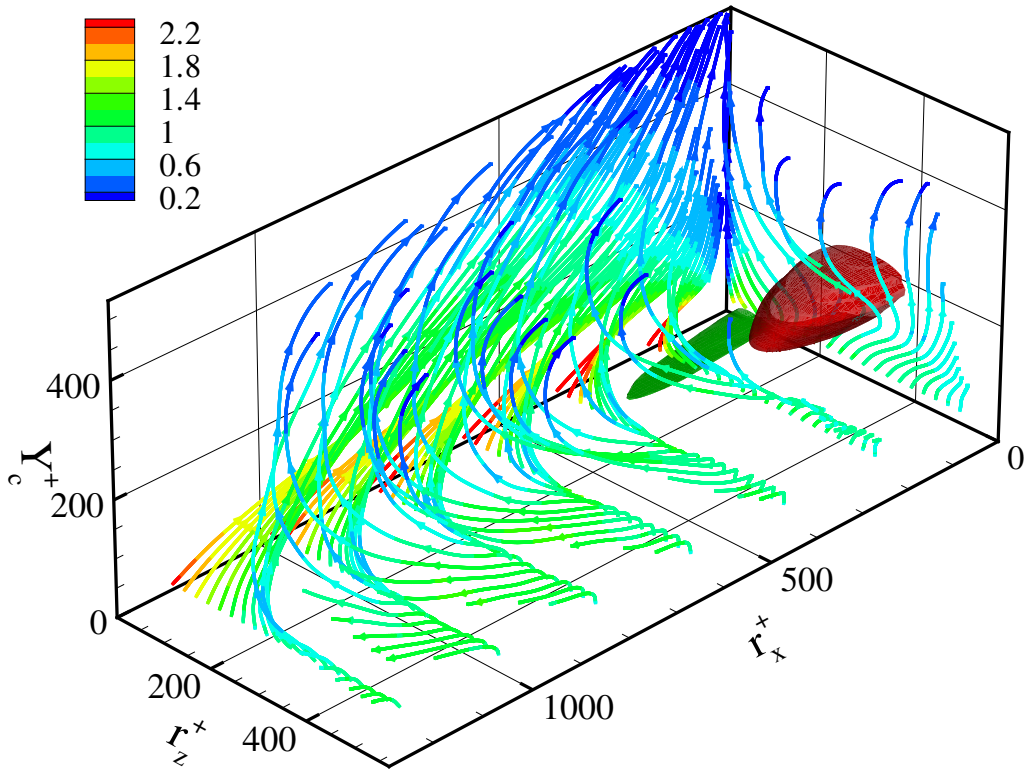

Figure 3.2: (r_x, r_z, Y_c)-projection ($r_y = 0$) of the augmented phase-space. Trajectories of the reduced hyper-flux (inertial component) $(\langle \delta u^2 \delta u \rangle, \langle \delta u^2 \delta w \rangle, \langle \delta u^2 v^* \rangle + 2\langle \delta p \delta v \rangle)$ (colours according to strength). These value are expressed in viscous units, the same convention is used in all the plots of this work. The two iso-surfaces of the energy source $\xi(r_x, r_z, Y_c)$ are selected to show the two local maxima, in the inner ($\xi^+ = 0.42$, green) and outer ($\xi^+ = 0.006$, red) regions, respectively.

addressing the trajectories of the hyper-flux. The data used for the analysis are those of the direct numerical simulation (DNS) of a channel flow at $Re_\tau = u_\tau h/\nu = 550$ reported in chapter 1.

3.1.1 The paths of energy

As established by equation 3.1, the scale-energy hyper-flux is driven by the source ξ. This term reaches its maximum in a range of small scales well within the buffer layer (green isosurface in figure 3.2). As we shall see, this

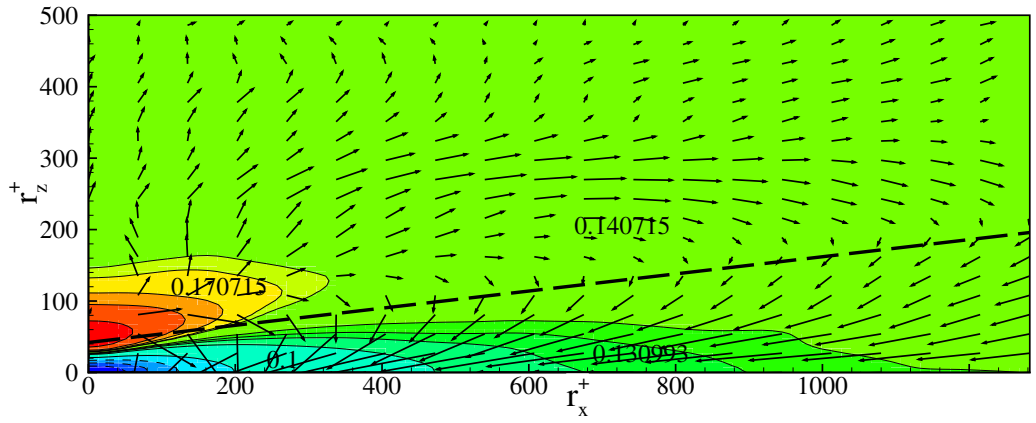

(a)

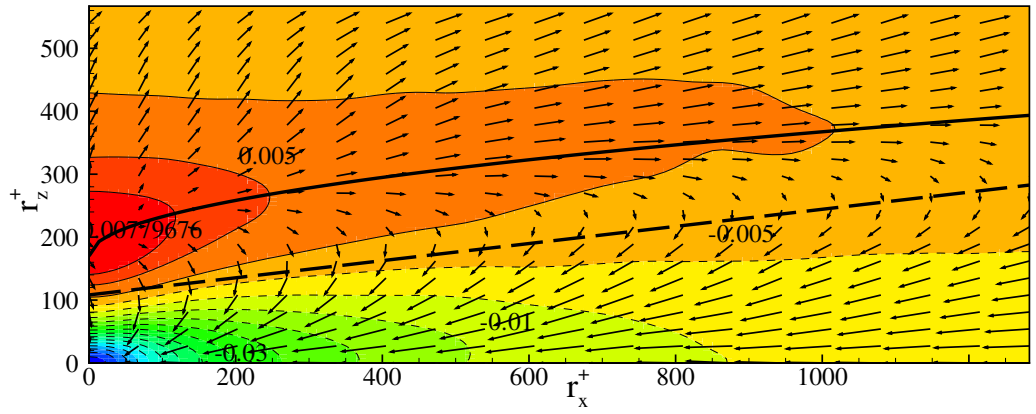

(b)

Figure 3.3: Projection of the reduced inertial hyper-flux and isolines of the energy source in the $Y_c^+ = 20$ (a) and $Y_c^+ = 110$ (b) planes.

region of the augmented space is one of the engines of wall-turbulence, and will be hereafter called the driving scale-range (DSR).

This is an interesting result showing how the classical paradigm of turbulence fails near the wall with the turbulent energy being generated amid the spectrum. The turbulent energy is not introduced at the top of the spectrum and there is not an isotropic recovery since anisotropic production does not decreases moving to small scales. The DSR is associated with a strong anisotropic energy injection at small scales, which leaves a deep footprint on the geometrical properties of the turbulence [7]. The trajectories of the issuing energy fluxes are markedly different from those of the classical theory, see the colored lines in the three-dimensional plot of figure 3.2, where the

colors encode the strength of the flux. As more clearly seen in figure 3.3(a), corresponding to an (r_x, r_z)-plane close to the center of the DSR ($Y_c^+ = 20$), the trajectories diverge from the DSR to feed other regions in the combined physical/scale space, see figure 3.4(b) for an (r_z, Y_c)-cut at $r_x = 0$ through the DSR. The vector field exhibits a spiraling behavior which starts from the buffer layer and diverge feeding longer and wider turbulent structures reaching the outer regions of the flow. Note the combined nature of the paths taken by the scale energy, which loops in the three-dimensional space moving from the DSR towards larger r_x and r_z while ascending towards increasing Y_c. A further distinguishing feature of figure 3.2 is the eventual convergence of the trajectories towards the zero-separation dissipative scales at $r_x = r_z = 0$. The overall picture conforms to a system of ascending spiral-like curves which end up in the small-scale range at different wall-normal positions to be understood as a Y_c-distributed dissipative range (DDR), sink of scale-energy. Overall, the energy transfer systematically takes place towards larger scales (reverse energy cascade) and in the upward direction before eventually bending towards the dissipative range (direct energy cascade). The present view is entirely consistent with the spectral description provided in [17], which however misses the multidimensional nature and the directionality of the process. We like to stress that a multidimensional description is crucial to understand the formation and sustainment of larger fluctuating structures fed by the energy excess in the near wall production region.

Unexpectedly, the phenomenon of the reverse energy cascade plays a central role for the generation of the characteristic long and wide fluctuations of wall-turbulence. As clearly shown by the projections in the space of scales, (r_x, r_z), figure 3.3(a) and (b), the energy fluxes diverge from the region of energy source at small scales and, through a reverse cascade, feed longer and wider fluctuations. Then, following a loop, the fluxes converge in a classical forward energy cascade reaching the region of energy sink (DDR) at the smallest scales where dissipation occurs. The coupling of the reverse energy cascade with the spatial fluxes is the basic element for the formation of the long turbulent fluctuations pattern usually observed in wall-flows from the wall to the core flow, figure 3.1.

In wall-turbulence the energy flux field $\mathbf{\Phi}(\mathbf{r}, Y_c)$ diverges from the energy source regions ($\xi(\mathbf{r}, Y_c) > 0$) and converges to the energy sink regions ($\xi(\mathbf{r}, Y_c) < 0$). This is a prerogative of wall-flows due to inhomogenity while in homogenous turbulence the source term satisfies the constrain $\xi_{hom}(\mathbf{r}) \leq 0$. In analogy with the Gauss's law for gravity and electromagnetism, the field of fluxes change from a monopolo to a dipole pattern. An electric field has sources at positive charges, sinks at negative charges, so electric field lines start at positive charges and end at negative charges potentially form-

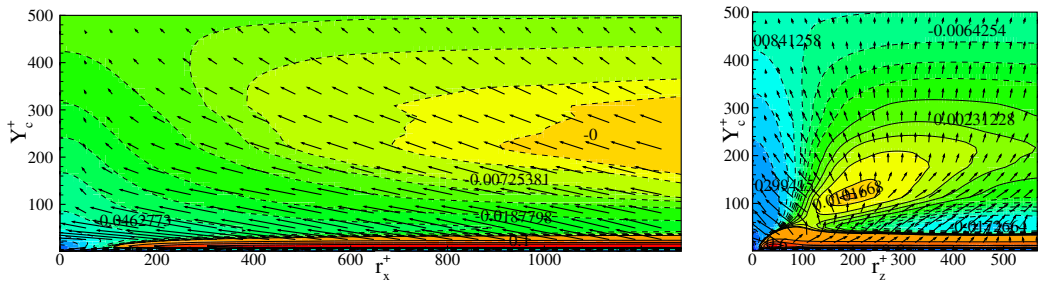

(a) (b)

Figure 3.4: Projection of the reduced inertial hyper-flux and energy source isolines in the $r_z = 0$ (a) and $r_x = 0$ plane (b).

ing closed loops, or extend to or from infinity. A gravitational field has no sources, it has sinks at masses, so gravitational field lines come from infinity and end at masses. The main energy source of the whole $(\mathbf{r}, Y_c)$-space is the DSR which is therefore responsible to feed from the small scales of the buffer layer most of the turbulent fluctuations at different scales and position of the flow.

3.1.2 The near-wall and outer peak of the energy source

The clear matching of scales, $20 < r_z^+ < 70$ for $r_x^+ < 200$, green isosurface in figure 3.2 and the isocontours of figure 3.3(a), actually suggests a strong connection of the DSR with the coherent structures involved in the near-wall cycle, see [66, 23, 33], and more specifically with the quasi-streamwise vortices. In this view, the near-wall cycle corresponds to the energy fluxes loop shown in figure 3.3(a). In particular, the energy source of the DSR can be thought as the scale-energy extracted from the mean flow to generate the quasi-streamwise vortices. A fraction of this energy is directly cascading down to small scales and dissipated, see 3.3(a). This phenomenon can be thought as the result of the bursting of these structures due to instability. The remaining fraction of energy is transfered to feed, through a reverse cascade, the streamwise velocity streaks, see 3.3(a). This phenomenon can be thought as the result of the interaction of the streamwise vortices with the mean shear. In the end, the energy associated to the streaks is cascading down to the smallest scales through a classical forward cascade and dissipated, see 3.3(a). This phenomenon can be thought as the result of the bursting of the streaks due to instability.

An amazing feature emerging from the present analysis is the existence of a rescaled replica of the processes described so far, associated with a

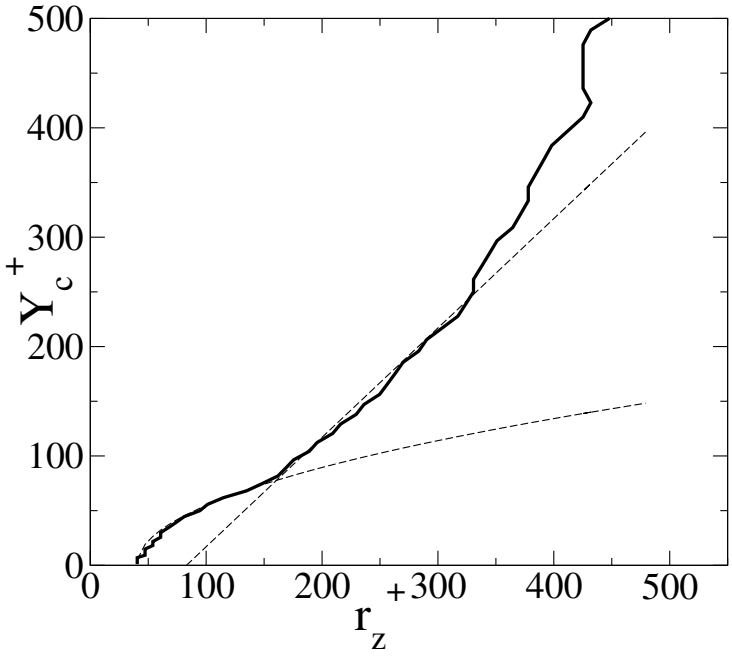

Figure 3.5: Locus of the energy source (ξ) maxima in the $r_x = 0$ plane.

second peak in the energy source, see the red isosurface displayed in figure 3.2. Still the energy loops in the augmented space, see figure 3.3(b) for a cut through the second peak, suggesting a dynamics pretty similar to that described for the DSR. As shown in figure 3.4(a) and 3.4(e), the region of excess production ($\xi > 0$) extends up to $Y_c^+ \approx 300$, though its intensity is substantially smaller than for the DSR. This second peak is presumably related to the outer mechanism reported in [34, 28] which has been shown to be self-sustaining [29]. For this particular simulation, this peak occurs at a spanwise scale of $0.36h$ which corresponds to the spanwise extension of the vortical structures reported in [28].

At given wall-distance the source maximum occurs for $r_x = 0$. Its location in the (r_z, Y_c)-plane, reported in figure 3.5, defines the typical spanwise scale of the energy source ξ. We recall the physical interpretation of the scale-energy source, which is especially clear for $r_x = 0$. A part from the base value provided by the Y_c dependent energy dissipation rate, the source is the correlation between streamwise and wall-normal velocity increments times the local average shear rate. Restricted to $r_x = 0$, this quantity is directly related to the spanwise co-spectrum which provides the spectral decomposition of the Reynolds stresses $-\langle uv \rangle$ responsible for turbulent production in the sense of Townsend's view [79]. We may regard the spanwise location of

the maxima as the typical dimension of the fluctuating motions which contribute more effectively to the build up of the Reynolds stresses. Near the wall, $Y_c^+ < 80$, this length scale increases quadratically, $r_z^+ \approx 35 + 0.02 Y_c^{+2}$, and keeps a finite value at the wall while the intensity of the maximum becomes vanishingly small. This is the region where the DSR occurs. Actually comparing figure 3.5 and 3.4(b), it is clear that within the DSR, $Y_c^+ < 30$, the length scale stays almost constant. This behavior would have been described in Townsend's terms as detached, i.e. independent of wall normal position, as opposed to attached meaning increasing linearly with wall distance. The detached nature of the structures involved in the near-wall cycle underlines that these structures feel the presence of the wall only indirectly and, therefore, behave more or less as in free shear flow. Since the spanwise extension is larger than twice the wall-distance, the cross-plane appereance of these eddies should be a swirling motion compressed in the wall-normal direction.

Moving away from the wall, a second behavior abruptly takes over for $100 < Y_c^+ < 0.4 Re_\tau$. In this region the single-point turbulent production roughly equals the energy dissipation, i.e. this is a putative equilibrium layer that would eventually develop into the log-layer expected to exist at extremely large Reynolds number. Here the spanwise scale of the energy source is to a very good degree linear with Y_c, $r_z^+ \approx 80 + Y_c^+$. This observation suggests that the turbulent production in this region would be related to the phenomenology proposed by Townsend [79] of active motion of attached eddies, where the attached eddies are considered as the maximal detached ones which are carrying Reynolds stresses. A further observation supports this statement. At given wall normal location, a definite correlation emerges in the (r_x, r_z)-planes between spanwise and streamwise scales, fitted to reasonable accuracy by a square-root law, $r_z \propto (r_x)^{1/2}$, solid line figure 3.3(b). This trend is actually similar to that reported in [34] for the spectral distribution of the Reynolds stress again in a context of active motion of attached eddies. Here, from the scalings we are observing, we clearly perceive that the outer peak of ξ is the result of a regeneration mechanism involving systems of attached eddies whose action should increase as the extent of the logarithmic layer with the Reynolds number. Establishing whether it scales in external units exceeds the computational power we have available. If confirmed, its presence could lead to clarify the influence of the external region on the inner layer and help setting the controversy concerning the mixed (inner/outer) scaling of certain observables, like energy spectrum and streamwise fluctuation intensity. Indeed, even if with the present data, the outer peak is very small compared to the near-wall peak, and, therefore the scale-energy fluxes are exclusively driven by the DSR, it is expected that for larger Reynolds

number the outer peak should increase its value modifying the scale-energy fluxes pattern up to the wall. For that reason this outer cycle should be able to actively modulate the generation of near-wall scales more and more increasing the Reynolds number. Whereas, the near-wall cycle related with the DSR should scale in inner variable and, therefore, should lead to the same energy source peak and energy fluxes pattern for different Reynolds number.

3.1.3 A reduced model of energy transfer

The scale-energy fluxes pattern shown in this section moves far away from those expected by the classical theory on turbulence such as the Kolmogorov cascade. Even if the Kolmogorov phenomenology is claimed to be universal for any flow at sufficiently high Reynolds number, does not extend to wall-turbulence for two reason. First, the expected isotropy recovery at small scales is not verified. The anisotropic energy production continuously inject energy at all scales even exhibiting a peak at small scales such as in the DSR. Therefore, the energy transfer is initialized at that small scales and not as commonly expected in the top of the spectrum. Second, this energy injection could exceed the rate of dissipation leading to regions of energy source, $\xi > 0$. Therefore, the energy transfer which is initialized at small scales, diverges, since $\xi > 0$, feeding both larger and smaller scales. The resulting unexpected paths taken by the scale energy flux in the combined physical-scale space may have huge repercussions on our theoretical understanding of wall-turbulence, with practical consequences for turbulence modeling. Let us try to grasp the essential aspects. At inertial scales the significant effects come from the transfer through the scales and from the spatial flux, $\partial\langle\delta u^2\delta u_i\rangle/\partial r_i + \partial\langle v^*\delta u^2\rangle/\partial Y_c \simeq \xi(\mathbf{r}, Y_c)$. Our numerical results show that the term $\partial\langle v^*\delta u^2\rangle/\partial Y_c$ at inertial separations is weakly dependent of the scales, see the scale-by-scale budgets shown in section 3.2, hence the inertial budget takes the simplified form

$$\frac{\partial\langle\delta u^2\delta u_i\rangle}{\partial r_i} = -\left[2\langle\delta u\delta v\rangle\left(\frac{dU}{dy}\right)^* + 4C(Y_c)\langle\epsilon^*\rangle\right], \tag{3.2}$$

where the multiplicative constant $C(Y_c)$ models the local scale-energy accumulation/release from/to the spatial fluxes. Given its weak scale-dependence, this process simply adds/subtracts energy for a fraction of the local energy dissipation rate. As shown in figure 3.6, $C(Y_c)$ increases the effective local energy dissipation in the whole flow except in the buffer layer. Indeed, the spatial flux redistributes the energy generated in the production region to the other region of the flow. For $Y_c^+ < 300$, the scatter of the points reported

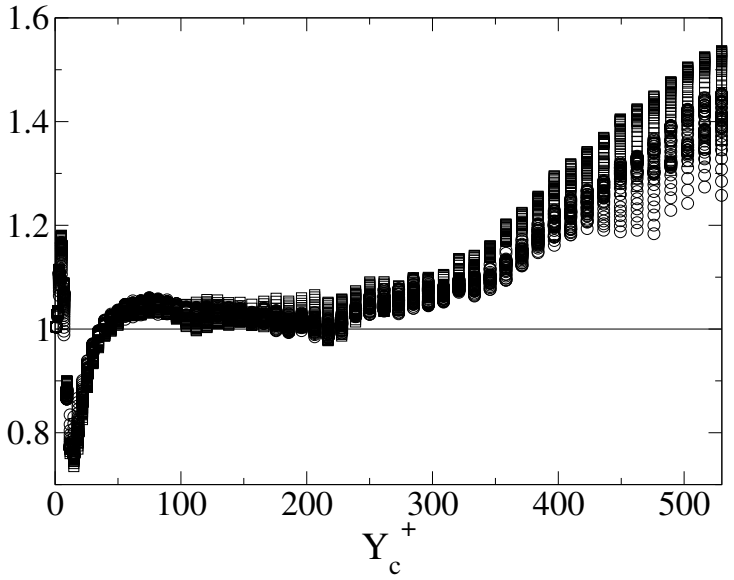

Figure 3.6: Y_c-behaviour of the model coefficient $C(Y_c)$ evaluated as $C(Y_c) = 1 + (\partial\langle v^*\delta u^2\rangle/\partial Y_c)/4\langle\epsilon^*\rangle$ for different streamwise and spanwise scales at inertial separation, i.e. for $(r_x^+ > 60, 0, 0)$ (circle) and $(0, 0, r_z^+ > 60)$ (square).

in figure 3.6 sustains the assumption made of a weak scale-dependence of the process of spatial flux. To note that for a wide range of wall-distance, $50 < Y_c^+ < 300$, $C(y)$ is constant and close to the unity. In this putative equilibrium region, the spatial flux is dynamically ineffective indipendently on the scale considered. The energy coming from the wall traverses this region to feed the core flow without interfere with the local dynamics. The spatial flux not adds/subtracts energy from this region. On the other hand, in the core flow, $C(Y_c)$ increases and shows a wide scatter highlighting a non negligble scale-dependence. For this reason, the reduced description 3.2 is inappropriate for the core region where production vanishes and the energy entirely comes from the spatial fluxes which are focalized on the large scales by the spiral-like behavior of the hyper-flux. This leads to recover in the bulk the classical picture of a small-scale equilibrium range as described by the Kolmogorov law, $\partial\langle\delta u^2\delta u_i\rangle/\partial r_i = -4\langle\epsilon^*\rangle$.

As shown in figure 3.7, the new relation 3.2 captures the physics of the shear dominated region of wall-turbulence away from the viscous sub-layer, where it reproduces the switch between source-like and sink-like scales which induces oppositely signed divergence of the scale-energy flux. Therefore, equation 3.2 reproduces both the forward and reverse cascade occurring si-

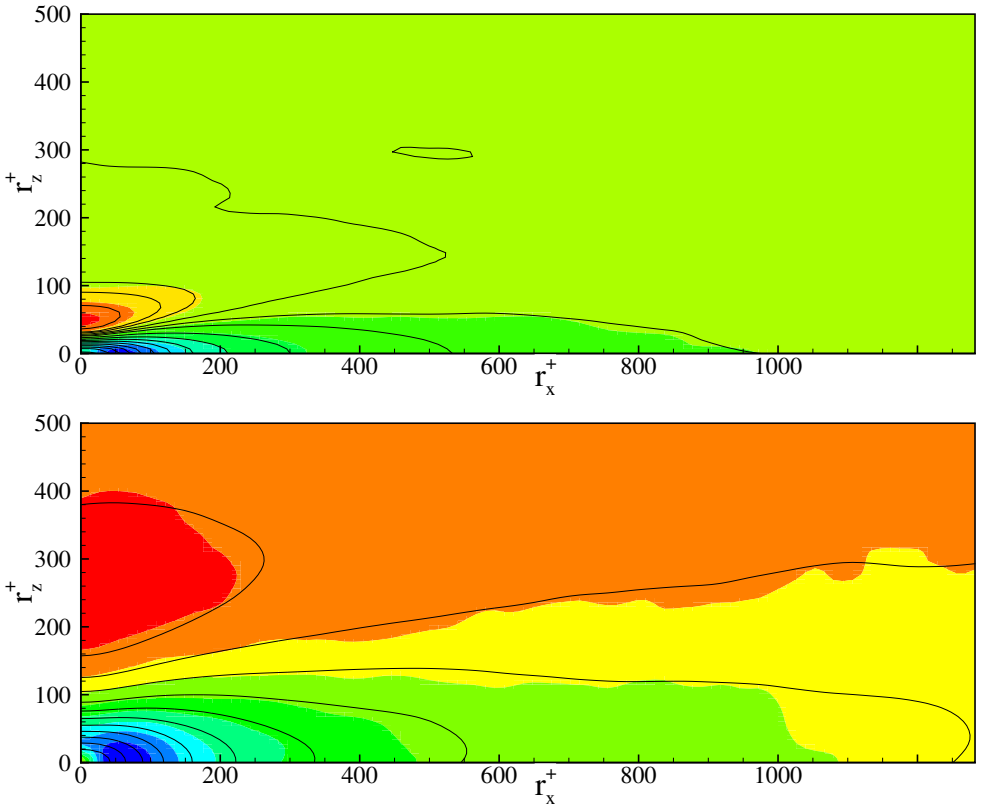

Figure 3.7: Scale-divergence of the inertial energy scale-transfer, $\partial\langle\delta u^2\delta u_i\rangle/\partial r_i$, (colors) and its model, equation 3.2, (lines) at $Y_c^+ = 20$ and $Y_c^+ = 150$ ($r_y = 0$), top and bottom panels, respectively.

multaneously in the space of scales of wall-turbulent flows. Let us notice that the range of scales of validity of equation 3.2 has not an upper bound but requires only scales large enough so that, $2\nu\partial\langle\delta u^2\rangle/\partial r_i r_i + \nu\partial^2\langle\delta u^2\rangle/2\partial {Y_c}^2 \ll -4\langle\epsilon\rangle$.

Starting from geophysics, the universal equilibrium range of high Reynolds number turbulence triggered the interest toward Large Eddy Simulation (LES), where the larger scales are directly computed, leaving to sub-grid stresses the duty to account in *almost universal* fashion for the dissipative energy sink. After decades of research efforts the wall region was recognized as extremely elusive. The reason is, as unequivocally shown here in quantitative terms, the focusing of energy generated at intermediate small scales near the wall to feed larger motions farther away from the wall. This leads to overwhelming difficulties for LES, since energy should emerge from nowhere

in the space of scale and position, to drive the quasi-coherent dynamics of the resolved scales. Equation 2.22 is a sound starting point to understand the issue, as its reduced model, equation 3.2, suggests. The augmented space actually matters for the filtering approach to the Navier-Stokes equations and, by addressing velocity increments, the formalism connects strictly to numerics, where derivatives are ratios $\delta u/r$ taken at numerical resolution scale.

In a context of Large Eddy Simulation, the term $\partial\langle\delta u^2\delta u_i\rangle/\partial r_i$ represents the energy transfer from resolved scales (at scales larger than $|\mathbf{r}|$) to subgrid scales (at scales smaller than $|\mathbf{r}|$), namely the so-called subgrid dissipation. Equation 3.2 indicates that this transfer should not be modeled proportional to the rate of dissipation as in a context of Kolmogorov cascade, $\partial\langle\delta u^2\delta u_i\rangle/\partial r_i = -4\langle\epsilon^*\rangle$, but the subgrid production should be also extimated in order to correctly capture the subgrid dissipation and the backward energy transfer of wall-turbulence. As an alternative, a classical LES model based on the Kolmogorov theory could be also considered but only when the subgrid scales lie in the region of the (r_x, r_z)-space where a classical forward energy cascade is recovered. To this aim, it is found that the smallest spanwise scales where the standard forward energy cascade occurs, increase moving to larger streamwise scales following a linear trend, $r_z \propto r_x$, in conjunction with a square-root dependence on the wall-distance, i.e. $r_z^+ = 0.12r_x^+ + 9(Y_c^+)^{1/2}$, dashed line figure 3.3(a) and (b). In this region a standard sub-grid model is expected to capture the physics. Filtering at larger scales, in the reverse energy cascade range, challenges for new models, which could take advantage of the new picture we are delineating with equation 3.2.

3.2 Scale-by-scale budget

As shown in figures 3.8(a) and (b), the istantaneous flow field of a wall-turbulent flow is characterized by turbulent fluctuations which are organized in thin and elongated structures. This strong diretionality leaves a deep anisotropic footprint in the geometrical properties of the turbulent generation mechanisms as shown in figures 3.8(c) and (d). In a statistical sense this anisotropy emerges in the form of energy fluxes loops in the space of scales as shown in the previous section.

In order to quantitatively assess this scenario, in this section a classical scale-by-scale budget is performed. As shown in [54], this procedure gives a rigorous description of the mechanisms through which the turbulent fluctuations are generated and sustained at different scales and wall-distances. In this paper, it was considered a scale-space averaged form which allowed to

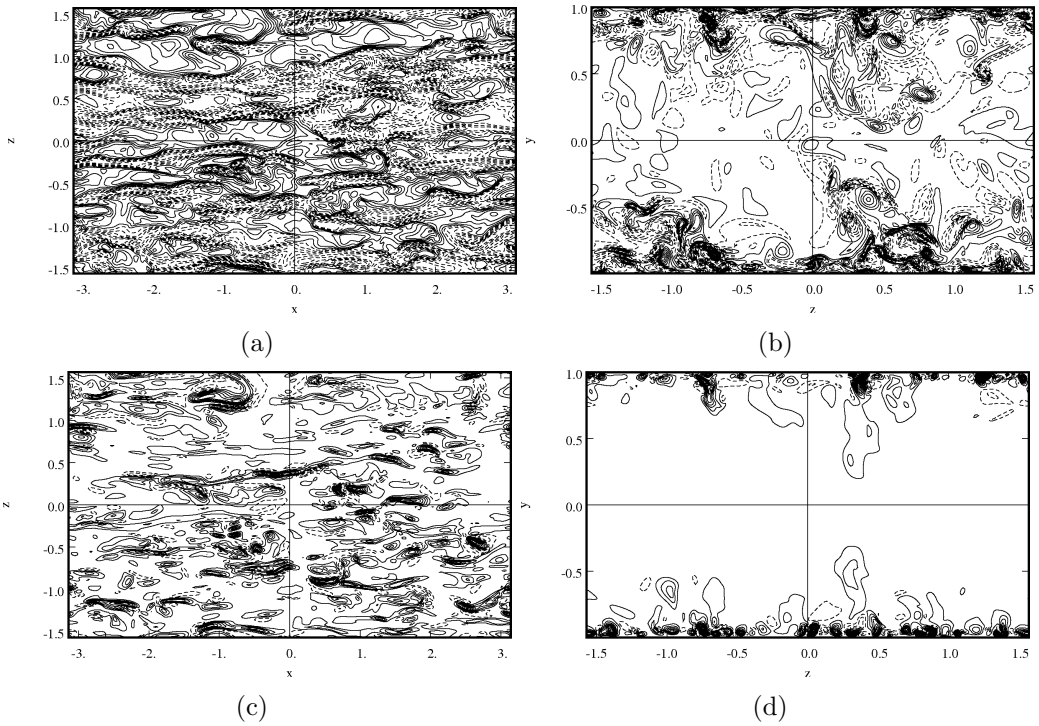

Figure 3.8: Isocontour of the streamwise velocity fluctuations in a xz-plane at $y^+ = 20$ (a) and of the streamwise vorticity, $\omega_x = (\partial w/\partial y - \partial v/\partial z)$ in a yz-plane (b). Isocontour of the istantaneous turbulent production, $uv(dU/dy)$ in a xz-plane at $y^+ = 20$ (c) and in a yz-plane (d).

analyse the different terms of the Kolmogorov equation 2.22 as function of a single scale parameter r. Despite the resulting easier interpretation of the results, the averaging operation in the space of scales hides the directionality of the energy processes which is instead crucial to the understanding of the wall-turbulent physics. For this reason, in this section the scale-by-scale budget will be performed in the $(r_x, 0, 0, Y_c)$ and $(0, 0, r_z, Y_c)$-space separately without any averaging procedure in order to highlight the anisotropic feature of the energy fluxes physics.

According to the analysis in section 3.1, the presence in the spectrum of scales of an excess of scale-energy $\xi(r, Y_c) > 0$ strongly modifies the scale-energy fluxes pattern of wall-flows from those usually observed and predicted in isotropic and homogeneous shear turbulence. In figures 3.9 the energy source ξ it is shown as function of the wall-distance at different streamwise (a) and spanwise (b) scales. Both plots highlight the buffer layer as the turbulent energy source region of wall-turbulence at the present moderate

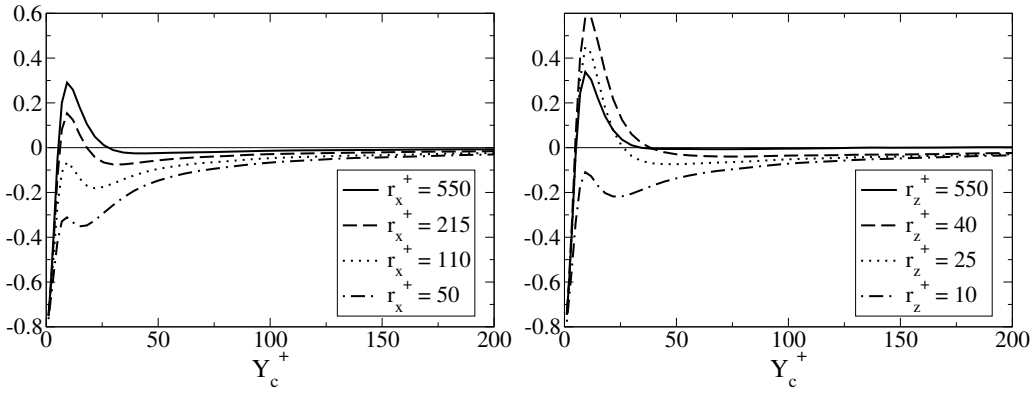

(a) (b)

Figure 3.9: Y-behaviour of the source term ξ for different streamwise (a) and spanwise (b) scales.

Reynolds number. Indeed, ξ reaches a positive value only in the buffer layer, while it is negative in the other regions of the flow which therefore are energy sink regions. However, the relevance of the energy source change depending on the specific streamwise and spanwise scales considered. As shown in figure 3.9(a), the scale-energy excess in the streamwise scales, $\xi(r_x, Y_c) > 0$, occurs only at the larger scales of the buffer layer. The anisotropic energy injection shows a monotonical decrease from large to small scales at all wall-distances. Whereas, in the spanwise scales, figure 3.9(b), the scale-energy excess occurring in the buffer layer is stronger and does not decrease at small scales. Indeed, the anisotropic energy injection increases from the largest to small scales reaching a maximum at scales $r_z^+ \approx 35$ (the center of the DSR) and then decreases up to approach a negative value at smaller and smaller scales. In order to higlight the completely different behaviour in the streamwise and spanwise scales note that the excess of scale-energy for small spanwise scales, as for $r_z^+ = 25$, is greater than the maximum occurring in the streamwise scales for $r_x^+ = 550$. Furthermore, in the streamwise scales a scale-energy lack, $\xi(r_x, Y_c) < 0$, can be observed already for scales $r_x^+ = 110$, while in the spanwise scales the scale-energy lack, $\xi(r_z, Y_c) < 0$, occurs only for very small scales as for $r_z^+ = 10$. The overall picture is the presence of a turbulent production region, the buffer layer, which is the main source of turbulent fluctuations in wall-turbulence at moderate Reynolds number. The unexpected result is the location of this energy source region in the space of scales. The anisotropic processes responsible for the generation of turbulent fluctuations are not located at large scales as in the classical concept of turbulence but amid the spectrum of scales.

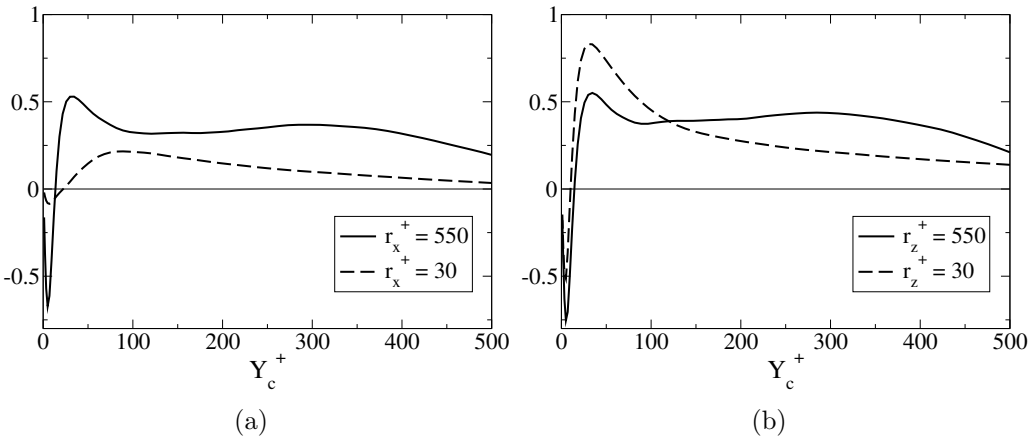

(a) (b)

Figure 3.10: Y-behaviour of the spatial flux Φ_c for different streamwise (a) and spanwise (b) scales.

Let us now consider the inhomogeneity of the flow. In figures 3.10 the spatial flux Φ_c is shown as function of the wall-distance at different streamwise (a) and spanwise (b) scales. In both plots it is possible to identify two regions, in which the flux is either positive, i.e. transfers energy towards the bulk of the flow, or negative, i.e. it is directed towards the wall. The energy source in the buffer layer is transferred via spatial flux to sustain the turbulence in the other regions of the flow. The absolute value of the spatial flux, $|\Phi_c|$, reaches a maximum between the buffer layer and both the log-layer and the viscous sublayer and then decreases both towards the wall and the channel center. This decrease implies that the scale-energy carried by the flux is progressively released to the turbulent fluctuations. This decrease is limited in the log-layer where the flux manifests a trend to form a plateau at large streamwise and spanwise scales. Asimptotically, as the Reynolds number is increased, Φ_c is known to approach a constant value in the log-layer [37]. As a consequence, the log-layer should be asymptotically traversed by an almost constant flux of energy, meaning that it does not need a replenishment of energy by the action of spatial flux, which does not interfere with the local dynamics.

Let us now consider the scale-space distribution of the inhomogeneous spatial flux. The importance of this process change for different streamwise and spanwise scales depending on the pattern the energy source ξ takes, see figures 3.9. In the spanwise scales, the inhomogeneous energy redistribution, $\Phi_c(r_z, Y_c)$, is larger at small scales than at large ones, see figure 3.10(b). Indeed, a larger amount of energy is available to be transferred at the small spanwise scales of the buffer layer than at the larger ones, see the behaviour

of ξ in the spanwise scales of the buffer layer in figure 3.9(b). Whereas, in the streamwise scales the spatial flux $\Phi_c(r_x, Y_c)$ classically decreases from large to small scales, see figure 3.10(a). Indeed, the same behaviour is observed for the energy source ξ in the streamwise scales of the buffer layer, figure 3.9(a).

In conclusion, in the classical notion of turbulence, the anisotropic energy injection and inhomogeneous fluxes are placed at large scales and an isotropy recovery occurs at small scales. The point here is that this picture fails in wall turbulence. The anisotropic and inhomogeneous processes does not show a decrease moving to small scales but concentrate deep inside the spanwise spectrum of scales. There is not a classical isotropy recovery. This scenario can be highlighted only with a multidimensional analysis and for that reason in the following sections a scale-by-scale analysis is performed in the $(r_x, 0, 0, |Y_c)$ and $(0, 0, r_z, |Y_c)$-space separately at two relevant distances from the wall, in the buffer and logarithmic layer, greatly extending the physical understanding obtained with a similar approach in [54].

3.2.1 The logarithmic layer

The scale-by-scale budget in the log-layer is shown in figures 3.11(a) and (b). At this location, the streamwise energy processes are characterized by a production of turbulent fluctuations at large scales, see figure 3.11(a). This production range is followed by a range dominated by the inertial energy cascade which is closed by diffusion at viscous scales. The energy cascade term, $-\partial\langle\delta u^2 \delta u_i\rangle/\partial r_i$, is always positive as the classical concept of the energy cascade, relation 2.19, leads to believe. Generally speaking, the classical picture of turbulence holds in the streamwise scales of the log-layer. The scale-energy is introduced at the largest scales by turbulent production and then is transferred to small scales by energy cascade and in the end is diffused by viscous forces. The dynamics of the log-layer in the streamwise spectrum reproduce the conditions of a locally homogeneous shear turbulence [6]. The only difference is the almost constant spatial flux of scale-energy which traverse the spectrum of scales to reach the bulk region of the flow. However, the divergence of this turbulent flux is sufficiently small in comparison with the other terms of the scale-by-scale budget to be dynamically ineffective, see 3.11(a).

At the same wall-distance, the scale-by-scale budget in the spanwise scales is characterized by a large-scale production range followed by an inertial energy cascade range and finally by a viscous diffusion range, see 3.11(b). Even if a classical picture of turbulence as those in the streamwise scales seems to occurs, the action of the scale-energy production is stronger and significantly acts at smaller scales. The energy injection leads to an excess of scale-energy, $\xi(r_z, Y_c) > 0$ (grey region of figure 3.11(b)), for scales $100 <$

$r_z^+ < 600$. Unexpectedly, even if the log-layer is a putative equilibrium layer where production and dissipation balance, there are regions in the space of scales where production still exceeds dissipation such as in the spanwise spectrum, leading to an energy source. As also suggested by the reduced model 3.2, this energy source, $\xi > 0$, is responsible for a positive divergence of the energy cascade, $-\partial\langle\delta u^2\delta u_i\rangle/\partial r_i < 0$, which means that both larger and smaller scales are fed by the inertial energy transfer. This range is the local origin of a scale-energy fluxes loop reported in figure 3.3(b), and, therefore, for the reverse energy cascade at these wall-distances.

Finally, it is important to note that the assumption of the reduced model 3.2 of a weakly dependence of the rate of spatial flux on the scales considered is verified at this wall-distance for scales sufficiently large so that $2\nu\partial\langle\delta u^2\rangle/\partial r_i r_i + \nu\partial^2\langle\delta u^2\rangle/2\partial {Y_c}^2 \ll -4\langle\epsilon\rangle$, see figures 3.11(a) and (b). In particular, in this region the divergence of the turbulent spatial flux is very small and, therefore, $C \approx 1$. Accordingly to the reduced model 3.2, this means that $\partial\langle\delta u^2\delta u_i\rangle/\partial r_i \approx \xi$. Indeed, the correspondence between $\xi > 0$ and $-\partial\langle\delta u^2\delta u_i\rangle/\partial r_i < 0$ is remarkable.

3.2.2 The buffer layer

Moving towards the wall, in the buffer layer, shown in figures 3.11(c) and (d), an excess of scale-energy, $\xi > 0$, appears also in the streamwise scales for scales $r_x^+ > 250$, the grey region in figure 3.11(c). Apart the phenomenon of the energy source, the turbulent dynamics in the streamwise spectrum of the buffer layer follow the classical picture of turbulence. The energy is provided at large scales and then is transferred to small scales and diffused by viscous forces. The energy source, ξ, manifests a monotonical decrease moving towards small scales. For this reason, a direct forward energy cascade takes place since displaces the energy, mostly provided at the large scales, towards the small ones. In the streamwise scales, the energy excess, $\xi > 0$, results only in the positive divergence of the spatial fluxes, $-\partial\langle v^*\delta u^2\rangle/\partial Y_c < 0$, which diverge in the buffer layer to feed both the near-wall and outer regions of the flow.

The most striking phenomenon of the buffer layer appears in the spanwise spectrum. In these scales the phenomenon of energy injection via turbulent production and the resulting scale-energy excess is more pronounced and acts at smaller and smaller scales. A very pronounced peak of scale-energy production occurs at small spanwise scales, $r_z^+ \approx 50$, see 3.11(d). Instead of what is commonly expected, the larger energy injection occurs at small scales than in the large ones. The anisotropic production does not show a monotonic decrease moving to small scales as in the streamwise spectrum, figure 3.11(c).

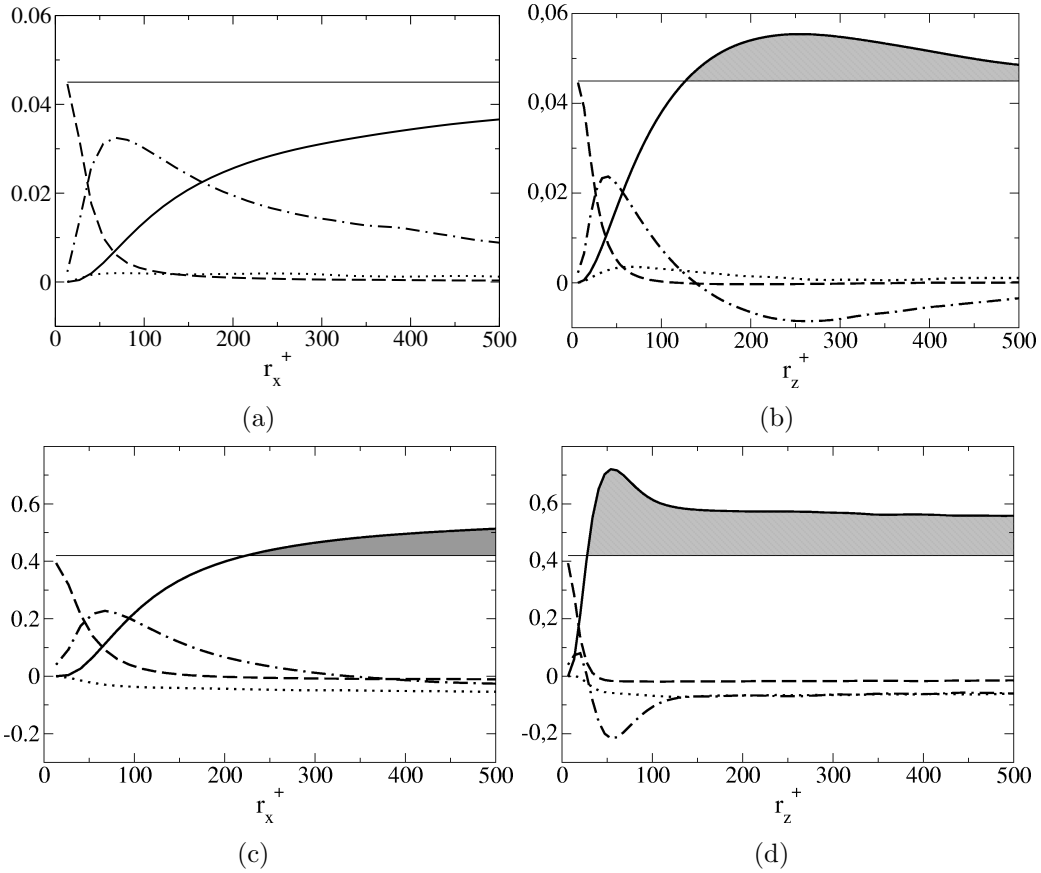

Figure 3.11: Scale-by-scale budget 2.22: turbulent production $-2\langle\delta u\delta v\rangle\,(dU/dy)^*$ (solid line), inertial rate of energy transfer $-\partial\langle\delta u^2\delta u_i\rangle/\partial r_i$ (dashed-dotted line), inertial rate of spatial flux $-\partial\langle v^*\delta u^2\rangle/\partial Y_c$ (dotted line), viscous diffusion rate $2\nu\partial^2\langle\delta u^2\rangle/\partial r_i\partial r_i(r_x,0,0,|Y_c)$ (dashed line) and dissipation $4\langle\epsilon^*\rangle$ (thin horizontal solid line). $(r_x,0,0,Y_c^+=160)$ (a); $(0,0,r_z,Y_c^+=160)$ (b); $(r_x,0,0,Y_c^+=20)$ (c); $(0,0,r_z,Y_c^+=20)$ (d). The grey regions highlight the energy source regions, $\xi>0$.

As suggested by the reduced model 3.2, this peak leads to a large peak of positive divergence of the inertial energy transfer, $\partial\langle\delta u^2\delta u_i\rangle/\partial r_i = max$, at small spanwise scales, which can be also graphically appreaciate in figure 3.3(a).

This range of spanwise scales, $30 < r_z^+ < 70$, previously called driving scale-range (DSR), is the leading source of scale-energy fluxes in wall-turbulence. In this scenario, the controversial reverse energy cascade is due

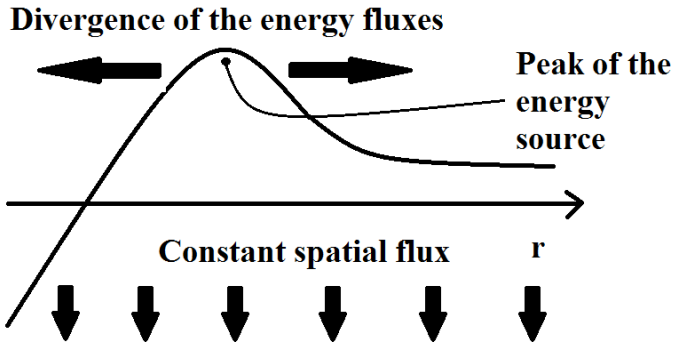

Figure 3.12: Sketch of the energy fluxes diverging from the peak of energy source ξ.

to the location of this energy source region (DSR) at small scales. The failure of the classical picture of turbulence in wall-flows, as described by the Kolmogorov theory, is the assumption that the energy is provided at the largest scales of motion. Indeed, this is the only one assumption that allows to expect a recovery of an inertial equilibrium range at small scales where the energy production/diffusion is negligible and the scale-energy is transfered from large to small scales at a constant rate proportional to the local energy dissipation, i.e. $\partial\langle\delta u^2\delta u_i\rangle/\partial r_i = -4\langle\epsilon\rangle$. In wall-turbulence the energy is provided deep inside the spectrum of scales. Furthermore, this energy injection exceeds dissipation, $\xi > 0$, leading to a positive divergence of the energy fluxes and, therefore, also to an opposite energy transfer mechanism, the reverse energy cascade, as sketched in figure 3.12.

Finally, it is important to note that the assumption used in the reduced model 3.2 of a weakly dependence of the rate of spatial flux on the scales considered is verified also at this wall-distance for scales sufficiently large so that $2\nu\partial\langle\delta u^2\rangle/\partial r_i r_i + \nu\partial^2\langle\delta u^2\rangle/2\partial {Y_c}^2 \ll -4\langle\epsilon\rangle$, see figures 3.11(c) and (d). In this region the divergence of the turbulent spatial flux cannot be neglected as in the log-layer. Indeed, the buffer layer is the region of the flow which mostly release energy to feed the turbulence in the other regions of the flow.

3.2.3 The characteristic scales of wall-turbulence

This scenario has a strong repercussion on the modelistic approach of wall-turbulence expecially in a context of Large Eddy Simulation where the concept of equilibrium range in the space of scales is widely used as basic inspiration for the development of LES models. In a LES context, the filter length

and the turbulence model physics are two aspects which are strongly coupled for the correct simulation of a turbulent field. Indeed, depending on the physical processes removed by the filtering operation, a certain LES model may gives or not good results. Therefore, it is very important to characterize the various regions of the combined scale/physical space where the relevant physical processes of wall-turbulence take place. This characterization will be shown instrumental for the analysis of the filtered dynamics examined in the next chapter 4.

In order to highlight the anisotropic nature of wall-turbulence, we identify the various regions of the $(r_x^+, 0, 0, Y_c^+)$ and $(0, 0, r_z^+, Y_c^+)$-plane separately where the relevant processes take place. Firstly the curve $l_{c_i}(Y_c)$ splits the space of scales into an inertial range at small r_i from a production dominated range at large r_i. This scale, identified as $\partial\langle\delta u^2\delta u_i\rangle/\partial r_i(l_{c_i}, Y_c) = -2\langle\delta u\delta v\rangle\left(dU/dy\right)^*(l_{c_i}, Y_c)$, is dimensionally related to the shear scale $L_s = \sqrt{\epsilon/|S^3|}$ which is found crucial for the small scale isotropy recovery [7] and for the subgrid stresses modelization [21]. According to the classical equilibrium theory for the log-layer, these scales, L_s and l_{c_i}, should behave linearly with the wall-distance, i.e. $L_s^+(Y_c^+) \approx l_{c_i}^+(Y_c^+) \approx kY_c^+$. Due to the assumption of isotropy made in this dimensional analysis, both the cross-over scales in the streamwise and spanwise spectrum should assume the same value and decrease linearly moving towards the wall. The cross-over scales l_{c_i} as function of the wall-distance are reported in figure 4.14. As expected, both l_{c_x} and l_{c_z} show a decrease moving towards the wall but they assume a very different values highlighting a strong anisotropic character of wall-turbulence. The smaller value of l_{c_z} with respect to l_{c_x} suggest that turbulent production in the spanwise scales is more effective even at very small scales. The value of these scales compared with the filter lenght will be shown foundamental for the understanding of the filtered dynamics shown in chapter 4.

Another important region which characterize the various regions of the combined scale/physical space where the relevant physical processes of wall-turbulence take place is the plane Ω_{E_i} of the (r_i, Y_c)-space where the energy cascade term changes sign, $-\partial\langle\delta u^2\delta u_i\rangle/\partial r_i < 0$. As previously shown, the presence of this region differentiates wall-turbulence from homogeneous turbulence where $-\partial\langle\delta u^2\delta u_i\rangle/\partial r_i$ is always positive since there are no energy source regions, $\xi_{hom} < 0$. This region, once integrated in the space of scales, is responsible for the reverse energy cascade and therefore will be hereafter referred to this phenomenon. The edge of this region is the scale $l_{E_i}(Y_c)$ which splits the space of scales into a forward cascade at smaller r_i from a reverse cascade at larger r_i. As shown in the previous sections, the positive divergence of the energy fluxes in the space of scales is concentrated in the spanwise scales. Indeed, as shown in figure 4.14, $-\partial\langle\delta u^2\delta u_i\rangle/\partial r_i < 0$ occurs

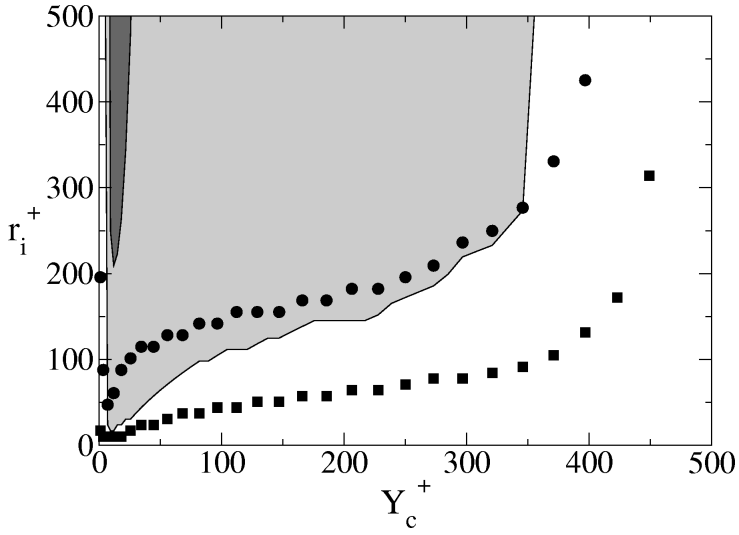

Figure 3.13: The characteristic lenght scales of wall-turbulence. The cross-over scales l_{c_x} (circle), l_{c_z} (square) and the reverse cascade regions Ω_{E_x} (dark grey region), Ω_{E_z} (grey region).

in a wider region up to the smallest scales in the spanwise scales while in the streamwise scales take place only in the buffer layer and for large scales. To note that Ω_{E_z} take place up to $Y_c^+ \approx 350$, meaning that this phenomenon is not confinated at the buffer layer but extend up to the outer flow and then disappears since the energy source for $Y_c^+ > 350$ is always negative, $\xi < 0$.

3.3 Turbulence regeneration cycles and reverse energy cascade

One of the most important features which characterize actual turbulent flows such as wall-bounded flows from the idealized flows such as isotropic turbulence is that the turbulent motion is self-sustained. The generation mechanisms of turbulent fluctations are embedded in the system rather than being provided by an external agent. In contrast with isotropic turbulence which requires a replenishment of the energy dissipated by the viscous forces, in wall-turbulence the turbulent fluctuations autonomously extract energy from the mean flow.

At moderate Reynolds number the main turbulent regeneration mechanisms reside close to the wall in the buffer layer. This is a region of net turbulence production, and there are convincing evidence that it contains well defined structures which interact between them forming self-sustaining cycles

of turbulent energy. Kinematic studies catalogue these structures [66, 81] and the dominant ones are classically referred to streamwise velocity streaks and quasi-streamwise vortices. The former consist of long arrays of alternating streamwise velocity fluctuations and the latter are relatively thin vortices elongated in the streamwise direction. The ciclic mechanism involving these structures starts from the energy extracted from the mean flow by the interaction of the streamwise vortices with the mean shear. In this process the streamwise create alternating streaks of longitudinal velocity fluctuations. These streaks in turn give rise to the vortices with a phenomenon of inflection instability. Due to the inflection occurring increasing downstream distance, the streaks exhibit rapid oscillations followed by a breakdown into finer-scale motions, known as bursting. The wall-turbulence is maintained by this cycle which is local to the near-wall region and can survive without any input from the core flow and for that reason has been called near-wall autonomous cycle [33].

At large Reynolds number flows, recent studies [29] conjecture the presence of a rescaled self-sustaining mechanism similar to the autonomous cycle observed in the buffer layer. This regeneration cycle should take place in the logarithmic region of wall turbulent flows and should verify some aspects of the Townsend's theory of wall-turbulence [79]. These outer dynamics involve large coherent structures corresponding to rescaled replica of the buffer layer structures, i.e. large scale streaks flanked by staggered streamwise swirling motion. In the previous sections, the associated turbulent production has been identified beyond any doubt by the use of the generalized Kolmogorov equation as a result of a mechanism composed by attached eddies. In this case the attached eddies have to be understood as composed by an active core region of swirling motion of dimensions in the cross stream plane $O(Y_c)$ which is responsible for turbulent production.

The overall picture conforms to regeneration cycles where the energy associated to the turbulent fluctuations is extracted from the mean flow by the action of vortices, is transferred toward long fluctuating streaks which in turn displace energy towards small scales with a bursting phenomena which creates the conditions to generate new vortices. The present view is entirely consistent with the behaviour of the energy fluxes reported in the previous sections. The streamwise vortices manifest a well defined spanwise scale where statistically a large part of the turbulent energy is extracted from the mean flow. From this characteristic spanwise length the turbulent energy is transferred to the large streamwise scales statistically referring to the long streaks and then flows down to the small scales classical referring to the statistically occurence of a Richardson cascade where the instability of large eddies generates smaller and smaller eddies.

Figure 3.14: “Adresovat a obrácený kaskáda” (“direct and inverse cascade”): charcoal drawing of Crôzevic Töerbor (1696).

In this view the dynamical processes related to the turbulent regeneration cycles correspond to the loop of energy fluxes in the space of scales of figures 3.3. Forward and reverse energy fluxes coexist in the space of scales highlighting in a statistical point of view the cyclic nature of the turbulent motion in wall-flows, see the picture reported in figure 3.14 which gives an artistic idea of the process. Hence, the reverse energy cascade is an expression of the cyclic self-sustaining mechanisms of wall-turbulence.

It is important to point out the distinguishing features of the back-scatter phenomena commonly adressed in the literature and the reverse cascade we are observing. It is well known that turbulent flows manifest events of energy back-scatter also in globally isotropic and homogenous conditions, [46, 36, 49]. These phenomena are local energy transfer mechanisms where fluctuations at small scales feed larger ones. Within the chaotic processes of

nonlinear interactions of turbulent fluctuations of different size, the energy back-scatter has been shown to occurs very frequently and in an intermittent manner. Despite their importance for the turbulence modeling, the back-scatter events are immersed in a forward energy transfer background and the resulting energy flux is from large to small scales as predicted by the Richardson energy cascade. When dealing with wall-flows, these phenomena become stronger and manifest coherence. As shown in [62], the coherency of the back-scatter events in the near-wall turbulence can be attributed to the dynamics of the turbulent structures involved in the self-sustaining mechanisms of this kind of flows. These back-scatter phenomena result in a net reverse energy flux in wall flows. Evidence of the reverse energy flux was provided in [54] with the analysis of the Kolmogorov equation and in a context of filtered dynamics in [24] with the analysis of the subgrid energy transfer. Both these works highlighted a net energy flux from small scales to larger ones in the buffer layer of wall bounded flows. Here, the multidimensional description of wall-turbulence revealed that this phenomenon is extended to almost all the flow. The reverse cascade systematically takes place at different wall distances forming a part of the energy fluxes loop which result from the cyclic regeneration mechanisms of wall-turbulence.

3.3.1 Practical implications

The present approach to wall turbulence based on the study of the generalized Kolmogorov equation and the resulting findings could be used for a wide range of applications. Here, some examples are suggested in the field of

- turbulence modeling;
- LES simulations of high Reynolds number flows without wall-resolution;
- turbulence control;

which will be handle in future works.

Regarding turbulence modeling, the study of the generalized Kolmogorov equation allows to evaluate the leading physical processes governing the turbulent motion in wall flows. In particular, the assessment of these processes in the augmented space of wall-turbulence actually matters for the filtering approach in the LES simulations as will be shown in the next chapter. Concerning the present findings, the new relation for the energy transfer, equation 3.2, is a clear starting point for the development of new turbulence models.

On the other hand, the unequivocally identification of an outer turbulent regeneration cycle allows to theorize the simulation of infinite Reynolds

number wall-turbulence through LES thecniques without near-wall resolution. Indeed, this outer cycle should increase its action moving to large Reynolds number up to overcomes the effects of the generation mechanisms of the buffer layer. If confirmed, one can expect that the turbulent properties of interest for the applications such as drag and large scale dynamics of the outer flow, should depend only on this outer cycle. The detailed description of these phenomenon given by the generalized Kolmogorov equation should be used to verify the outer scaling of the turbulent production related to this object and, in case, to assess in the augmented space the interactions with the near-wall region adressing the energy fluxes at the interface of these two layers. The clear understanding of these interacting phenomena would help in the LES simulation without near-wall resolution which require appropriate boundary conditions and well-established wall-modeling [61].

Finally, the systematic characterization of the most active range of scales at different wall-distances given by the analysis of the generalized Kolmogorov equation should help setting the control techniques with the aim of drag reduction. Indeed, many attempts to control drag have centred on weakening the turbulent structures involved in the turbulence regeneration mechanisms. Hence, the identification at different wall-distances of the three-dimensional scales statistically emerging as relevant for the turbulent production will be an useful indication for the development of control techniques for drag reduction. Furthermore, the identification of the turbulent energy paths will be also used for the control of the mixing properties of wall-turbulent flows.

Chapter 4

Filtered dynamics

The physical understanding of wall-turbulence gained in the previous chapter will be used in this part of the thesis to understand the filtered wall-turbulent dynamics. The analysis of the filtered velocity field is foundamental in the context of Large Eddy Simulation (LES) where a filtering operation is used and a model is added to the Navier-Stokes equation to account for the effects of the unresolved scales of motion. The analysis of the energy transfer mechanisms in a filtered wall-turbulent flow has been traditionally accomplished via the turbulent kinetic energy balance, as in [24], or via analysis of the energy spectra, as in [17]. Here, in order to adapt the physical insight obtained in the previous chapter, the Kolmogorov equation is applied, for the first time, to a filtered wall-turbulent velocity field. Contrarly to the classical kinetic energy balance and spectral approach, the Kolmogorov equation generalized to filtered wall-turbulence allows to account in a single framework for both spatial fluxes and energy transfer across the scales. The results will show what effects the subgrid scales have on the resolved motion in both physical and scale space, singling out the prominent role of the filter scale compared to the cross-over scale between production dominated scales and inertial range, l_c, and the reverse energy cascade region Ω_B. The systematic characterization of the subgrid stresses physics as function of the filter scale, l_F, and of the wall-distance, Y_c, will be instrumental for a correct use of the LES models in the simulation of wall-turbulence. Finally, we will briefly discuss how the filtered Kolmogorov equation can be used as a new tool for the assessment of LES models and for the development of new ones. As example, some classical purely dissipative eddy viscosity models will be analyzed via an *a priori* procedure.

4.1 Introduction

It is well established that in turbulent flows the energy carrying structures are directly affected by the boundary conditions, hence they are highly non universal and generally anisotropic, while the small scales tend to be more homogeneous and isotropic than the large ones. Therefore, it is thought that relatively simple and universal models can be used to describe the last part of the energy spectrum, when, for example, a Large Eddy Simulation (LES) approach is required for the computation of moderately large Reynolds number flows.

In LES, a low-pass filtering operation is used to decompose the velocity field, $u_i^\star$, into the sum of a filtered (or resolved) component, $\bar{u}_i^\star$, and a residual unresolved component (or subgrid scale motion, SGS), $u_i^{\star sgs}$, see figure 4.1, so that the resulting filtered velocity field can be adequately resolved on a relatively coarse grid and the total velocity field has the decomposition,

$$u_i^\star(\mathbf{x},t) = \bar{u}_i^\star(\mathbf{x},t) + u_i^{\star sgs}(\mathbf{x},t)$$

Once defined the filtering operation, the evolution equation of the filtered velocity field, $\bar{u}_i^\star$, can be obtained by applying this operation to the Navier-Stokes equations yelding to

$$\frac{\partial \bar{u}_i^\star}{\partial x_i} = 0$$

$$\frac{\partial \bar{u}_i^\star}{\partial t} + \frac{\partial \bar{u}_i^\star \bar{u}_j^\star}{\partial x_j} = -\frac{1}{\rho}\frac{\partial \bar{p}^\star}{\partial x_i} + \nu \frac{\partial^2 \bar{u}_i^\star}{\partial x_j^2} - \frac{\partial \tau_{ij}^\star}{\partial x_j} \tag{4.1}$$

where the effects of the small unresolved scales appears in the subgrid stress tensor $\tau_{ij}^\star = \overline{u_i^\star u_j^\star} - \bar{u}_i^\star \bar{u}_j^\star$ which must be modeled. In order to develop subgrid scale models, it is useful to understand the physical phenomena that the models should represent. Arguably, the most important effect of the subgrid scales on the large ones, and the one that the models must represent accurately, is the energy exchange that results from the interaction between resolved and subgrid motion, e.g. see [67]. In this context, most of the commonly used LES models assume that the main role of the subgrid scales is to remove energy from the large resolved motion and dissipate it through the action of a diffusion mechanism analogous to the viscous forces, see [69] and [46]. These assumptions are based on the idea of an inertial range in the spectrum of scales. Indeed, as asserted by the 4/5 law, [40], in the inertial range the energy flux is independent of the scale under consideration, is from large to small scales and it is proportional to the viscous energy dissipation. This picture is claimed to be highly universal. No matter what

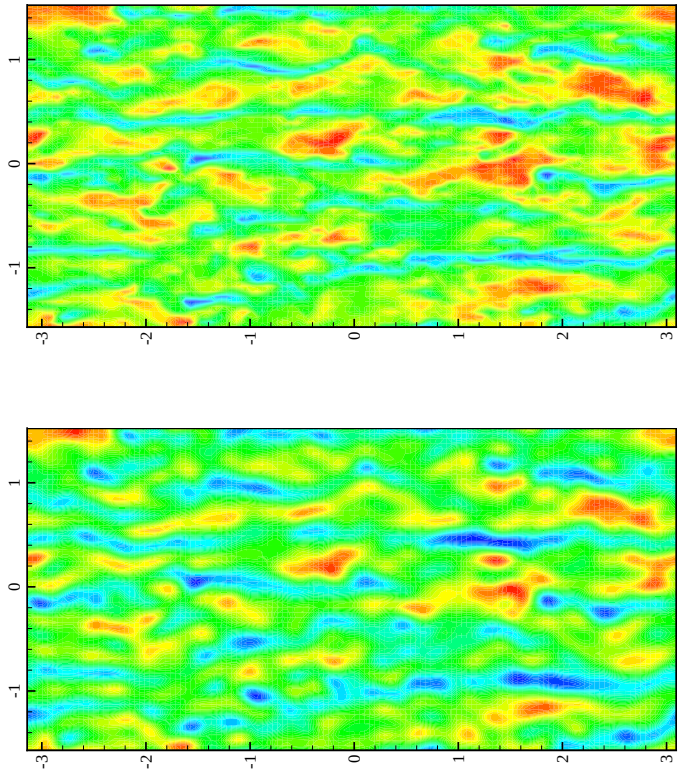

Figure 4.1: Istantaneous isocontours of the fluctuating streamwise velocity field in a wall-parallel plane at $y^+ = 60$ of a turbulent channel flow. Top: unfiltered velocity field. Down: filtered velocity field.

the large scale processes which feed turbulence are, the small scales of large Reynolds number flows are believed to behave according to this scenario and many LES models take inspiration from it. Indeed, in the early attempts, the Kolmogorov energy cascade concept was instrumental in proposing to reproduce the inertial range effects by defining a suitable eddy viscosity, [74] and [51]. On the other hand, the scale-invariance assumption of the inertial range was used both to postulate that the features of the subgrid velocity field are similar to that at large resolved scales, [3], and more recently to develop a dynamic procedure for the evaluation of an improved eddy viscosity coefficient, [22].

This kind of approach has given good results in homogeneous and in unbounded shear flows but less in wall turbulence. In fact, in such flows, as

shown in the previous chapter, the anisotropic turbulent production affects most of the turbulent eddies and the shear is sufficiently strong to hinder isotropy recovery even at small inertial scales, see also [1], [7] and [30]. Beside these observations, the single most striking phenomenon is the complete modification of the Richardson scenario up to a reverse energy cascade in the form of energy fluxes loops shown in chapter 3.

Such a rich scenario has been classically addressed for the assessment of energy exchange between resolved and unresolved scales. As far as these ideas are concerned, we should mention the work of Domaradzky et al. [17] where a spectral analysis of the energy transfer among wavenumbers belonging to the wall-parallel directions was performed for two datasets of confined turbulent flows, i.e. Rayleigh-Benard convection and a channel flow, at moderate Reynolds number. This work considers the instantaneous interscale energy transfer between modes at a given distance from the wall. In order to assess the nonlinear triadic interactions, at the basis of the energy cascade, the spectrum is divided into well defined regions and the transfer between these bands is studied. One of the main findings is that energy transfer processes are mostly between contiguous bands but due to nonlocal interactions and this information should be valuably used when modeling subgrid stresses is addressed. In a complementary way, some issues related to the inhomogeneity of the channel flow are discussed by Härtel et al. [24]. In this contribution the authors analyzed the behavior of the subgrid stresses and their effects on the single-point turbulent kinetic energy balance, highlighting in particular the presence of a backward energy transfer in the buffer layer when a certain value of the cutoff filter is chosen. Similar aspects are also discussed in Piomelli et al. [62], again for a channel flow, where an analysis of the transport equation for the subgrid stresses is performed. Forward and backward subgrid energy transfer is related to the dynamics of the quasi-streamwise vortices which live in the wall region, extrapolated via conditional averages of the velocity field. More in the context of computational issues for LES simulations, Bagget et al. [2] pointed out the importance in identifing the anisotropic dynamics in shear flows. Indeed, in wall bounded flows, the lower bound limit for the size of anisotropic eddies decreases with wall-distance, leading to a large number of degrees of freedom which should be computed explicitly when for example isotropic models are used.

In the present work we intend to extend these ideas by addressing the dynamics of the coupling between the subgrid and resolved scales simultaneously in the physical and scale space. The observed spiral-like behaviour of the energy fluxes and the phenomenon of energy source, shown in chapter 3, will be considered in a context of filtered dynamics and subgrid scale physics. To this aim, an appropriate extension of the Kolmogorov equation to a fil-

tered case, proposed here for the first time, is used adding those related to the subgrid scales to the processes accountable for in the turbulent channel flow. The resulting approach allows for the evaluation of the contributions due to the subgrid terms, at different values of the filter length, for different scales and wall-distances. The analysis enables us to appreciate when subgrid stresses become relevant in the dynamics of the resolved motion and, if this is the case, the physical nature of their action that should be considered when modeling is proposed. In the context of LES modeling, the possibility of using the filtered Kolmogorov equation as a new tool for the assessment of proposed models and for the development of new ones will be outlined. Indeed, as pointed out in [57] for isotropic turbulence, the filtered Kolmogorov equation provides the correct framework to evaluate if the energy transfer rate is correctly reproduced.

The data used for the analysis are those of the direct numerical simulation (DNS) of a channel flow at $Re_\tau = u_\tau h/\nu = 300$ reported in chapter 1. The simulation has been carried out with a resolution in wall units of $\Delta x^+ = \Delta z^+ = 3.64$. This very high resolution, quite unique for a turbulent channel flow, has been chosen, at the expense of the Reynolds number achievable, to capture the phenomena occurring in the dynamics of the velocity field up to the dissipative scale and to better appreciate the alterations taking place in the statistics when the small scales effects are removed by an explicit filtering. The turbulent fields are filtered with respect to the wall-parallel directions only, using a sharp cutoff filter in wavenumber space. Let us notice that such a procedure is quite established for the analysis of the physical behavior of the subgrid scales. In the present work we choose to analyze firstly results for filter lengths from $l_F^+ = 15$ to $l_F^+ = 120$ equal in the two directions parallel to the wall. This choice is aimed to study the effects of the subgrid scales as a function of a single filter parameter, varying with respect to the relevant scales of wall-turbulence. In the end, different filter lenghts in the streamwise and spanwise scales, l_{Fx} and l_{Fz}, will be also analysed to highlight the anisotropic physics of filtered wall-turbulence. However, the analysis presented in the following sections has been performed disregarding the filtering operation in the wall-normal direction. Indeed, in the near-wall resolved LES simulations the required wall-normal resolution cannot be reduced such as in the homogeneous directions and, therefore, we expect a prominent role of the horizontal filter scales.

4.2 The Kolmogorov equation for filtered velocity field

In analogy with equation 2.22, an evolution equation for the filtered second order structure function, $\langle \delta\bar{u}^2 \rangle = \langle \delta\bar{u}_i \delta\bar{u}_i \rangle$, is derived and discussed for the first time. Following the classical Reynolds decomposition, it is possible to derive an evolution equation for the filtered fluctuating velocity field, $\bar{u}_i(\mathbf{x}, t)$. Subtracting this equation written in two different points, $\mathbf{x}$ and $\mathbf{x}'$, it is possible to obtain the evolution equation for the filtered velocity increments, $\delta\bar{u}_i(\mathbf{x}, t)$. This equation, once multiplied by $\delta\bar{u}_i$ and averaged, leads to the generalized Kolmogorov equation specialized for filtered velocity field which under some simplifications due to the symmetries of the channel reads as,

$$\frac{\partial \langle \delta\bar{u}^2 \delta\bar{u}_i \rangle}{\partial r_i} + \frac{\partial \langle \delta\bar{u}^2 \delta U \rangle}{\partial r_x} + 2\langle \delta\bar{u}\delta\bar{v} \rangle \left(\frac{dU}{dy} \right)^* + \frac{\partial \langle \bar{v}^* \delta\bar{u}^2 \rangle}{\partial Y_c} = -4\langle \bar{\epsilon}^* \rangle$$

$$+2\nu \frac{\partial \langle \delta\bar{u}^2 \rangle}{\partial r_i \partial r_i} - \frac{2}{\rho} \frac{\partial \langle \delta\bar{p}\delta\bar{v} \rangle}{\partial Y_c} + \frac{\nu}{2} \frac{\partial^2 \langle \delta\bar{u}^2 \rangle}{\partial {Y_c}^2} - 4\langle \epsilon^*_{sgs} \rangle - 4 \frac{\partial \langle \tau^*_{ij} \delta\bar{u}_i \rangle}{\partial r_j} - \frac{\partial \langle \delta\tau_{i2} \delta\bar{u}_i \rangle}{\partial Y_c}, \quad (4.2)$$

where $\tau_{ij} = \overline{u_i u_j} - \bar{u}_i \bar{u}_j$ are the subgrid stresses, $\bar{\epsilon} = \nu(\partial\bar{u}_i/\partial x_j)(\partial\bar{u}_i/\partial x_j)$ is the resolved viscous pseudo-dissipation, $\epsilon_{sgs} = -\tau_{ij}\bar{S}_{ij}$ is the energy exchange between resolved and subgrid scales usually called *subgrid dissipation* with $\bar{S}_{ij} = 1/2(\partial\bar{u}_i/\partial x_j + \partial\bar{u}_j/\partial x_i)$ the resolved strain-rate tensor and $\langle \cdot \rangle$ stands for average in the homogeneous directions. Let us point out that for this particular choice of the filter $\bar{U} = U$, i.e. there is no alteration of the mean profile.

Equation 4.2 allows for the analysis of how the resolved processes change as function of the filter scale l_F in different regions and scale range and to appreciate the effects of subgrid stresses both in physical and scale space. The three new terms represent the effects of the subgrid stresses on the resolved motion. In particular,

$$-4\langle \epsilon^*_{sgs} \rangle$$

represents the net energy flux between grid and subgrid motion, while

$$-4 \frac{\partial \langle \tau^*_{ij} \delta\bar{u}_i \rangle}{\partial r_j} \qquad \text{and} \qquad - \frac{\partial \langle \delta\tau_{i2} \delta\bar{u}_i \rangle}{\partial Y_c},$$

are the resolved energy displacement in the space of scales and physical space, respectively, due to grid/subgrid nonlinear interactions. At large separations, equation 4.2 approaches an asymptotic behaviour given by the single-point resolved turbulent kinetic energy budget 4.6. For example, the large scale

limit of the resolved energy fluxes among scales and wall-distances due to subgrid stresses, i.e. $-4\partial\langle\tau^*_{ij}\delta\bar{u}_i\rangle/\partial r_j$ and $-\partial\langle\delta\tau_{i2}\delta\bar{u}_i\rangle/\partial Y_c$, approach both with the same value the single-point term of subgrid spatial flux, $-\partial\langle\tau_{i2}\bar{u}_i\rangle/\partial y$, which appears in equation 4.6. Hence, equation 4.6 represents the large scale boundary condition for the corresponding terms in equation 4.2.

In order to highlight the energy processes across scales, it is useful to consider an r-averaged form of equation 4.2. In the case of unbounded flows, the r-average can be performed integrating equation 4.2 over a ball of radius r in the space of scales.[1] Indeed, this procedure allows to identify the transport terms in the space of scales as representative of the energy fluxes,

$$\frac{1}{V_r}\int_{B_r}\nabla_r\cdot\left(\bar{\mathbf{\Phi}}_r+\mathbf{\Phi}_r^{sgs}\right)dV_r=\frac{1}{V_r}\int_{\partial B_r}\left(\bar{\mathbf{\Phi}}_r+\mathbf{\Phi}_r^{sgs}\right)\cdot\mathbf{n_r}dS_r$$

with

$$\bar{\mathbf{\Phi}}_r=\langle\delta\bar{u}^2\delta\bar{u}_i\rangle+\langle\delta\bar{u}^2\delta U\rangle-2\nu\nabla_r\langle\delta\bar{u}^2\rangle$$

$$\mathbf{\Phi}_r^{sgs}=4\langle\tau^*_{ij}\delta\bar{u}_i\rangle$$

where $\mathbf{n_r}$ is the outward normal to the ball B_r of radius r and volume V_r. However, the geometry of the channel makes impossible to average over spheres with radius larger than the distance of their center from the wall. Furthermore, this operation would also imply an average over Y_c loosing the information about the local contribution of inhomogeneous fluxes to the balance 4.2. For these reasons, instead of considering a 3D average of equation 4.2 in the space of scales, we set $r_y=0$ and average only along homogeneous directions, considering a square domain, Σ, of side r belonging to wall-parallel planes, see [54] for the details. This procedure allows to analyze the terms of equation 4.2 as a function of a single scale parameter r and of the wall-distance Y_c. Considering that the second term of the left-hand side of equation 4.2 vanishes since $\delta U=0$ for $r_y=0$, the r-averaged form of equation 4.2 follows as,

$$\bar{T}_r+T_r^{sgs}+\bar{\Pi}+\bar{T}_c+T_c^{sgs}=\bar{E}+\bar{D}_r+\bar{P}+\bar{D}_c+E_{sgs}\tag{4.3}$$

where

$$\bar{T}_r=\frac{1}{r^2}\int_\Sigma\frac{\partial\langle\delta\bar{u}^2\delta\bar{u}_i\rangle}{\partial r_i}\,dr_xdr_z,\;\;\bar{D}_r=\frac{1}{r^2}\int_\Sigma 2\nu\frac{\partial^2\langle\delta\bar{u}^2\rangle}{\partial r_i\partial r_i}\,dr_xdr_z,$$

[1] To note that the classical form of the Kolmogorov equation 2.12, expressed in terms of longitudinal velocity increments, is exactly an r-average over a ball of radius r.

are the contributions to the scale-space energy transfer due to the inertial fluctuations and viscous diffusion.

$$\bar{T}_c = \frac{1}{r^2}\int_\Sigma \frac{\partial\langle\bar{v}^*\delta\bar{u}^2\rangle}{\partial Y_c}\,dr_x dr_z,\;\; \bar{D}_c = \frac{\nu}{r^2}\int_\Sigma \frac{\partial^2\langle\delta\bar{u}^2\rangle}{2\partial {Y_c}^2}\,dr_x dr_z,\;\; \bar{P} = \frac{2}{r^2}\int_\Sigma \frac{-\partial\langle\delta\bar{p}\delta\bar{v}\rangle}{\rho\partial Y_c}\,dr_x dr_z,$$

are the inhomogeneous contributions to the spatial flux related to the inertial fluctuations, viscous diffusion and pressure-velocity correlation.

$$\bar{\Pi} = \frac{1}{r^2}\int_\Sigma 2\langle\delta\bar{u}\delta\bar{v}\rangle\left(\frac{dU}{dy}\right)^*\,dr_x dr_z,\;\; \bar{E} = \frac{1}{r^2}\int_\Sigma -4\langle\bar{\epsilon}^*\rangle\,dr_x dr_z,$$

are the energy production by mean shear and the rate of energy dissipation. The subgrid stresses affect the resolved motion with a redistribution of resolved energy in the space of scales and physical space,

$$T_r^{sgs} = \frac{1}{r^2}\int_\Sigma -4\frac{\partial\langle\tau_{ij}^*\delta\bar{u}_i\rangle}{\partial r_j}\,dr_x dr_z,\;\; T_c^{sgs} = \frac{1}{r^2}\int_\Sigma -\frac{\partial\langle\delta\tau_{i2}\delta\bar{u}_i\rangle}{\partial Y_c}\,dr_x dr_z$$

and with a draining or sourcing of resolved energy,

$$E_{sgs} = \frac{1}{r^2}\int_\Sigma -4\langle\epsilon_{sgs}^*\rangle dr_x dr_z.$$

It is useful to recast equation 4.3 in a simpler form. In the absence of subgrid stresses, the amount of energy which is effectively available at a given wall-distance Y_c is provided by the local resolved production $\bar{\Pi}$ plus all the terms corresponding to the spatial flux of energy towards or from the location considered. By considering the overall turbulent transport in the wall-normal direction we can define an effective resolved production,

$$\bar{\Pi}_e = \bar{\Pi} + \bar{T}_c - \bar{P}.$$

Clearly, the single contributions are not positive definite, but their sum must be positive since it represents the only production mechanism of the flow. Analogously, the contributions of diffusive nature can be added to form an effective resolved dissipation rate,

$$\bar{E}_e = \bar{E} + \bar{D}_r + \bar{D}_c$$

With these definition, the r-averaged balance is expressed in a compact form as

$$\left(\bar{\Pi}_e + T_c^{sgs}\right) + \left(\bar{T}_r + T_r^{sgs}\right) = \left(\bar{E}_e + E_{sgs}\right). \tag{4.4}$$

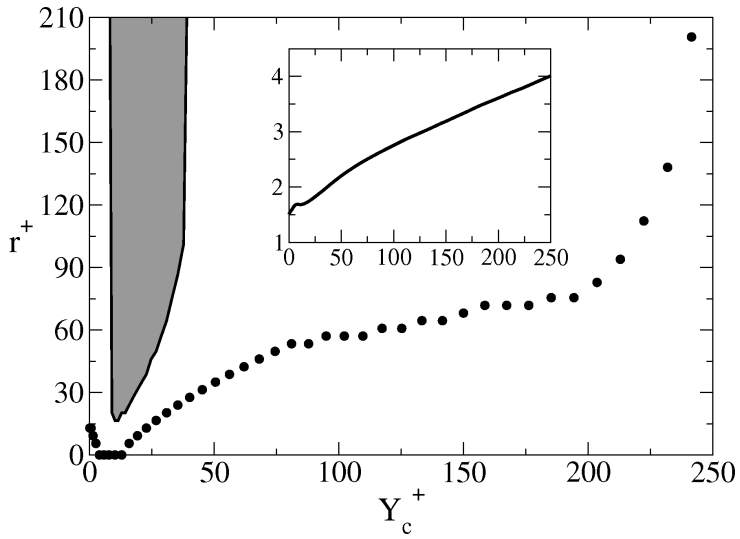

Figure 4.2: Characteristic length scales of the r-averaged energy processes in equation 4.5; the cross-over scale l_c^+ (circle), the reverse energy cascade region Ω_B (grey region) whose edge is the scale l_B^+. In the inset plot it is shown the Kolmogorov scale η^+.

In the absence of subgrid stresses, $\tau_{ij} = 0$ for $l_{Fi} \to 0$, the balance 4.4 reduces to the r-averaged form of the unfiltered Kolmogorov equation, 2.22,

$$\Pi_e + T_r = E_e \tag{4.5}$$

which has to be read as: transfer across scales plus effective production equals effective dissipation. In this context, the filtered dynamics follow the same picture but with the presence of subgrid stresses which alter these phenomena through three different mechanisms. A true source or sink of resolved energy, E_{sgs}, which increases/decreases the effective production or equivalently the effective dissipation. A modification of the resolved energy transfer phenomena due to nonlinear interactions involving subgrid fluctuations which increase/decrease the inhomogeneous spatial flux of resolved energy, with T_c^{sgs}, and the energy transfer across resolved scales, with T_r^{sgs}.

4.3 The filtered wall-turbulent dynamics

In this section, a detailed analysis of the filtered wall-turbulent dynamics is performed via the scale-energy balance 4.3. Energy transfer in the resolved motion will be discussed and emphasis will be spent on the action of the

subgrid stresses on the resolved motion in both physical and scale space, underlining the role of the filter scale compared to the relevant scales of wall-turbulence. As shown in section 3.2.3 for the turbulent channel flow case at $Re_\tau = 550$, these scales are: the cross-over scale, l_{ci}, which divide the turbulent fluctuations governed by anisotropic production from those dominated by inertial energy transfer and the scale, l_{Ei}, which separetes positive and negative inertial fluxes divergence among scales. In a context of r-averaged dynamics, equation 4.5, these scales become scalar quantities, namely l_c and l_B, which define the cross-over scales between the correspective r-averaged processes. To note that the rates of energy transfer in the space of scales become pseudo-fluxes due to the r-average operation, namely T_r and D_r.

In figure 4.2 it is shown the cross-over scale $l_c^+(Y_c^+)$ identified as $\Pi(l_c^+, Y_c^+) = T_r(l_c^+, Y_c^+)$ which splits the space of scales into an inertial range at small r^+ from a production dominated range at large r^+ and the reverse cascade region $\Omega_B(r^+, Y_c^+)$ where the energy cascade term T_r changes sign. The edge of this region is the scale $l_B^+(Y_c^+)$ which splits the space of scales into a forward cascade at smaller r^+ from a reverse cascade at larger r^+.

The scale l_c shows a decrease moving from the bulk of the flow to the walls without marked differences with the behaviour of the non averaged scales l_{ci}. Whereas, contrarily to the non averaged energy processes, the r-averaged pseudo-flux T_r show a reverse cascade only in the buffer layer. The net pseudo-flux, T_r, coming out from the square domain Σ, becomes positive only close to the wall, hiding the energy fluxes loops emerging from the multidimensional analysis of chapter 3. Hereafter, we will refer to as reverse and forward cascade (or equivalently Richardson cascade) in a r-averaged point of view which indicate respectively the outgoing and incoming pseudo-flow of energy from the square domain Σ. However, it is important to keep in mind that the energy fluxes loop in the space of scales and systematically show a reverse energy flux not only in the near-wall region as shown in chapter 3.

In the next section we will analyze results for filter lengths from $l_F^+ = 15$ to $l_F^+ = 120$ equal in the two directions parallel to the wall. This choice will allow to study the effects of the subgrid scales as a function of a single filter parameter, varying with respect to the scalar relevant scales of wall-turbulence, namely l_c and l_B.

4.3.1 The resolved turbulent kinetic energy

Before discussing the scale by scale balances for the filtered Kolmogorov equation, we briefly discuss some results obtained with the resolved single-

point turbulent kinetic energy $\bar{q} = \bar{u}_i\bar{u}_i/2$. The evolution equation for $\langle\bar{q}\rangle$ in a turbulent channel flow is

$$\frac{d\bar{\phi}}{dy} + \frac{d}{dy}\langle\bar{u}_i\tau_{i,2}\rangle = -\langle\bar{u}\bar{v}\rangle\frac{dU}{dy} - \langle\bar{\epsilon}\rangle - \langle\epsilon_{sgs}\rangle, \tag{4.6}$$

where $\bar{\phi} = (\langle\bar{q}\bar{v}\rangle + \langle\bar{p}\bar{v}\rangle/\rho - \nu d\langle\bar{q}\rangle/dy)$. In the absence of subgrid stresses, $\tau_{ij} = 0$, equation 4.6 reduces to the classical balance of turbulent kinetic energy, $q = u_iu_i/2$,

$$\frac{d\phi}{dy} = -\langle uv\rangle\frac{dU}{dy} - \langle\epsilon\rangle, \tag{4.7}$$

where $\phi = (\langle qv\rangle + \langle pv\rangle/\rho - \nu d\langle q\rangle/dy)$. Equation 4.7 has to be read as: the rate of spatial flux equals the balance between production and dissipation. In this context the filtered dynamics follow the same picture but with the presence of subgrid stresses which alter the balance with two mechanisms. A true source or sink of resolved energy, $\langle\epsilon_{sgs}\rangle$, which increases/decreases the resolved energy available at a given location and an additional inhomogeneous flux due to nonlinear phenomena involving inertial fluctuations at subgrid scales. Basically, the analysis of equation 4.6 allows to evaluate the subgrid stresses effects and the resolved energy processes in the physical space for various filter lengths, see also [24] for a discussion of the turbulent channel flow.

In figure 4.3(a) the resolved energy production by mean shear, $-\langle\bar{u}\bar{v}\rangle dU/dy$, and the resolved viscous dissipation, $-\langle\bar{\epsilon}\rangle$, are shown for three values of the filter length l_F^+. In the core flow, the former remains unaltered and a depletion of the latter at increasing filter scale is observed. On the contrary, approaching the wall, both these quantities decrease with l_F^+. Indeed, while dissipation is always present at the small subgrid scales even in the center of the channel, the production mechanism involves more and more the subgrid scales moving towards the wall as the shear scale, $L_s \approx ky^+$, diminishes. The figure 4.3(b) shows $-\langle\epsilon_{sgs}\rangle$ at the same values of l_F^+. From the inspection of the plot the role of the *subgrid dissipation* is deduced. Resolved turbulent kinetic energy is drained in the core flow and in the viscous sublayer while in the buffer layer, for the larger filter scales, it becomes opposite in sign in an increasing region, implying that the subgrid scales feed the large scale of motion, i.e. a backward energy transfer occurs, see [24] for a similar discussion.

The backward energy transfer can be related to the excess of turbulent energy in the subgrid scales due to the large subgrid turbulent production. To quantify this observation let us consider, $[(\pi - \bar{\pi}) - (\langle\epsilon\rangle - \langle\bar{\epsilon}\rangle)]$, where $\bar{\pi} = -\langle\bar{u}\bar{v}\rangle dU/dy$ and $\pi = -\langle uv\rangle dU/dy$. This quantity represents somehow

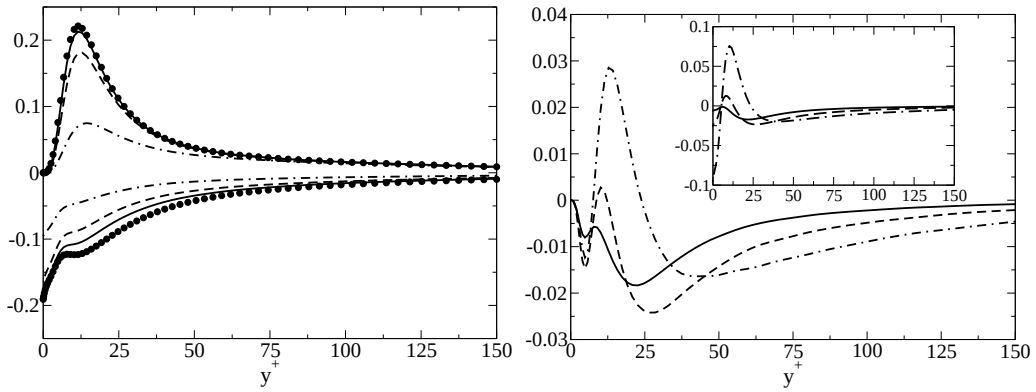

Figure 4.3: (a) y-behavior of production and dissipation. (b) *Subgrid dissipation*, $-\langle\epsilon_{sgs}\rangle$, and in the inset, $[(\pi-\bar{\pi})-(\langle\epsilon\rangle-\langle\bar{\epsilon}\rangle)]$. DNS (circle), $l_F^+=20$ (solid line), $l_F^+=30$ (dashed line) and $l_F^+=60$ (dashed-dotted line).

the net balance of energy production and dissipation acting in the subgrid scales. Indeed, the spectral cutoff filter used allows to divide the unfiltered turbulent kinetic energy production and dissipation into the sum of two distinct contributions from resolved and subgrid scale. The same applies for the turbulent kinetic energy where $\langle u^2\rangle=\langle\bar{u}^2\rangle+\langle u_{sgs}^2\rangle$ with $2\langle\bar{u}u_{sgs}\rangle=0$, see [69]. From the inset of figure 4.3(b), it is observed that dissipation is dominant in the subgrid scales in the core flow and the viscous sublayer where a draining of resolved energy occurs, $-\langle\epsilon_{sgs}\rangle<0$. Whereas, in the subgrid scales of the buffer layer, production overcomes the viscous effects leading to a subgrid energy excess which feeds the resolved motion. Indeed, the corrispondance between the region where $[(\pi-\bar{\pi})-(\langle\epsilon\rangle-\langle\bar{\epsilon}\rangle)]>0$ and the region where $-\langle\epsilon_{sgs}\rangle>0$ is remarkable. The present view is entirely consistent with the scenario highlighted in chapter 3 where it is shown that the turbulent energy is mostly generated amid the spectrum of the near-wall region in the so-called driving scale range DSR.

It is worth anticipating that the different behaviors in the bulk, logarithmic and buffer regions can be easily related to the two scenarios that will be discussed in the next sections respectively.

4.3.2 Scale by scale budget in the logarithmic and bulk region

To ease the comprehension of the results in this region of the flow, let us recall that the logarithmic layer is characterized, see figure 4.2, by one relevant length, i.e. the cross-over scale l_c^+. Such parameter represent somehow the border of the production dominated range. In figure 4.4(a) and (b), the scale energy balance 4.3 in one representative plane for $l_F^+ = 30$ is shown. At this location the filter scale is always smaller than the cross-over scale, $l_F^+ < l_c^+$ and the subgrid scale dynamic reduces to the Richardson energy cascade. Such condition leads to a preservation of the value for the statistical observables of the resolved fields, i.e. $E_e \approx \bar{E}_e + E_{sgs}$, $\Pi_e \approx \bar{\Pi}_e$, $T_r \approx \bar{T}_r$. Indeed, for $l_F^+ < l_c^+$ the energy production in the subgrid scales is negligible and the value obtained for the filtered field equals the unfiltered one, $\Pi \approx \bar{\Pi}$. Therefore, the rate of energy exchange between resolved and subgrid motion, E_{sgs}, is exclusively determined by the viscous dissipation in the subgrid scales, implying that $E \approx \bar{E} + E_{sgs}$, i.e. the sum of the subgrid and resolved viscous dissipation equals the unfiltered rate of energy dissipation.

In these regions of the flow, the subgrid stresses effects of resolved scale-energy redistribution in physical and scale space, namely T_c^{sgs} and T_r^{sgs}, are both negligible as shown in figure 4.4(a). This is very important in a context of subgrid stresses modeling. Indeed, the main goal of most LES models is the correct estimation of the energy exchange between grid/subgrid motion, E_{sgs}, assuming that the resolved energy redistribution due to subgrid stresses is negligible.

The common interpretation of E_{sgs} is a measure of the rate of energy transfer between scales larger and smaller than l_F^+. However, in a wall flow this rate of energy flux is predominantly determined by the balance between processes of energy production and dissipation in the subgrid scales. Indeed, from figure 4.5 showing E_{sgs} for different filter lengths and wall distances in the logarithmic and bulk regions, it is noticeable that as l_F^+ approaches the Kolmogorov scale η^+, E_{sgs} decreases since a larger fraction of energy dissipation occurs due to the resolved flow. When l_F^+/η^+ is larger, E_{sgs} increases monotonically accounting more and more for the energy dissipation, up to approach the cross-over scale, $l_F^+/l_c^+ \approx 1$, where a maximum is observed. For filter scales larger than the cross-over scale, $l_F^+/l_c^+ > 1$, E_{sgs} decreases since production starts to be significant in the subgrid range and hence E_{sgs} does not account exclusively for the energy dissipation but for the balance between energy source and sink processes occurring simultaneously in the subgrid scales. As a consequence $\bar{E} + E_{sgs} \ll E$ and $\bar{\Pi} \ll \Pi$.

To ease the interpretation of the plot in figure 4.5, let us consider that in

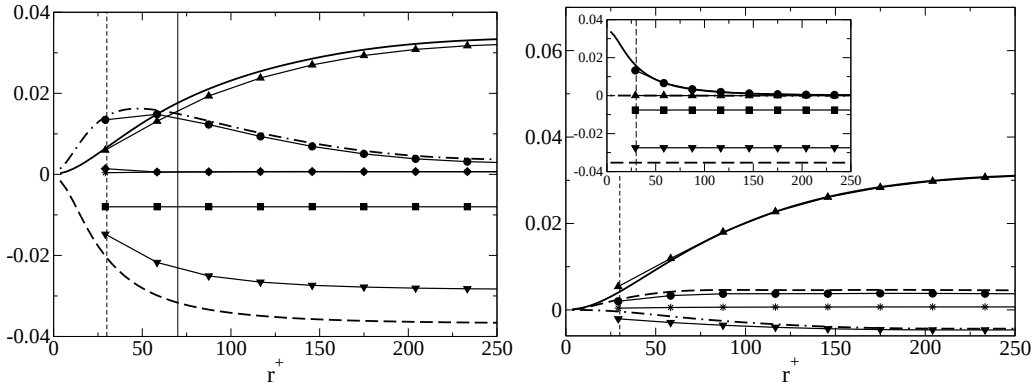

Figure 4.4: Scale-energy balance in the logarithmic layer at $Y_c^+ = 160$ for the unfiltered (lines) and filtered field at $l_F^+ = 30$ (symbols). (a) The terms of equation 4.4. Filtered field: $\bar{E}_e$ triangles down, $-\bar{\Pi}_e$ triangles up, $-\bar{T}_r$ circles, $-\bar{T}_r^{sgs}$ diamonds, $-\bar{T}_c^{sgs}$ stars and $\bar{E}_{sgs}$ squares. Unfiltered field: E_e dashed line, $-\Pi_e$ solid line and $-T_r$ dashed dotted line. (b) Contributions to the effective production. Filtered field: $-\bar{\Pi}$ triangles up, $-\bar{P}$ triangles down, $-\bar{T}_c$ circles and $-T_c^{sgs}$ stars. Unfiltered field: $-\Pi$ solid line, $-P$ dashed dotted line and $-T_c$ dashed line. Inset of (b): contribution to the effective dissipation. Filtered field: $\bar{E}$ triangles down, E_{sgs} squares, $\bar{D}_r$ circles and $\bar{D}_c$ triangles up. Unfiltered field: E dashed line, D_r solid line and D_c dashed dotted line. The vertical solid and dashed line are l_c^+ and l_F^+ respectively.

higher Reynolds number flows, when a large separation between l_c^+ and viscous scales occurs in the logarithmic and bulk regions, a plateau is expected for $\eta^+ \ll l_F^+ \ll l_c^+$. In this range the *subgrid dissipation* should equal the total amount of viscous dissipation, $E_{sgs}(l_F^+) \approx E$, with a negligible contribution from the resolved scales, $\bar{E}(l_F^+) \approx 0$. The extension of this plateau represents a measure of the amplitude of the inertial equilibrium range increasing with the distance from the wall. Since in such a range a Kolmogorov scaling sets in, $\langle \delta u^2 \delta u_i \rangle r_i / r \propto -\langle \epsilon^* \rangle$, the behavior of $E_{sgs}(l_F^+)$ which is expected to be the same as those of the third order structure function evaluated at the filter scale $(\langle \delta u^2 \delta u_i \rangle r_i / r)|_{l_F^+}$, see [9], should therefore equals E independently on the filter scale under consideration.

These results show the logarithmic layer as a region where the dominant energy processes can be reproduced with the resolved scales with the exception of a fraction of viscous dissipation which can be recovered with E_{sgs} if $l_F^+ < l_c^+$. The subgrid scales are dominated by a classical Richardson energy cascade closed by viscous diffusion at small scales. Therefore, the main

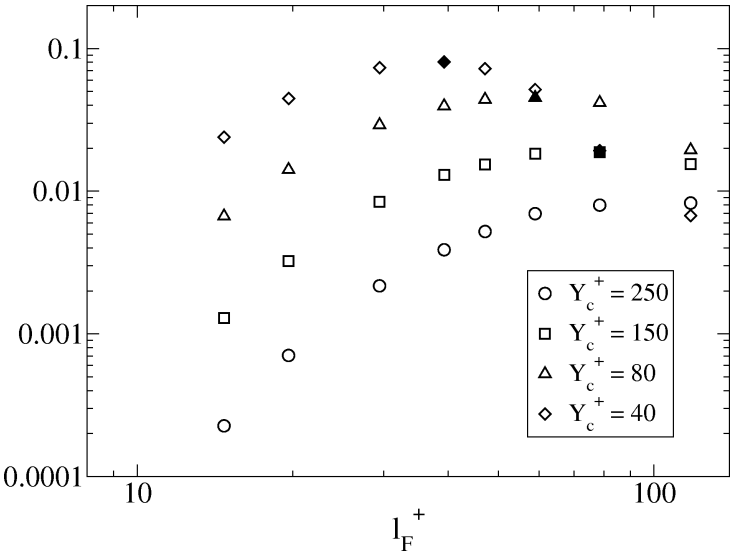

Figure 4.5: Scaling of the *subgrid dissipation* $-E_{sgs}(l_F^+)$ as a function of the filter scale l_F^+ for different wall distances. The filled symbols correspond to $l_F^+/l_c^+ = 1$.

role of the subgrid scales is to drain resolved energy, $E_{sgs} < 0$, without redistribution effects, $T_c^{sgs} \approx T_r^{sgs} \approx 0$. This kind of phenomenology can be reproduced with good results with the common used purely dissipative eddy viscosity models as shown in section 4.4. The present scenario should be substantially Reynolds number independent with an unaltered role of the filter position with respect to the cross-over scale. The only expected difference is quantitative, since the value of the cross-over scale could change due to the appeareance of longer and wider structures in this region for larger Reynolds number. Indeed, as reported in [71], an increase of l_c^+ is observed when the same present approach is applied to datasets with larger values of the friction Reynolds number.

In the bulk flow, the physics governing the subgrid motion is still the same of that reported for the log-layer. Indeed, in this region the cross-over scale l_c^+ is very large up to infinity in the core of the channel where production vanishes. Therefore, the filter scale l_F^+ is always reasonably smaller than l_c^+. In these conditions, the subgrid motion is characterized by a Richardson energy cascade and, therefore, drain resolved energy, $E_{sgs} < 0$, without resolved energy redistribution effects, $T_c^{sgs} \approx T_r^{sgs} \approx 0$, as shown in figure 4.6(b) for two different filter scales. We would like to stress that even if in the bulk the subgrid stresses dynamics are the same of those of the log-layer, there

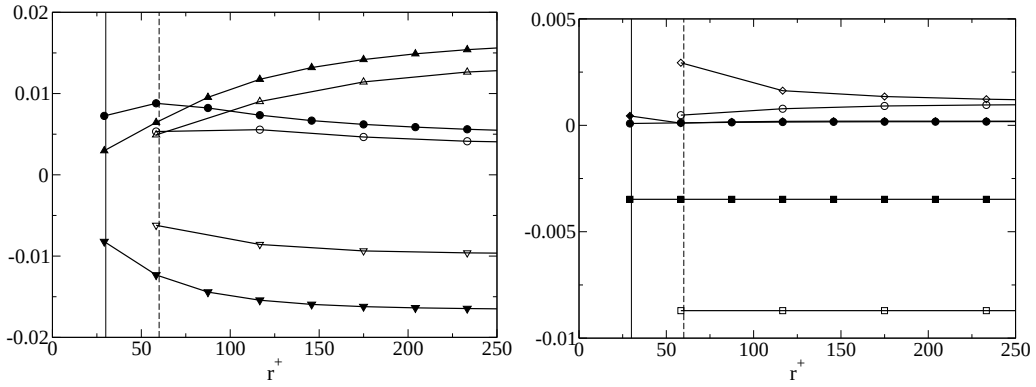

(a) (b)

Figure 4.6: Effect of the filter scale at $Y_c^+ = 220$ for $l_F^+ = 30$ (filled symbols) and $l_F^+ = 60$ (open symbols). (a) $-\bar{\Pi}_e$ triangles up, $\bar{E}_e$ triangles down and $-\bar{T}_r$ circles. (b) $-T_r^{sgs}$ diamonds, $-T_c^{sgs}$ circles and E_{sgs} squares. The vertical solid and dashed line are $l_F^+ = 30$ and $l_F^+ = 60$ respectively.

is a change in the dynamics of the resolved ones that should be considered with some care. In fact, as shown in figure 4.6(a), a depletion of the physics captured with the resolved motion is observed despite $l_F^+ < l_c^+$. The resolved effective production $\bar{\Pi}_e$ is considerably smaller with respect to the unfiltered one (not reported) and a depletion is observed increasing the filter scale even if both the filters shown, $l_F^+ = 30$ and $l_F^+ = 60$, are smaller than the cross-over scale. The observed depletion in the effective production is due to a poorly resolved spatial transfer rather than to an error in the evaluation of the local production, hence this could be regarded as a non local effect potentially worsened by a not fully resolved physics in the buffer layer as will be shown in the next section.

4.3.3 Scale by scale budget in the buffer layer

The physical scenario of the buffer layer is enriched by the presence of a range of scales where a reverse energy transfer occurs, namely the area Ω_B in figure 4.2. In this region the cross-over scale is very small, the filter scale is always larger than l_c^+ and the physics captured by the resolved field is largely affected by the position of the filter scale l_F^+ with respect to the edge of the region Ω_B, namely the scale l_B^+.

The scale-energy budget in the buffer layer for $l_F^+ = 30$ is reported in figure 4.7(a) and (b) for $Y_c^+ = 12$, corresponding to the peak of the turbulent production. At this location $l_F^+ > l_B^+$ and it is shown that, since a non-

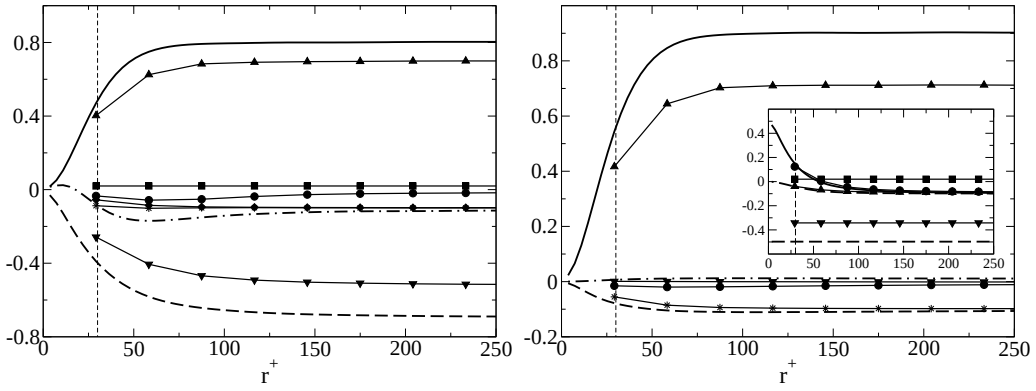

Figure 4.7: Scale-energy balance in the buffer layer for $Y_c^+ = 12$. See caption of figure 4.4.

negligible part of the production acts in the subgrid scales, $\bar{\Pi} \ll \Pi$, see figure 6(b). Approaching the buffer layer the cross-over scale l_c^+ reaches the Kolmogorov scale η^+, as shown in figure 4.2, and the anisotropic action of turbulent production is relevant at all scales. In this region, the most significant scales of motion are not those greater than l_c^+ but those belonging to the reverse cascade region Ω_B. To corroborate the role of Ω_B, a comparison between the unfiltered and filtered mixed structure functions, $-\bar{S}_{12}(r^+) = -\langle \delta\bar{u}\delta\bar{v} \rangle$, evaluated at $Y_c^+ = 25$ and averaged on a square of dimension r^+, is reported in figure 4.8 for different values of the filter length l_F^+. The r^+-dependence of $-\bar{S}_{12}(r^+)$, that is the scale-dependent component of the resolved turbulent production, recovers the unfiltered behavior only for $l_F^+ < l_B^+$. Otherwise, the scale-energy production reproduced with the resolved scales is very poor, meaning that a large energy injection due to production occurs in the subgrid scales. The edge of the reverse cascade region, the scale l_B, is the r-averaged footprint of the near-wall peak of energy source, DSR, and, consequently of the peak of energy fluxes divergence reported in chapter 3. For that reason, the scale l_B is the relevant scale to be considered when a filtering operation is used since it marks a range of scales characterized by a large turbulent production from which the energy fluxes depart to both smaller and larger scales and other regions of the flow.

In this region of the flow, the rate of energy exchange between grid/subgrid motion, E_{sgs}, is not determined by the viscous dissipation, but by the balance between production, which is never negligible ($l_c^+ \to \eta^+$), and dissipation in the subgrid scales, therefore $\bar{E} + E_{sgs} \ll E$ see the figure 4.7(a) and (b). The resolved field cannot reproduce the unfiltered physics because most of

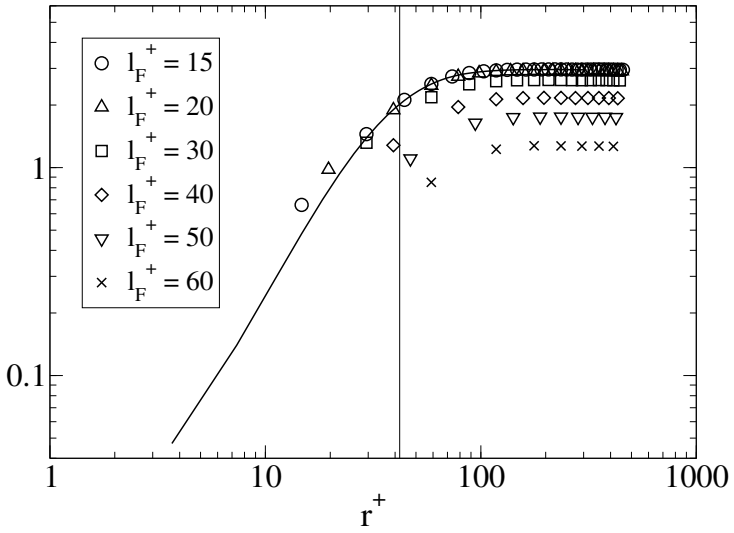

Figure 4.8: Scaling of the averaged filtered mixed structure function, $-\bar{S}_{12} = -\langle \delta\bar{u}\delta\bar{v} \rangle$, for different filter scale l_F^+ in the buffer layer $Y_c^+ = 25$. Comparison with the unfiltered mixed structure function $-S_{12} = -\langle \delta u \delta v \rangle$ (solid line). The vertical line represents the scale l_B^+ at $Y_c^+ = 25$.

the energy processes act in the subgrid scales and the role of E_{sgs} is strongly modified up to a backward energy transfer, $E_{sgs} > 0$ when $l_F^+ > l_B^+$, leading to an energy flux from subgrid to resolved scales, as for the location $Y_c^+ = 12$. As shown in figure 4.3(b), the intensity of the backward energy transfer and the region of the flow involved increase with the filter scale l_F^+. Indeed, as shown in figure 3.3, representing the non averaged multidimensional energy fluxes, for large square domain of side r^+ corresponding to the filter lengths considered, the amount of reverse energy fluxes covered increases.

Furthermore, for $l_F^+ > l_B^+$, the nonlinear interactions in the resolved scales do not reproduce the energy flux across scales, T_r, and the spatial flux T_c, as shown in the figure 4.7(a) and (b). While, on the other hand, the subgrid stresses significantly act in the energy redistribution with T_r^{sgs} and T_c^{sgs} meaning that most of the resolved processes depends on the scales below l_F^+. In order to better exploit the role of the filter length, in figure 4.9(a) and (b) the comparison between two balances at different value of l_F^+, smaller and larger than l_B^+, is reported. It is interesting to observe that the contribution of T_r^{sgs} and T_c^{sgs} in the case $l_F^+ = 60$, the one larger than l_B^+, is fundamental in reproducing the energy redistribution mechanisms, while for $l_F^+ = 30$ is negligible.

The effects of nonlinear interactions, T_r^{sgs}, as function of the wall-distance

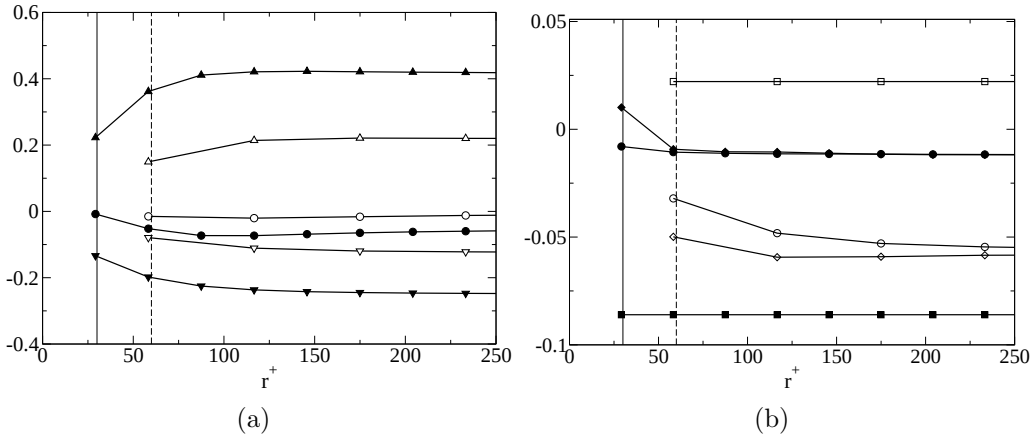

Figure 4.9: Effects of the filter scale in the buffer layer at $Y_c^+ = 25$. See caption of figure 4.6.

and evaluated at a scale $r^+ = l_F^+ = 30$, are shown in the figure 4.10(a) where also T_r and $\bar{T}_r$ appear. In the bulk of the channel the transfer is only due to the nonlinear interactions in the resolved scales, $\bar{T}_r$, while T_r^{sgs} is negligible. Approaching the wall, the subgrid interaction term, T_r^{sgs}, becomes more and more significant highlighting a strong coupling between subgrid and resolved motion occurring in the buffer layer. This statistical occurrence can be presumably attributed to the fact that when $l_F^+ > l_B^+$ both subgrid and resolved scales belong to the same coherent motion. Indeed, the multidimensional analysis, reported in chapter 3, show the DSR, and consequently the scale l_B in the r-averaged framework, as the result of the coherent dynamics involved in the near-wall cycle. The same phenomenology is observed also for other scales and filters considered, here not shown, and for the spatial fluxes T_c, $\bar{T}_c$ and T_c^{sgs} shown in the figure 4.10(b) in the same conditions. In general, it is very important to estimate the subgrid nonlinear energy distribution effects in the buffer layer for $l_F^+ > l_B^+$ in order to correctly reproduce the near-wall regeneration mechanisms.

As suggested in chapter 3, in the buffer layer an intermediate range of scales exists, the DSR, which loses energy to feed both larger (reverse energy cascade) and smaller (forward energy cascade) scales in the same physical location and other range of scales of the adjacent regions of the flow via spatial flux. In the present framework, the scale $l_B^+(Y_c^+)$ can be thought as the center of this range of scales. This range, responsible for the backward energy transfer, is related to the dynamics of the coherent structures producing turbulent fluctuations, see [62]. When $l_F^+ > l_B^+$, a large fraction of this range belongs to the subgrid scales and therefore both T_r^{sgs} and T_c^{sgs} account for a

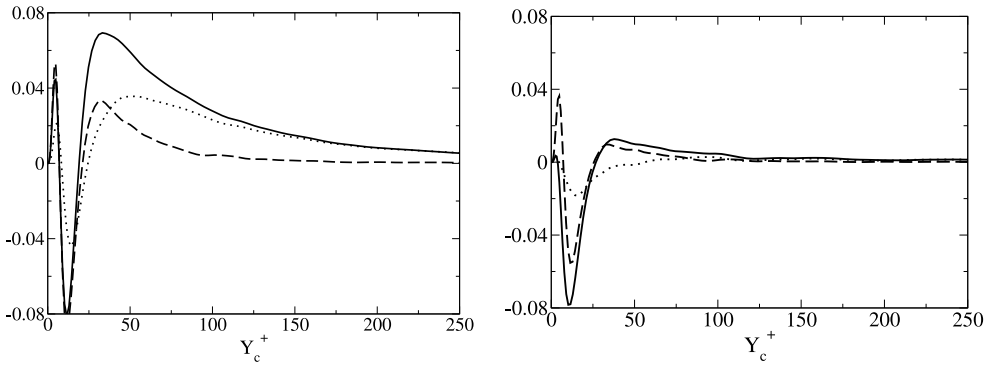

Figure 4.10: (a) Y_c-behavior of $-T_r$ (solid line), $-\bar{T}_r$ (dotted line) and $-T_r^{sgs}$ (dashed line) for $r^+ = 30$ and $l_F^+ = 30$. (b) Y_c-behavior of $-T_c$ (solid line), $-\bar{T}_c$ (dotted line) and $-T_c^{sgs}$ (dashed line) for $r^+ = 30$ and $l_F^+ = 30$.

significant part of the energy cascade and spatial fluxes in the resolved scales and the resolved physics is very poor. Furthermore, in these conditions a large energy-excess due to turbulent production occurs in the subgrid scales as highlighted in figure 4.8, feeding the backward energy transfer, $E_{sgs} > 0$.

In a context of Large Eddy Simulation of wall flows it is very important to capture the physics of the buffer layer because this region is responsible for the sustainment of turbulence. However, according to the present results, the filtered velocity field is able to capture the turbulent dynamics only when the filter scale allows for the resolution of the reverse energy cascade region Ω_B. Otherwise, the resolved physics is very poor, see figure 4.9(a), where $\bar{\Pi}_e$, $\bar{T}_r$ and $\bar{E}_e$ recover the unfiltered physics (not shown) only for $l_F^+ = 30$, which is outside Ω_B, and are underestimated otherwise. Furthermore, if $l_F^+ > l_B^+$, LES models should be able to reproduce a backward energy transfer and the complex but significant nonlinear phenomena of energy redistribution due to subgrid stresses.

The incorrect resolution of the leading physical processes of the buffer layer affects the flow, especially in the core region, via spatial energy fluxes. In figure 4.11(a) and (b) the Y_c^+-behavior of the r-averaged resolved spatial flux $\bar{\Phi}_c = \langle \bar{v}^* \delta \bar{u}^2 \rangle + 2\langle \delta\bar{p}\delta\bar{v} \rangle/\rho - \nu d\langle \delta\bar{u}^2 \rangle/2dY_c$ is shown in comparison with the unfiltered one Φ_c for large and small scales and different filter length. It is also shown $\bar{\Phi}_{c+sgs} = \bar{\Phi}_c + \langle \delta\tau_{i2}\delta\bar{u}_i \rangle$ which accounts for the energy redistribution in physical space due to subgrid stresses.

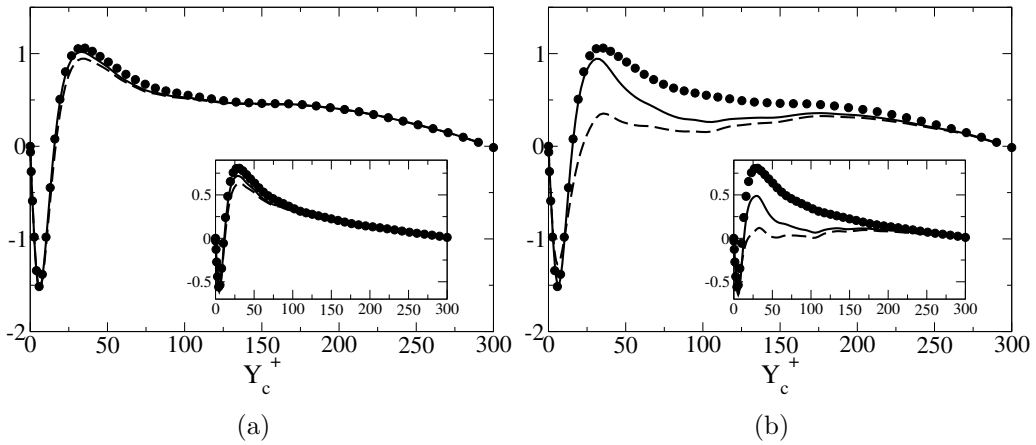

Figure 4.11: Y_c-behavior of the r-averaged spatial flux for large scales $r^+ = 310$ and small scales $r^+ = 30$ (inset plots). The unfiltered spatial flux Φ_c (circle), the resolved spatial flux $\bar{\Phi}_c$ (dashed line) and the resolved and subgrid spatial flux $\bar{\Phi}_{c+sgs}$ (solid line). (a) $l_F^+ = 15$ and (b) $l_F^+ = 30$.

When the filter length allows to capture the whole region Ω_B, as for $l_F^+ = 15$ shown in figure 4.11(a), the amount of resolved energy which leaves the buffer layer to feed the viscous sublayer and the core flow recovers the unfiltered process, $\bar{\Phi}_c \approx \Phi_c$, for both large and small scales. The subgrid stresses effects are negligible, $\bar{\Phi}_c \approx \bar{\Phi}_{c+sgs}$. Otherwise, a depletion of the resolved spatial flux is observed as for $l_F^+ = 30$ shown in figure 4.11(b). In this case the filter scale not allows to resolve the region Ω_B and the subgrid stresses accounts for a significant part of the resolved energy redistribution in physical space.

The reduction in the resolved spatial energy fluxes strongly affects the dynamics of the turbulent fluctuations in the core flow. Indeed, the turbulence in this region is sustained by the energy incoming from the wall since production goes to zero. The resolved physics in this region is strongly altered even if the local main processes are captured, i.e. if $l_F^+ < l_c^+$. As shown in figure 4.6(a) for $Y_c^+ = 220$, a depletion of the resolved statistical observable occurs moving from $l_F^+ = 30$ to $l_F^+ = 60$ even if both the filter length are smaller than l_c^+. Indeed, for $l_F^+ = 60$ a larger fraction of the region Ω_B is not resolved leading to a stronger decrease of the spatial fluxes which feed this region.

It should be pointed out that in the same conditions the dynamics of the logarithmic region remains unaffected. Indeed in the log-layer these effects are negligible even if a large decrease of the resolved spatial flux occurs as

shown in figure 4.11(a) and (b). In fact being the spatial flux almost constant, the amount of energy carried out by it is not released in this region. Therefore, despite the large value of the spatial flux in the log-layer, its divergence is sufficiently small in comparison with the other terms of the scale-by-scale budget 2.22 and 4.2 to be dynamically ineffective. The inhomogeneity plays here only a minor role which is also expected to vanish for larger Reynolds number. Therefore, the condition $l_F^+ < l_c^+$ presented in the previous section is still sufficient to ensure that the main physical processes of the log-layer are well reproduced with the resolved scales.

4.4 Behaviour of the classical LES models

In this section, a methodology for using the filtered Kolmogorov equation 4.2 as a new tool for the assessment of LES models will be briefly outlined. An *a priori* analysis of the most common and widely used eddy viscosity models will be shown as an example, but the same procedure could be performed also for the *a posteriori* analysis and for other LES models. The systematic characterization of the subgrid stresses physics as function of the filter scale and of the wall-distance, performed in the previous sections, will be shown instrumental for the correct use of given LES models in the simulation of wall-turbulence.

According to the idea of isotropic recovery at small scales of all types of flow for sufficiently large Reynolds number, the eddy viscosity models assume that the energy exchange between resolved and subgrid scales is similar to the viscous dissipation, leading to subgrid stresses in the form, $\tau_{ij} - 1/3\tau_{kk}\delta_{ij} = -2\nu_T\bar{S}_{ij}$. In fact, when isotropic conditions are recovered, equation 2.22 leads to an energy exchange across the filter scale,

$$\left.\frac{\partial\langle\delta u^2\delta u_i\rangle}{\partial r_i}\right|_{l_F} = -4\nu\langle S_{ij}S_{ij}\rangle\,, \tag{4.8}$$

which is similar to E_{sgs} evaluated with eddy viscosity, i.e. $E_{sgs} = -8\nu_T\langle\bar{S}_{ij}\bar{S}_{ij}\rangle$. Let us note that in expression (4.8) the pseudo-dissipation $\langle\epsilon\rangle$ is replaced with the proper dissipation $\nu\langle S_{ij}S_{ij}\rangle$ since in homogeneous conditions these terms are coincident. Accordingly to the results in the previous sections, this kind of subgrid stresses physics implemented by the eddy-viscosity models should give good results only when the filter used is $l_F < l_c$ far from the wall, leading to subgrid dynamics governed by a Richardson cascade, and $l_F < l_B$ in the wall-region, in order to have at least a drain of resolved energy, $E_{sgs} < 0$. Nevertheless, the analysis of the eddy-viscosity models will be shown for $l_F > l_B$.

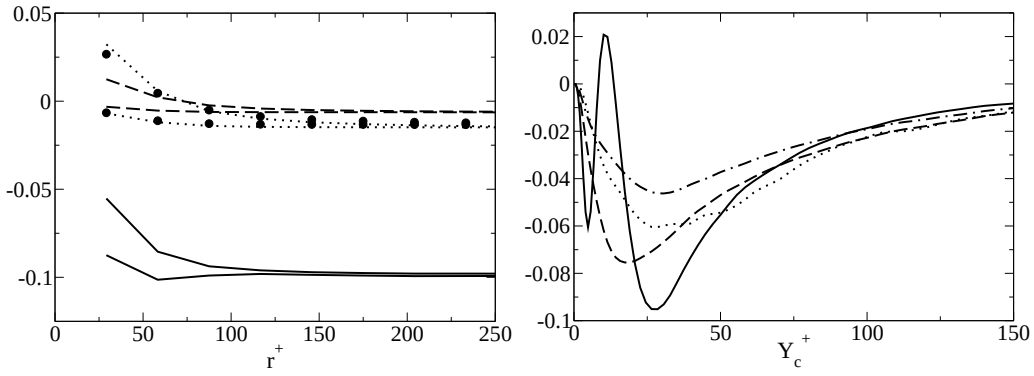

(a) (b)

Figure 4.12: (a) $-T_r^{sgs}$ and $-T_c^{sgs}$ evaluated with the Smagorinsky (circles), Smagorinsky shear-improved (dashed lines), dynamic Smagorinsky (dotted lines) and with the filtered DNS (solid lines) for $l_F^+ = 30$ in the buffer layer $Y_c^+ = 12$. (b) Y-behavior of E_{sgs} estimated with exact subgrid stresses (solid line) and with Smagorinsky (dashed line), Smagorinsky shear-improved (dashed-dotted line) and dynamic Smagorinsky (dotted line) for $l_F^+ = 30$.

The simplest and most commonly used eddy viscosity model is the one developed by Smagorinsky [74], where it is assumed that $\nu_T = (C_s l_F)^2 |\bar{S}|$. This model is known to give good results in homogeneous and isotropic turbulence but it is too dissipative in the near-wall turbulence. To alleviate this deficiency, for wall-bounded flows the Smagorinsky constant C_s is often multiplied by a damping factor depending on the wall-normal distance, see [80]. Instead, in other models like Smagorinsky shear-improved, [47], the eddy viscosity takes into account mean-shear effects, and, therefore the non-isotropic nature of near-wall turbulence, and naturally decreases to zero at the wall, i.e. $\nu_T = (C_s l_F)^2 (|\bar{S}| - |\langle \bar{S} \rangle|)$.

More in general, the Smagorisky approach can be improved to a large degree via a dynamic procedure, [22], where the model coefficient is evaluated from the resolved motion and it is applied to the subgrid scales assuming the scale-invariance suggested by the relation (4.8). Formally, this methodology is based on the Germano identity, $L_{ij} = T_{ij} - \tilde{\tau}_{ij}$, which relates the resolved turbulent stresses $L_{ij} = \widetilde{\bar{u}_i \bar{u}_j} - \tilde{\bar{u}}_i \tilde{\bar{u}}_j$, the subgrid stresses τ_{ij}, and the subtest stresses $T_{ij} = \widetilde{u_i u_j} - \tilde{u}_i \tilde{u}_j$ where $\tilde{(\cdot)}$ denotes a test filter applied at a scale $\alpha\, l_F$, with $\alpha = 2$ the commonly used value. Assuming scale-invariance, the same Smagorinsky model approximation is used for both the subgrid and subtest stresses allowing to calculate the Smagorinsky coefficient with a least-squares error minimization procedure, [50], $C_s^2 = -\langle L_{ij} M_{ij} \rangle / \langle M_{ij} M_{ij} \rangle$, where

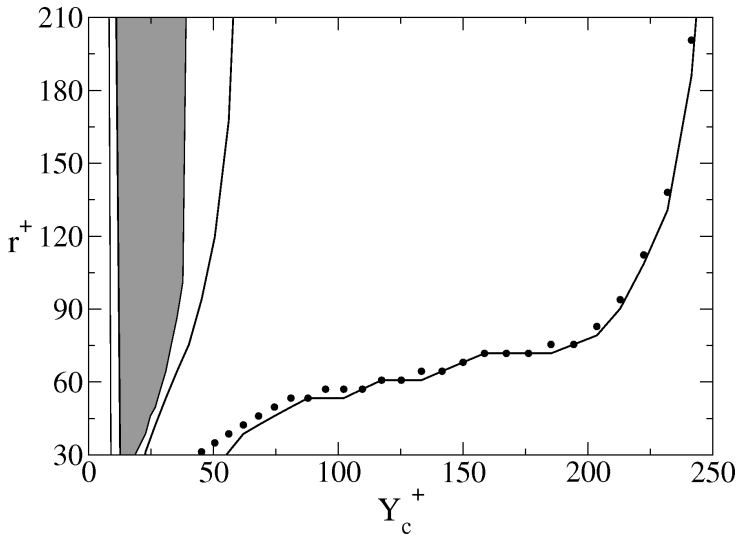

Figure 4.13: The cross-over l_c^+ and reverse cascade scale l_B^+ evaluated with the filtered velocity field for $l_F^+ = 30$ (lines) and compared with the unfiltered values.

$M_{ij} = l_F^2(\alpha^2|\tilde{\bar{S}}|\tilde{\bar{S}}_{ij} - \widetilde{|\bar{S}|\bar{S}_{ij}})$. These three models will be here addressed in the framework of the filtered Kolmogorov equation.

The predicted subgrid stresses for $l_F^+ = 30$ lead to negligible energy redistribution effects in physical and scale space, T_r^{sgs} and T_c^{sgs}, also in the buffer layer where the filter scale l_F^+ lies within the region of the reverse energy transfer Ω_B, see figure 4.12(a). No relevant differences between the three models are observed in the predicted very small T_r^{sgs} and T_c^{sgs}. As shown in the previous sections this is a satisfactory behavior in the logarithmic and bulk flow but not in the wall region where the energy redistribution due to subgrid stresses should be very significant when $l_F > l_B$. This incorrect behavior is due to the linear relation between subgrid stresses τ_{ij} and resolved strain-rate $\bar{S}_{ij}$ which is at the base of the eddy viscosity formulation. On the contrary, the energy redistribution terms, i.e. T_r^{sgs} and T_c^{sgs}, are an expression of the nonlinearity in the Navier-Stokes equations which shows a strong coupling of the subgrid and resolved scales in the buffer layer.

As expected, the predicted energy exchange between resolved and subgrid scales, E_{sgs}, figure 4.12(b), shows a good behavior in the logarithmic and bulk flow where for $l_F^+ < l_c^+$ an r-averaged forward energy cascade occurs in the subgrid scales. Conversely, in the buffer layer with $l_F^+ > l_B^+$, production, occurring even at small scales, leads to the impossibility for the eddy viscosity models to reproduce a E_{sgs} which should exhibit a backward energy transfer.

Given this limitation, the two refined models are only able to determine more accurately the location of the maximum of the energy transfer at $Y_c^+ = 30$, see dotted and dash-dotted lines in figure 4.12(b), while the expected backscatter appears as a reduced value of the *subgrid dissipation*. No approach based on the eddy viscosity concept can reproduce the backward energy transfer and hence for this kind of models the optimal filter scale is $l_F^+ < l_B^+$ in the near-wall region and $l_F^+ < l_c^+$ in the logarithmic region. The cross-over l_c^+ and reverse cascade scale l_B^+ estimated with the filtered velocity field are reported in figure 4.13. A good agreement with the unfiltered value of these scales is observed, meaning that information from the resolved field can be in principle extracted to predict an optimal filter scale at different wall-distances and Reynolds number without any a priori knowledge.

4.5 Correct resolution of the wall-turbulent physics

Summarizing, the results of the previous sections single out, in a quantitative way, the prominent role of the filter scale compared to the relevant scales of the channel in the different regions of the flow. In the logarithmic region, the dominant energy processes can be reproduced with the resolved scales when $l_F^+ < l_c^+$. In this case the missing fraction of viscous dissipation can be recovered with E_{sgs} since the subgrid scales are dominated by a classical Richardson energy cascade closed by viscous diffusion at small scales. The role of the subgrid scales is to drain resolved energy, $E_{sgs} < 0$, without redistribution effects, $T_c^{sgs} \approx T_r^{sgs} \approx 0$. This kind of phenomenology can be reproduced to a good degree with the commonly used dissipative eddy viscosity models. In the buffer layer, the scale l_B^+ marks an intermediate range of scales, the DSR for the r-averaged processes, which loses energy to feed both larger (reverse energy cascade) and smaller (forward energy cascade) scales in the same physical location and other range of scales of the adjacent regions of the flow via spatial flux. When $l_F^+ > l_B^+$, a large fraction of this range belongs to the subgrid scales and therefore both T_r^{sgs} and T_c^{sgs} account for a significant part of the energy cascade and spatial fluxes in the resolved scales. Hence when this is the case the poorly resolved physics of the buffer layer affects the dynamics of the turbulent fluctuations of the whole domain via spatial fluxes especially in the core flow. Furthermore, in these conditions a large energy-excess due to turbulent production occurs in the subgrid scales, feeding the backward energy transfer, $E_{sgs} > 0$. Indeed, when $l_F^+ > l_B^+$ a large decrease in the resolved production is observed. This energy

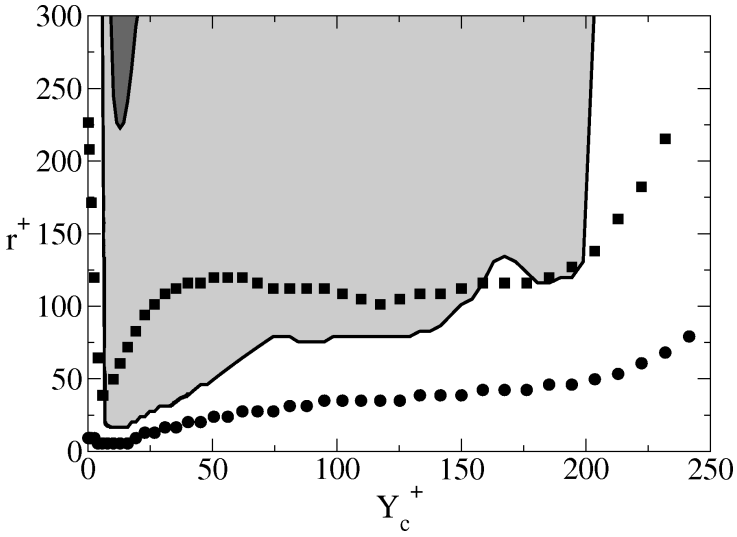

Figure 4.14: The cross-over scale l_{cz} (circle), l_{cx} (square) and the reverse cascade plane Ω_{Ez} (grey region), Ω_{Ex} (dark grey region).

excess feeds the backward energy transfer observed in the buffer layer.

While we are confident that this analysis, where a single filtering parameter has been introduced, is sufficient to describe the role of the filter length in capturing the physics of wall turbulence, richer physics is expected to be revealed when investigating the streamwise and spanwise energy processes separately. This procedure should highlight the anisotropic physics of wall-turbulence allowing for an enlarged analysis of the role of optimal values of the filter scales in the streamwise and spanwise direction separately. Indeed, as shown in chapter 3, a multidimensional analysis is crucial for the description of the wall-turbulent physics.

For these reasons, in this section we extend the analysis of the filtered wall-turbulent dynamics accounting for the anisotropic behaviour exhibited by the non averaged relevant scales l_{c_i} and l_{E_i} previously introduced in section 3.2.3. The scale-by-scale budget will be performed using a spectral cutoff filter with different lenghts in the streamwise and spanwise directions in order to separately verify the conditions $l_{F_x} < l_{c_x}$, $l_{F_z} < l_{c_z}$ and $l_{F_x} < l_{E_x}$, $l_{F_z} < l_{E_z}$.

In figure 4.14, the scales l_{c_i} and l_{E_i} are shown as a function of the wall-distance for the channel flow case at $Re_\tau = 300$. From this figure emerges that the bounding condition for the filter length in the streamwise direction is the value of l_{c_x} in the logarithmic region. While in the spanwise direction is the value of l_{E_z} in the buffer layer. For that reason we consider a filter with $l^+_{F_x} = 60$ and $l^+_{F_z} = 15$ which satisfies these constraints. This filter will be denoted as l_{Fmix}. The resulting statistics will be compared to that obtained

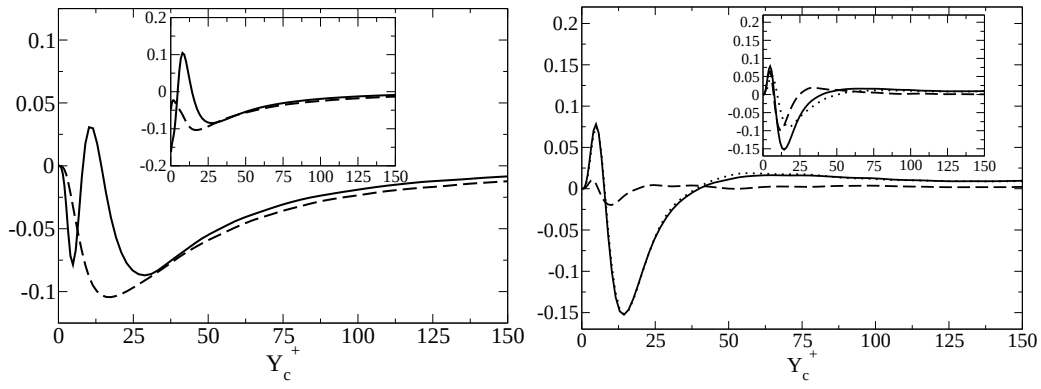

(a) (b)

Figure 4.15: (a) Subgrid dissipation, E_{sgs}, and excess of scale-energy in the subgrid scales, $[(\pi - \bar{\pi}) - (\langle\epsilon\rangle - \langle\bar{\epsilon}\rangle)]$ (inset). l_F solid line and l_{Fmix} dashed line. (b) T_r (solid line), $\bar{T}_r$ (dotted line) and $\bar{T}_r^{sgs}$ (dashed line) for l_{Fmix} and l_F (inset).

with a filtered field with $l_F^+ = 30$ equals in the homogeneous directions which will be denoted as l_F. This filtered field has the same amount of small scales removed by the filtering operation as l_{Fmix}.

As shown in figure 4.16(a) and (b), the scale-by-scale budget in the log-layer obtained with the filter l_{Fmix} is essentially the same for l_F. Indeed, in this region the conditions $l_{F_x} < l_{c_x}$ and $l_{F_z} < l_{c_z}$ are verified for both the filters considered. Hence, in both cases the resolved field is able to reproduce the physics of this region with a missing fraction of energy dissipation which is recovered with E_{sgs}. The role of the subgrid stresses is to drain resolved energy, $E_{sgs} < 0$, without resolved energy redistribution effects in physical and scale-space, $T_r^{sgs} \approx T_c^{sgs} \approx 0$.

In the buffer layer, the use of l_{Fmix} leads to an energy exchange between resolved and subgrid scales, E_{sgs}, which drains resolved energy, see figure 4.15(a). The backward energy transfer observed for l_F is absent. When $l_{F_x} < l_{E_x}$ and $l_{F_z} < l_{E_z}$ the process of viscous dissipation dominates the subgrid scales also in the buffer layer where otherwise an energy-excess is observed, see the inset of plot 4.15(a). Therefore, in the subgrid scales prevail the viscous effects of dissipation and then of absorption of resolved scale-energy. Indeed, as shown in section 3.2, considering that the scales l_{E_i} represent the edge of the energy fluxes at positive divergence and, therefore, of the scales of energy source, it is clear that when $l_{F_x} < l_{E_x}$ and $l_{F_z} < l_{E_z}$ the larger energy production and larger scale-energy fluxes divergence occur in

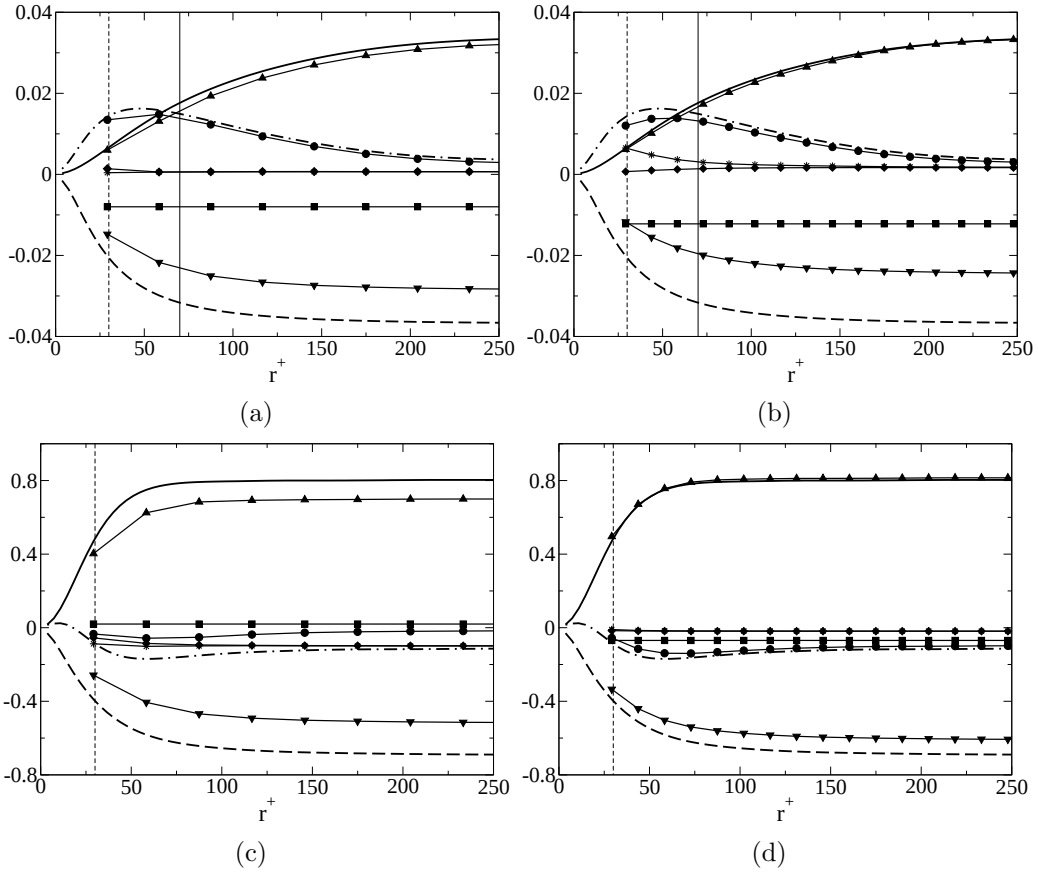

Figure 4.16: Scale-by-scale budget in the log-layer, $Y_c^+ = 160$, (a)(b) and buffer layer, $Y_c^+ = 12$, (c)(d) with l_F (a)(c) and l_{Fmix} (b)(d). Filtered field: $\bar{E}_e$ dashed line, $-\bar{\Pi}_e$ solid line, $-\bar{T}_r$ dashed dotted line, $-\bar{T}_r^{sgs}$ dotted line, $-\bar{T}_c^{sgs}$ dashed-dashed-dotted line and $\bar{E}_{sgs}$ dashed-dotted-dotted line. Unfiltered field: E_e triangle down, $-\Pi_e$ triangle up and $-T_r$ circle.

the resolved motion and therefore $E_{sgs} < 0$ and the subgrid stresses effects of redistribution of resolved energy in physical and scale-space, T_r^{sgs} and T_c^{sgs} are negligibles. As shown in figure 4.15(b), the energy transfer across scales is determined by nonlinear interaction in the resolved scales also in the buffer layer for the filter l_{Fmix}, i.e. $\bar{T}_r$ is the dominant nonlinear processes while T_r^{sgs} is negligible. Otherwise, the opposite occurs as for l_F. The same conclusions apply also for the spatial flux $\bar{T}_c$ and T_c^{sgs} (not reported).

When $l_{F_i} < l_{E_i}$ the main physical processes belong to the resolved motion allowing to recover the unfiltered dynamics also in the near-wall region. As shown in figure 4.16(c) and (d), for filter l_{Fmix}, $\bar{\Pi}_e \approx \Pi_e$, $\bar{T}_r \approx T_r$ and $\bar{E}_e + E_{sgs} \approx E_e$. The subgrid stresses drain resolved energy, $E_{sgs} < 0$, recovering

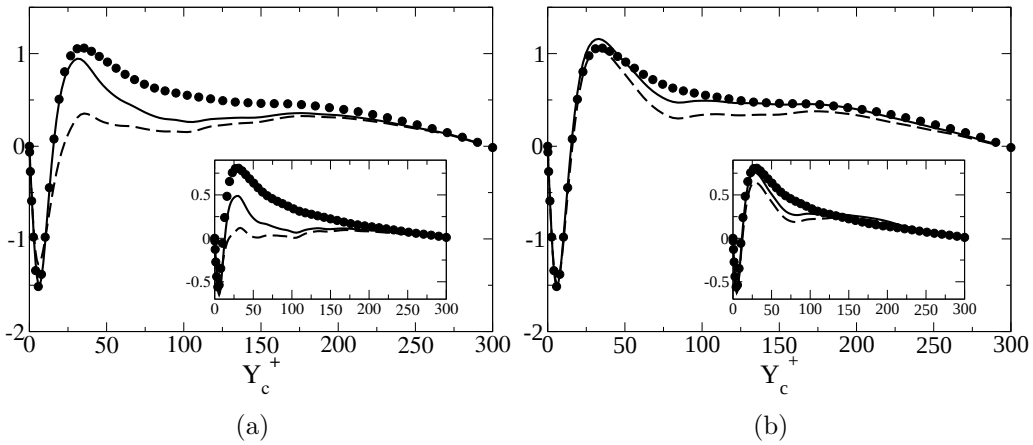

Figure 4.17: Y_c-behavior of the r-averaged spatial flux for large scales $r^+ = 310$ and small scales $r^+ = 30$ (inset plots). The unfiltered spatial flux Φ_c (circle), the resolved spatial flux $\bar{\Phi}_c$ (dashed line) and the resolved and subgrid spatial flux $\bar{\Phi}_{c+sgs}$ (solid line). (a) l_F and (b) l_{Fmix}.

the missing fraction of dissipation and $T_r^{sgs} \approx T_c^{sgs} \approx 0$. Otherwise, for l_F, the resolved physics is very poor $\bar{\Pi}_e < \Pi_e$, $\bar{T}_r < T_r$, $\bar{E}_e + E_{sgs} < E_e$ and the subgrid scales strongly affect the resolved motion with a backward energy transfer, $E_{sgs} > 0$, and with large T_r^{sgs} and T_c^{sgs}.

The correct resolution of the leading physical processes of the turbulent production region leads to a correct extimation of the spatial fluxes which sustain the turbulent motion in the core region of the flow. As shown in figure 4.17, for the filter case l_{Fmix} the r-averaged amount of resolved energy which leaves the buffer layer to feed the viscous sublayer and the core flow recovers the unfiltered process, $\bar{\Phi}_c \approx \Phi_c$ for both large and small scales with subgrid stresses effects negligible, $\bar{\Phi}_c \approx \bar{\Phi}_{c+sgs}$. Otherwise, for filter lenghts which not allow to resolve the reverse cascade region, as for the filter l_F, a depletion of the r-averaged resolved spatial flux is observed with subgrid stresses accounting for a significant part of the resolved energy distribution in physical space. Even if the very large scales of motion of the core region are reasonably well resolved in LES simulation, the correct resolution of the buffer layer guarantees the proper sustainment of these turbulent dynamics.

In conclusion, the results of this paragraph single out the need to adopte a filter which satisfyies the constrain $l_{F_x} < l_{c_x}$ and $l_{F_z} < l_{E_z}$ leading to $l_{F_x}^+ < 100$ and $l_{F_z}^+ < 20$, in order to correctly capture the main physical processes of wall-turbulence. With these limits, the near-wall resolved LES of very high Reynolds number wall-bounded flows may not be possible. As shown in

section 4.4, a runtime extimation of the relevant scales, l_{c_i} and l_{E_i}, should be used to predict from the resolved field an optimal filter scale for different wall-distances and also Reynolds number in order to save computational resources. Indeed, while the spanwise filtering constrain, l_{E_z}, should scale in viscous units, the streamwise one should have a Reynolds number dependence since l_{c_x} is expected to increase its value for larger Reynolds number, as reported in [71].

4.6 Towards a backward energy transfer LES model

It is well known that the most important feature of LES models for the unresolved subgrid scales should be their ability to accurately reproduce the energy transfer between the resolved and subgrid scales. This physical process, represented in the present work by the term E_{sgs}, has been shown to have very different roles depending on the amount of scales removed by the filtering operation, l_{F_i}, and on the wall-distance considered. In particular, in the production region for the filter scale values commonly used for the LES simulation of near-wall resolved wall-turbulence, a net energy flux takes origin in the subgrid scales to feed the resolved motion. This aspect is of fundamental importance for the correct simulation of wall bounded flows as highlighted in chapter 3. The reverse energy cascade is the basic element for the formation of the characteristic long turbulent fluctuations of this kind of flows and also for the correct extimation of the filtered dynamics as shown in the previous paragraphs.

According to these points, it is very important to develop new LES models able to capture the physics of the reverse energy cascade, since the most used ones are based on the Kolmogorov theory on the energy cascade where

$$\frac{\partial \langle \delta u^2 \delta u_i \rangle}{\partial r_i} = -4\langle \epsilon^* \rangle, \tag{4.9}$$

and, therefore, are purely dissipative. In this context, the reduced model for the energy cascade, equation 3.2, here reported for the sake of clarity,

$$\frac{\partial \langle \delta u^2 \delta u_i \rangle}{\partial r_i} = -\left[2\langle \delta u \delta v \rangle \left(\frac{dU}{dy} \right)^* + 4C(Y_c)\langle \epsilon^* \rangle \right]$$

can be seen as a starting point for the development of new LES models replacing the classical Kolmogorov relation 4.9. This relation suggests to model the energy flux between resolved and subgrid scales with the energy

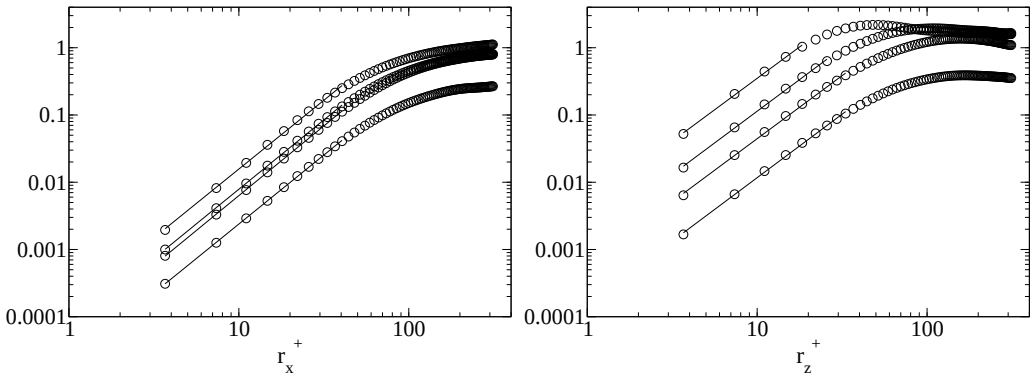

Figure 4.18: Scaling mixed structure function, $-S_{12}$, for different wall-distances from $Y_c^+ = 12$ to $Y_c^+ = 250$ as a function of the streamwise (left) and spanwise (right) scales. The fitted lines correspond to a power law with exponents 2.04 and 1.88 for the streamwise and spanwise scales respectively.

source/sink occurring in the subgrid motion. In a context of LES simulations, the extimation of the subgrid energy source/sink can be obtained using only information from the large resolved motion. In this view, the rate of dissipation in the subgrid scales can be extimated using the classical concept of eddy viscosity whose basically idea is exactly to properly account for dissipation in the subgrid motion through a mechanism analogous to the viscous forces. Whereas, the subgrid turbulent production can be roughly extimated using the amount of production at the smallest resolved scales opportunely projected in the whole subgrid space. In figure 4.18, it is shown the $(r_x^+, 0, 0, |Y_c^+)$- and $(0, 0, r_z^+, |Y_c^+)$-behaviour of the mixed structure function $-S_{12}^+ = -\langle \delta u \delta v \rangle^+$ which is the scale-dependent part of the turbulent production. A well defined behaviour at small scales is observed at different wall-distances corresponding to $-\langle \delta u \delta v \rangle (r_x^+, 0, 0, |Y_c^+) \propto r_x^{+2.04}$ and $-\langle \delta u \delta v \rangle (0, 0, r_z^+, |Y_c^+) \propto r_z^{+1.88}$. These power laws suggest similarity at the smallest scales which can be used to roughly extimate the averaged turbulent production in the subgrid scales. It is important to mention that an universal exponent for the mixed structure function already exists in literature based on dimensional prediction by Lumley [52]. This exponent corresponds to 4/3 and should be found in the equilibrium layer of wall-flows [30] for scales below the shear scale where an isotropic recovering behaviour occurs.

According to these arguments the energy flux between resolved and subgrid scales in wall-turbulence could be written in the streamwise and spanwise

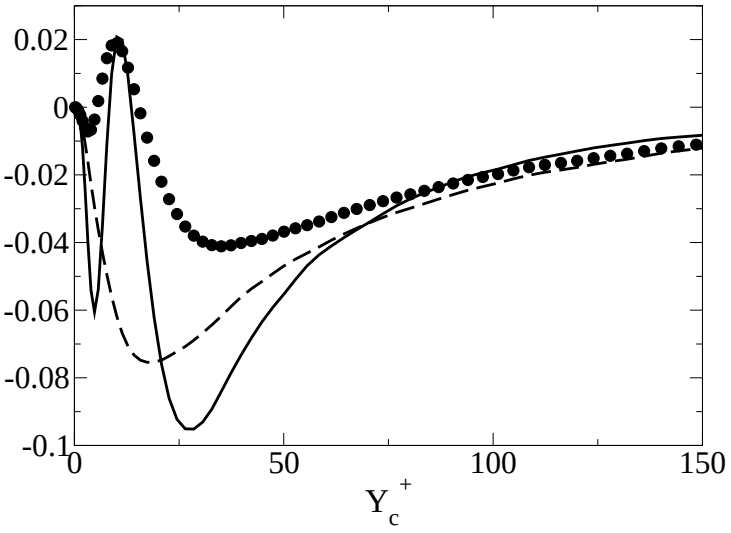

Figure 4.19: Comparison between the exact subgrid energy flux, E_{sgs}, for filter length scale $l_F = 30^+$ (line) and the subgrid dissipation predicted by the Smagorinsky model (dashed line) and by the proposed new one, equation 4.10, (circle) as a function of wall distance.

scales respectively as,

$$-\left[\frac{2}{3}\,\langle\delta\bar{u}\delta\bar{v}\rangle|_{(l_{F_x},0,0)}\left(\frac{dU}{dy}\right)^{*}+8\nu_T\langle\bar{S}_{ij}\bar{S}_{ij}\rangle\right]$$

and

$$-\left[\frac{2}{3}\,\langle\delta\bar{u}\delta\bar{v}\rangle|_{(0,0,l_{F_z})}\left(\frac{dU}{dy}\right)^{*}+8\nu_T\langle\bar{S}_{ij}\bar{S}_{ij}\rangle\right]$$

which highlight that the new term takes into account not only production but also the anisotropy of the flow. The factor 1/3 of the production terms derives from the application of the similarity concept previously introduced. Indeed, considering a subgrid production which follows a power law such as, $-\langle\delta u\delta v\rangle(r_i^+,|Y_c^+) = Ar_i^{+2}$, with the coefficient A determined by turbulent production at the smallest resolved scales as boundary condition, the resulting mean value obtained by an integral in the subgrid space of scales is $-\langle\delta u\delta v\rangle(l_{F_i}^+,|Y_c^+)/3$. Considering now the r-averaged processes, the new formulation leads to

$$E_{sgs}\approx-\left[\frac{1}{3}\,\bar{\Pi}\big|_{l_F}+8\nu_T\langle\bar{S}_{ij}\bar{S}_{ij}\rangle\right] \tag{4.10}$$

whose prediction, with ν_T evaluated with the classical Smagorinsky model, is reported in figure 4.19 as a function of the wall-distance for the filter case $l_F^+ = 30$ and it is compared with the exact E_{sgs} and the one predicted with the Smagorinsky model. The new formulation predicts with a good approximation the energy exchange between resolved and subgrid scales in the logarithmic and bulk flow where $l_F < l_c$ and the subgrid scales drain resolved energy. As expected, no relevant differences with the classical eddy viscosity formulation emerge in these regions of the flow. Conversely, in the buffer layer where $l_F > l_B$, the new formulation is able to determine accurately the location of the maximum energy transfer at $Y_c^+ = 30$ and $Y_c^+ = 12$ corresponding to the peaks of draining and sourcing of resolved energy respectively. Apart the absolute value, the correspondence of the behaviour of the new formulation with those of the exact E_{sgs}, suggests that this line of reasoning could be very promising.

In this view, the subgrid stress tensor, $\tau_{ij}^\star$, should be composed by a linear part in analogy with the viscous forces responsible for dissipation and by a nonlinear part which expresses the inertial interactions between fluctuations of different sizes at the base of turbulent production and of the inertial energy fluxes such as T_r^{sgs} and T_c^{sgs} which have been shown foundamental in the previous paragraphs. While the classical eddy viscosity concept can be used for the linear part of the subgrid stress tensor, in the present framework, the velocity increments appear as the natural candidate for the nonlinear part. As a confirmation, in the work [5], the velocity increments tensor $\delta\bar{u}_i\delta\bar{u}_j$ has been used for the modelization of the subgrid stresses and has been shown, both in *a priori* and *a posteriori* tests, to give a good extimation of both forward end backward energy transfer. Summarizing, the model for the subgrid stresses emerging from the present analysis should take the form,

$$\tau_{ij}^\star = A\delta\bar{u}_i\delta\bar{u}_j - 2\nu_T\bar{S}_{ij} \tag{4.11}$$

where, as suggested by [5], the resolved velocity increments should be evaluated for separation vector $r_i(\mathbf{x}) = 2\Delta x_i(\mathbf{x})$, where $\Delta x_i(\mathbf{x})$ is the grid interval at position $\mathbf{x}$. This operation highlights that the anisotropy of the mesh and, consequentely, of the flow, is implicitly accounted for in the present model by the definition of the three-dimensional velocity increment. The constant A should account for the projection of the increments at grid scales to the subgrid motion using similarity. This constant could be set a priori as previously shown for E_{sgs} or could be solved dynamically as proposed by [19]. However, both, the extimation procedure for the constant A and the analysis of the separation vector to be considered for the resolved velocity increments should be well assessed in the framework of the present model. Unfortunately, at the moment of the compilation of the present PhD thesis this is what has

been done but in the next future works these questions will be adressed and eventually *a posteriori* analysis will be done.

Chapter 5

Conclusions

The current understanding of the physics of wall turbulent flows is essentially based on two classical theories, one concerning the dynamics of the small scales and the other concerning the description of the near-wall layer of wall-bounded flows. The first one is based on the phenomenology of the turbulent energy cascade from the large production scales to the small dissipative ones and has been developed in the context of homogeneous isotropic turbulence. The second one follows from the classical division of wall bounded turbulent flows in a near-wall, inner region, and an outer region populated by large turbulent fluctuations. These two distinct regions are coupled through an overlap region which exhibits a large degree of universality in the form of the so-called law of the wall. These two theories belong to the singular perturbations analysis where the viscous effects are confined to a vanishingly narrow range and are foundamental in the identification of the large Reynolds number asymptotics of the Navier-Stokes equations. Even if the viscous effects are negligible at any finite scale or wall-distance for infinity Reynolds number, there should be finite limits for the viscous dissipation and for the wall shear stress.

The dual nature of these theories arises from the fact that the description is given in the space of scales in one case while in the other is given in physical space. In this context, the generalized Kolmogorov equation, originally derived in [26], represents the link between these two classical approaches to wall turbulence. This equation provides a realistic description of small scale turbulence when inhomogeneity and anisotropy are present. This kind of approach has been used in the present work in order to analyze the energy processes in the augmented space of wall turbulence, (r_x, r_y, r_z, Y_c), i.e. in the three dimensional space of scales and wall-normal direction.

The main results of the present work can be divided into two parts which, however, are closely related each other. One concerning the behaviour of the

energy fluxes and the other concerning the filtered dynamics both in the augmented space of wall turbulent flows.

Energy fluxes in wall turbulent flows

The generalized Kolmogorov equation has been applied to DNS data of a turbulent channel flow at $Re_\tau = 550$ in order to describe the energy fluxes simultaneously occurring in the space of scales and in the physical space of wall-turbulent flows. This analysis revealed an unexpected behavior of the energy fluxes which consists of spiral-like paths in the combined physical/scale space where the controversial reverse energy cascade plays a central role. The energy fluxes diverge from the small scales of the buffer layer to feed longer and wider turbulent fluctuations reaching the outer regions of the flow. The overall picture conforms to a loop in the space of scales where scale-energy is transferred towards larger r_x and r_z while ascending towards increasing Y_c and eventually converging towards the zero-separation, $r_x = r_z = 0$, dissipative scales. In this view, a net energy flux from small to large scales systematically take place at different wall-distances and not only in the near-wall region.

Two dynamical processes are identified as driving mechanisms for the fluxes, one in the near wall region and a second one further away from the wall. The former, stronger one, is related to the dynamics involved in the near-wall turbulence regeneration cycle. The associated strong anisotropic energy injection at small scales, here called driving scale-range (DSR), leaves a deep footprint on the geometrical properties of turbulence with turbulent energy generated amid the spectrum. The second dynamical process suggests an outer self-sustaining mechanism which is asymptotically expected to take place in the eventual logarithmic layer. The associated turbulent energy production occurs at wall-normal positions and scales that make it suspect of a result of turbulent mechanisms composed by attached eddies, in the sense of Townsend's theory, whose activity should increase as the extent of the log-layer with the Reynolds number. If confirmed, its presence could lead to clarify the influence of the external region on the inner layer and help setting the controversy concerning the mixed inner/outer scaling of certain observable like energy spectrum and streamwise fluctuation intensity.

The observed behavior of the energy fluxes and of the turbulent production mechanisms conflicts with the classical notion of Richardson cascade, and may have strong repercussions on both theoretical and modeling approaches to wall-turbulence. For this reason, a simple model for the energy transfer among scales has been proposed and shown to be able to capture most of the rich dynamics of the shear dominated region of the flow. In

particular, this new relation reproduces the switch between source-like and sink-like scales which induce oppositely signed divergence of the scale-energy fluxes at the base of the observed forward and reverse energy cascade simultaneously occurring in the space of scales.

Filtered dynamics

A generalized Kolmogorov equation specialized for filtered velocity field has been applied to filtered DNS data of a turbulent channel flow at $Re_\tau = 300$. The analysis of this equation allows the assessment of the filtered wall-turbulent physics and the subgrid stresses dynamics both in physical and scale space as a function of the filter length. The capability of the filtered velocity field to capture the wall-turbulent physics has been investigated. The results, obtained with an r-averaged form of the filtered Kolmogorov equation, single out, in a quantitative way, the prominent role of the filter scale compared to the relevant scales of the channel in the different regions of the flow.

In the logarithmic region, the dominant energy processes can be reproduced with the resolved scales when $l_F < l_c$. In this case the missing fraction of viscous dissipation can be recovered with E_{sgs} since the subgrid scales are dominated by a classical Richardson energy cascade, in the r-averaged sense, closed by viscous diffusion at small scales. The role of the subgrid scales is to drain resolved energy, $E_{sgs} < 0$, without redistribution effects, $T_c^{sgs} \approx T_r^{sgs} \approx 0$. This kind of phenomenology can be reproduced to a good degree with the commonly used dissipative eddy viscosity models.

In the buffer layer, the scale l_B marks an intermediate range of scales, the r-averaged form of the DSR, which loses energy to feed both larger (reverse energy cascade) and smaller (forward energy cascade) scales in the same physical location and other range of scales of the adjacent regions of the flow via spatial flux. When $l_F > l_B$, a large fraction of this range belongs to the subgrid scales and therefore both T_r^{sgs} and T_c^{sgs} account for a significant part of the energy cascade and spatial fluxes in the resolved scales. Hence, in this case the poorly resolved physics of the buffer layer affects the dynamics of the turbulent fluctuations of the whole domain via spatial fluxes especially in the core flow. Furthermore, in these conditions, $l_F > l_B$, a large energy-excess due to turbulent production occurs in the subgrid scales. This energy excess feeds the backward energy transfer observed in the buffer layer, $E_{sgs} > 0$. According to this phenomenology the analysis of the LES models has shown the incapability of the eddy viscosity models to reproduce the filtered near-wall physics when $l_F > l_B$.

These results, obtained with the r-averaged form of the filtered Kol-

mogorov equation, have been also extended through the analysis of the non averaged filtered Kolmogorov equation. This procedure highlights the anisotropic physics of wall-turbulence allowing for an enlarged analysis of the optimal values of the filter scales in the streamwise and spanwise directions separately. In this view the scalar r-averaged scales l_c and l_B become the vectors l_{c_i} and l_{E_i} which exhibit a very different behaviour in the streamwise and spanwise directions. The results single out the need to adopte a filter which satsfies the constrain $l_{F_x} < l_{c_x}$ and $l_{F_z} < l_{E_z}$ leading to $l^+_{F_x} < 100$ and $l^+_{F_z} < 20$, in order to correctly capture the main physical processes of wall-turbulence. With these limits, the near-wall resolved LES of very high Reynolds number wall-bounded flows may not be possible. A runtime extimation of the relevant scales, l_{c_i} and l_{E_i}, has been shown to be in principle used to predict from the resolved field an optimal filter scale for different wall-distances and also Reynolds numbers in order to save computational resources.

A new picture for the development of LES models has been also outlined. Starting from the simplified relation for the energy transfer, a new class of LES models which takes into account both nonlinear and linear interactions at the base of turbulence production and dissipation, respectively, has been proposed. This kind of approach aims to model the phenomenon of backward energy transfer which have to be considered for the filter lengths commonly used in practice.

Finally, the generalized Kolmogorov equation specialized for filtered velocity fields has been shown to be an helpful statistical tool for the assessment of LES models and for the development of new ones. As example, some classical purely dissipative eddy viscosity models have been analyzed via an *a priori* procedure.

Appendix A

Relation between scale energy, velocity correlations and energy spectrum

One of the most used statistical observable of the present work of thesis is the second order structure function or the scale energy as it is called. But in the study of turbulent flows are often used other quantities such as the energy spectrum and the two-points velocity correlations. These objects are closely related between them. For example the energy spectrum contains essentially the same information of the structure function but expressed differently, providing a quantification of the energy at given scale of motion. In order to better understand the real meaning of these quantities, in the present section the relation between scale energy, velocity correlation and energy spectrum will be shown.

Considering velocity increments in the homogeneous directions, the variance of velocities at different points is the same and the second order structure function can be written,

$$\langle \delta u_i^2 \rangle (r_x, 0, 0, Y_c) = 2[\langle u^2 \rangle (1 - C_{xuu}) + \langle v^2 \rangle (1 - C_{xvv}) + \langle w^2 \rangle (1 - C_{xww})]$$

$$\langle \delta u_i^2 \rangle (0, 0, r_z, Y_c) = 2[\langle u^2 \rangle (1 - C_{zuu}) + \langle v^2 \rangle (1 - C_{zvv}) + \langle w^2 \rangle (1 - C_{zww})]$$

where

$$C_{s,u_i u_i} = \frac{\langle u_i(x_s) u_i(x_s + r_s) \rangle}{\langle u_i^2 \rangle}.$$

For $r \gg l$ where l is the relevant correlation lenght, quantities evaluated at different point are uncorrelated and the structure function $\langle \delta u_i^2 \rangle$ reduces, within a factor 4, to the turbulent kinetic energy $(1/2)\langle u_i^2 \rangle$. For $r \leq l$, the

structure function behaviour is closely related to the velocity correlation and, therefore, also to the energy spectrum. The direct correspondence between structure function and energy spectrum is expressed as,

$$\langle \delta u_i^2 \rangle (r_x, 0, 0, Y_c) = 4 \int_0^\infty \left(\hat{E}_{uu}(k_x) + \hat{E}_{vv}(k_x) + \hat{E}_{ww}(k_x) \right) (1 - cos(k_x r_x))\, dk_x$$

$$\langle \delta u_i^2 \rangle (0, 0, r_z, Y_c) = 4 \int_0^\infty \left(\hat{E}_{uu}(k_z) + \hat{E}_{vv}(k_z) + \hat{E}_{ww}(k_z) \right) (1 - cos(k_z r_z))\, dk_z$$

or equivalently,

$$\frac{1}{4}\langle \delta u_i^2 \rangle (r_x, 0, 0, Y_c) = \frac{1}{2}\langle u_i^2 \rangle - \int_0^\infty \left(\hat{E}_{uu}(k_x) + \hat{E}_{vv}(k_x) + \hat{E}_{ww}(k_x) \right) cos(k_x r_x) dk_x$$

$$\frac{1}{4}\langle \delta u_i^2 \rangle (0, 0, r_z, Y_c) = \frac{1}{2}\langle u_i^2 \rangle - \int_0^\infty \left(\hat{E}_{uu}(k_z) + \hat{E}_{vv}(k_z) + \hat{E}_{ww}(k_z) \right) cos(k_z r_z) dk_z$$

where it is used,

$$R_{ii}(r_s) = \int_0^\infty \hat{E}_{ii}(k_s) cos(k_s r_s) dk_s$$

that is the inversion formula of

$$\hat{E}_{ii}(k_s) = \frac{2}{\pi} \int_0^\infty R_{ii}(r_s) cos(k_s r_s) dr_s$$

which is the diagonal of

$$\hat{E}_{ij}(r_s) = \frac{1}{\pi} \int_{-\infty}^{+\infty} R_{ij}(r_s) e^{-ik_s r_s} dr_s$$

considering that, for $i = j$, $R_{ii}(r_s)$ is real and an even function of r_s. Therefore, the energy associated at a given scale r is the difference between the total kinetic energy and the integral in the wavenumber space of the spectral energy multiplied by a cosine which frequency depends on r. The same occurs when the energy spectrum is expressed in terms of structure functions. For small values of r, the energy spectrum is correlated with a low frequency cosine in wavenumber space. Whereas, for high values of r, the energy spectrum is correlated with an high frequency cosine in wavenumber space. Apart the different definition of turbulent scale-energy given by the energy spectrum and the structure function, there is not a definite correspondence between wavelenght $2\pi/k$ and scale r. The link between the turbulent scales defined in spectral space with the energy spectrum and in physical

space with the structure function or the velocity correlation is given by the frequency of a cosine function.

Other aspects relating structure functions and energy spactra can be obtained via the analysis of the second order longitudinal structure functions in isotropic turbulence. As done in [15], the longitudinal second order structure function can be written as

$$\langle \delta u_{||}^2 \rangle = 2u^2(1-f) \tag{A.1}$$

where

$$R_{||}(r) = u^2 f(r) \text{ and } R_{\perp\perp}(r) = u^2 g(r)$$

In isotropic conditions we have that

$$\hat{E}(k) = \frac{2}{\pi}\int_0^\infty R(r) kr sen(kr) dr \tag{A.2}$$

obtained after integrating in the space (r, θ, ϕ) over θ and ϕ and using isotropic hypotheses. Then,

$$R(r) = \frac{u^2}{2r^2}\left(r^3 f\right)' = \int_0^\infty \hat{E}(k)\frac{sen(kr)}{kr} dk \tag{A.3}$$

and integrating in r this relation to obtain f and substituting it in relation A.1, yelds

$$\langle \delta u_{||}^2 \rangle = \frac{4}{3}\int_0^\infty \hat{E}(k) H(kr) dk \tag{A.4}$$

where

$$H(x) = 1 + \frac{3cos(x)}{x^2} - \frac{3sen(x)}{x^3} \tag{A.5}$$

The function $H(x)$, for small x it grows as $H(x) \approx x^2/10$ and for large x approaches an asymptote $H = 1$ in an oscillatory manner. A rough approximation to $H(x)$ is given by,

$$\hat{H}(x) = \begin{cases} (x/\pi)^2 & , x < \pi \\ 1 & , x > \pi \end{cases}$$

Regarding $H(kr)$ as a weighting function, filtering $E(k)$, then we should get a reasonable estimate of $\langle \delta u_{||}^2 \rangle$ substituting H by $\hat{H}$ and obtaining,

$$\langle \delta u_{||}^2 \rangle \approx \frac{4}{3}\int_{\pi/r}^\infty \hat{E}(k) dk + \frac{4}{3}\frac{r^2}{\pi^2}\int_0^{\pi/r} k^2 \hat{E}(k) dk \tag{A.6}$$

This relation allows the interpretation of the longitudinal structure function as a measure of the spectral energy contained at wavelenghts smaller than r and of the spectral dissipation at wavelenghts larger than r.

Apart the different interpretation of the turbulent scales and of the scale energy given by the energy spectrum and the structure function, it is finally interesting to note that the balance equations of these two objects have very similar aspects. For example, the inertial energy transfer rate, $\partial\langle\delta u^2\delta u_j\rangle/\partial r_j$, which appears in the evolution equation of the structure function, is equal to the energy transfer rate term appearing in the evolution equation of the velocity correlation, $\partial(\langle u_i' u_i u_j\rangle\rangle - \langle u_i' u_i u_j\rangle)/2\partial r_j$, where $u_i' = u_i(x')$ and $x' = x_s + r_s$. This term, once transformed in the Fourier space, gives the classical energy cascade term $j\mathbf{k}\cdot\hat{\mathbf{T}}_r(\mathbf{k})$ of the spectral energy equation. Indeed,

$$\langle\delta u^2\delta u_j\rangle = \langle(u_i - u_i')(u_i - u_i')(u_j - u_j')\rangle =$$

$$\langle u_i' u_i' u_j\rangle - \langle u_i u_i u_j'\rangle + 2\langle u_i' u_i u_j\rangle\rangle - 2\langle u_i' u_i u_j\rangle$$

where the additional terms $\langle u_i u_i u_j\rangle - \langle u_i' u_i' u_j'\rangle$ are canceled by homogeneity. Applying the divergence operator in the space of scales $\partial/\partial r_j$, by incompressibility, the first two terms vanish and, within a factor 4, the energy transfer rate term of the velocity correlation, $\partial(\langle u_i' u_i u_j\rangle\rangle - \langle u_i' u_i u_j\rangle)/2\partial r_j$, is obtained. Therefore, the energy transfer rate in the space of scale of the structure function, $\partial\langle\delta u^2\delta u_j\rangle/\partial r_j$, expresses the same physics of the energy transfer in the spectral space of the spectral energy $j\mathbf{k}\cdot\hat{\mathbf{T}}_r(\mathbf{k})$.

Appendix B

Spectral equation in wall-turbulence

In the present work of thesis, the generalized Kolmogrov equation has been used as basic tool for the multidimensional analysis of the turbulent energy processes occurring both in physical and scale space. Indeed, the second order structure function, at the base of this description, can be thought as the amount of energy at scale $|\mathbf{r}|$ and it is a function of the location $\mathbf{X}_c$. Analogously to this quantity, the energy spectrum, $\hat{E}(\mathbf{k}, \mathbf{X}_c)$, can be used to describe simultaneously the scale- and spatially-dependent turbulent dynamics. Indeed, the energy spectrum contains essentially the same informations of the second order structure function but expressed differently.

In the present section, the balance equation for the energy spectrum, analogous to that of the second order structure function, is derived and discussed. Some results will be presented in order to identify the counterpart in the spectral space of the main findings of the present thesis reported in chapter 3.

Summing the Navier-Stokes equations for the istantaneous velocity fluctuations applied to two different point, x_i and x'_i, and cross-multiplied by the velocity fluctuations $u_i = u_i(x_i)$ and $u'_i = u_i(x'_i)$, it is possible to obtain, once averaged, the balance equation for the two-point velocity correlation for fully inhomogeneous and anisotropic turbulence,

$$\frac{\partial \langle u_i u'_i \rangle}{\partial t} + \frac{\partial}{\partial X_{cj}} \langle (u_i u'_i) u^*_j \rangle + \frac{\partial}{\partial r_j} \langle (u_i u'_i) \delta u_j \rangle + \langle u'_i u_j \rangle \left(\frac{\partial U_i}{\partial x_j} \right)^* + 2 \frac{\partial}{\partial X_{cj}} \langle (u_i u'_i) U^*_j \rangle$$

$$+ \frac{\partial}{\partial r_j} \langle (u_i u'_i) \delta U_j \rangle = -\frac{1}{\rho} \frac{\partial}{\partial X_{ci}} \langle (p u'_i + u_i p') \rangle - \frac{1}{\rho} \frac{\partial}{\partial r_i} \langle (p u'_i - u_i p') \rangle$$

$$+\frac{\nu}{2}\frac{\partial^2\langle u_i u_i'\rangle}{\partial X_{cj}^2}+2\nu\frac{\partial^2\langle u_i u_i'\rangle}{\partial r_j^2} \tag{B.1}$$

where δ, * and X_{cj} have the same meaning of those in equation 2.22. This equation specialized for the symmetries of the channel reads,

$$\frac{\partial\langle u_i u_i'\rangle}{\partial t}+\frac{\partial}{\partial Y_c}\langle(u_i u_i')v^*\rangle+\frac{\partial}{\partial r_j}\langle(u_i u_i')\delta u_j\rangle+2\langle u'v\rangle\left(\frac{dU}{dy}\right)^*=$$

$$-\frac{1}{\rho}\frac{\partial}{\partial Y_c}\langle(pv'+vp')\rangle+\frac{\nu}{2}\frac{\partial^2\langle u_i u_i'\rangle}{\partial Y_c^2}+2\nu\frac{\partial^2\langle u_i u_i'\rangle}{\partial r_j^2}, \tag{B.2}$$

where it is considered that the separation vector lies in the homogeneous directions. This expression represents the dynamics governing the two-point correlations through the space of scales and physical space. It is straightforward to show that, for $r = 0$, equation B.2 reduces to the turbulent kinetic energy balance.

Equation B.2 can be used to derive the balance equation for the spectral energy density which in the channel reads, $\hat{E}(\mathbf{k}, Y_c)$. Indeed,

$$\hat{E}(\mathbf{k}, Y_c)=\frac{1}{(2\pi)^3}\int_{\mathbb{R}^3}\langle u_i u_i'\rangle(\mathbf{r}, Y_c)e^{j\mathbf{k}\cdot\mathbf{r}}d^3\mathbf{k},$$

and the equation for the spectral energy density can be obtained considering the Fourier transform of the terms of equation B.2 in the homogeneous directions, i.e. $\mathbf{k} = (k_x, k_z)$,

$$\frac{\partial\hat{E}(\mathbf{k}, Y_c)}{\partial t}+\frac{\partial\hat{T}_c(\mathbf{k}, Y_c)}{\partial Y_c}-j\mathbf{k}\cdot\hat{\mathbf{T}}_r(\mathbf{k}, Y_c)+\hat{\Pi}(\mathbf{k}, Y_c)=$$

$$-\frac{1}{\rho}\frac{\partial\hat{P}(\mathbf{k}, Y_c)}{\partial Y_c}+\frac{\nu}{2}\frac{\partial^2\hat{E}(\mathbf{k}, Y_c)}{\partial Y_c^2}-2\nu k^2\hat{E}(\mathbf{k}, Y_c). \tag{B.3}$$

where $\hat{T}_c(\mathbf{k}, Y_c)$ is the inertial spatial flux of spectral energy, $\hat{\mathbf{T}}_r(\mathbf{k}, Y_c)$ is the inertial energy transfer among wavenumbers, $\hat{\Pi}(\mathbf{k}, Y_c)$ is production of spectral energy by mean-shear, $\hat{P}(\mathbf{k}, Y_c)$ is the spatial flux due to pressure-velocity correlation and $2\nu k^2\hat{E}(\mathbf{k}, Y_c)$ is the rate of energy dissipation.

B.0.1 Results

Purpose of this section is the analysis of the energy processes in spectral space as described by equation B.3. We will briefly outline the main features of the spectral energy fluxes in comparison to those observed in physical

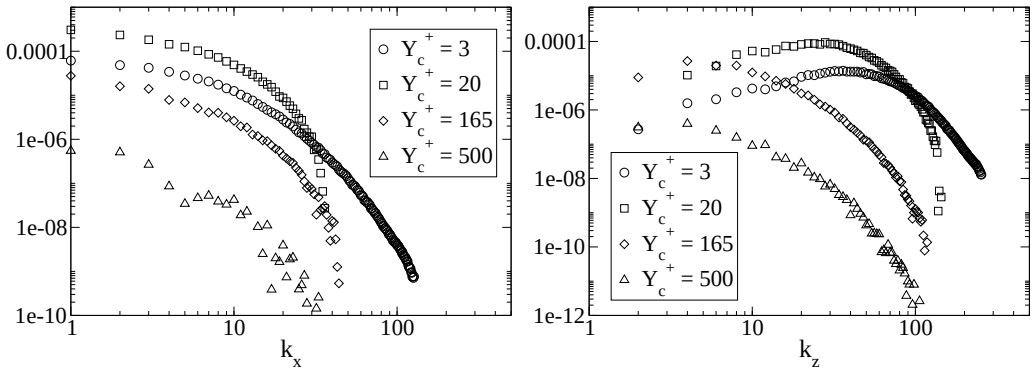

Figure B.1: 1D-spectral turbulent production, $-\hat{\Pi}^{1D}$, among different streamwise (a) and spanwise (b) wavenumbers and wall distances.

space with the balance equation of the structure function, equation 2.22. As shown in appendix A, there is not a definite relation between scales in the spectral space and physical space, hence, in the present analysis we will not refer to the exact values of relevant scales emerging from the spectral analysis but only to the geometrical properties the energy processes take in the spectral space. For simplicity we will analyze the various processes in the (k_x, Y_c)- and (k_z, Y_c)-space separately using the balance equations for the one-dimensional energy spectra $\hat{E}^{1D}(k_x, Y_c)$ and $\hat{E}^{1D}(k_z, Y_c)$ obtained with integration of equation B.3 over the k_z- and k_x-direction, respectively. The data used are those of the turbulent channel flow case at $Re_\tau = 550$.

First of all it si important to note that the rate of energy dissipation in equation B.3 is a function of the wavenumber vector k_i considered and not only of the wall-distance Y_c. In the Kolmogorov equation the rate of energy dissipation, $\langle\epsilon\rangle$, is a function only of the spatial location due to inhomogeneity. The role of $\langle\epsilon\rangle$ is to impose the velocity rate of energy conversion into heat at given wall-distance and the various terms of the budget balance with this rate in the respective scale range. In spectral space this term is absent and replaced by $-2\nu k^2 \hat{E}$. This term weight, among the different spectral wavenumbers, the relative rate of energy dissipation. It is a spectral decomposition of the rate of energy conversion into heat.

In chapter 3, the anisotropic mechanisms of energy injection of wall-turbulent flows has been shown responsible to leave a marked footprint on the geometrical properties of the turbulent energy fluxes. In figure B.1, the one-dimensional spectral turbulent production term, $-\hat{\Pi}^{1D}$, is shown in the (k_x, Y_c)- and (k_x, Y_c)-space. $-\hat{\Pi}^{1D}$ shows a marked different behaviour in the streamwise and spanwise spectrum. In particular, the spanwise spectrum

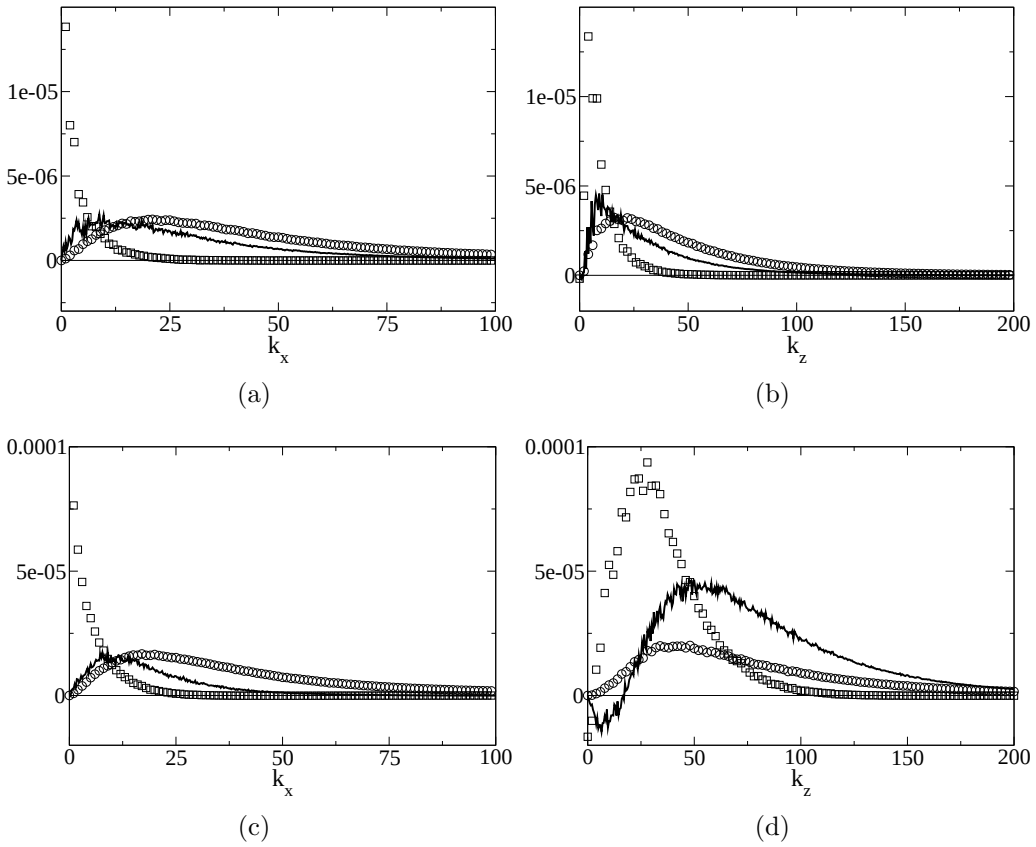

Figure B.2: 1D-spectral energy budget in the logarithmic layer at $Y_c^+ = 165$ (a) and (b) and in the buffer layer at $Y_c^+ = 20$ (c) and (d). Turbulent production, $-\hat{\Pi}^{1D}$ (square), inertial energy transfer among wavenumbers, $\hat{T}_{r_i}^{1D}$ (solid line) and viscous dissipation, $2\nu k^2 \hat{E}^{1D}$ (circle). These processes are shown as function of the streamwise wavenumber, k_x, in (a) and (c) and of the spanwise wavenumber, k_z, in (b) and (d).

is systematically characterized by an anisotropic energy injection at higher wavenumbers with resepct the streamwise one and moving toward the wall a maximum is observed. The action of turbulent production does not decrease moving to small scales but a well defined spectral band of spanwise scales is responsible for a large production mechanism amid the spectrum of scales. This maximum is not marked as those of the production term for the Kolmogorov equation but still exists. The turbulent dynamics in the spanwise scales raise a well defined statistical scale both in the spectral and Kolmogorov analysis, contrarly, to the streamwise spectrum where it is not

possible to define characteristic scales of large turbulent activity.[1]

In figures B.2, the spectral scale-by-scale budgets in one rapresentative plane of the logarithmic and buffer layer, are shown. The one-dimensional spectral turbulent production, $-\hat{\Pi}^{1D}$, dissipation, $2\nu k^2 \hat{E}^{1D}$, and inertial energy flux among wavenumbers, $\hat{T}^{1D}_{r_i}$, are shown in the (k_x, Y_c)- and (k_x, Y_c)-space. In the logarithmic layer, shown in figures B.2(a) and (b), no marked differences between the streamwise and spanwise energy processes are observed. A classical picture of turbulence occurs. The turbulent energy is produced at the largest scales, then is transferred to the small ones where viscous dissipation dominates. Qualitatively, the only difference is that the spanwise processes act at smaller scales, i.e. higher wavenumbers. To note that the wavenumber range considered in figures B.2 is different for the streamwise and spanwise processes, respectively (k_x goes from 0 to 100 while k_z goes from 0 to 200).

In the buffer layer, shown in figures B.2(c) and (d), the turbulent production mechanisms are stronger and significantly act at higher wavenumbers. In particular, in the spanwise spectrum, the energy injection manifests a peak amid the spectrum and both, forward and reverse cascade, are observed. While, in the streamwise spectrum the energy production still shows a maximum at the largest scales, and a forward energy flux displaces this energy excess toward smallest scales dominated by viscous dissipation. In conclusion, the emerging picture is consistent with the physical descripiton given in chapter 3 with the generalized Komogorov equation.

The data presented here are preliminary results of a more extended work of comparison between the spectral and the Kolmogorov approach. In this sense, further analysis including the behaviour of the spectral energy fluxes in the (k_x, k_z, Y_c)-space are needed in order to describe the spectral counterpart of the spiral-like paths of energy shown in chapter 3. As an anticipation, in figure B.3, the projection in the (k_z, Y_c)-plane of the inertial energy fluxes of equation B.3 written in the (k_x, k_z, Y_c)-space is shown. The energy provided at the small scales of the buffer layer, see the isocontour of figure B.3, is transferred to both large and small scales. The coupling of the reverse cascade with the spatial flux towards the bulk of the flow appears as the basic element for the formation of the wider fluctuations of the outer flow.

[1] In the spectral analysis of this section, premultiplied spectra will not used. Even if this observables allow to define well defined scales of large turbulent activity also in the streamwise spectrum, the resulting physical meaning is not clear, at least, for the knowledge of the author.

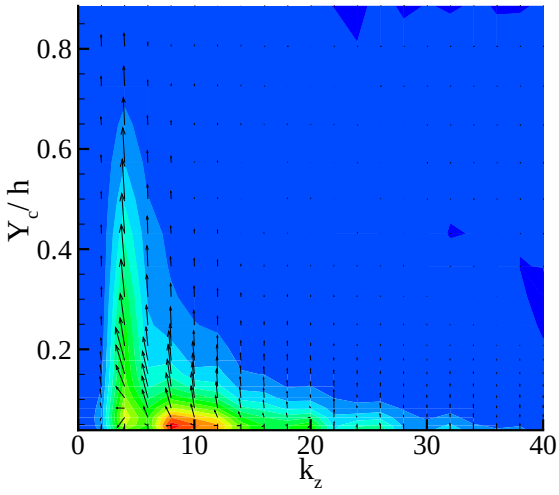

Figure B.3: Isocontours of the spectral turbulent production in a (k_z, Y_c)-plane. The vectors are the spectral energy transfer in wavenumber/physical space, $(\hat{T}_{r_z}, -\hat{T}_c)$.

Appendix C

On solenoidal Lamb vector fluctuations and turbulent energy fluxes

In the previous sections, the turbulent energy fluxes have been shown driven by regions of energy source which seem to be a result of the action of the coherent swirling motion of the near-wall turbulence. In more general cases, the every turbulent dynamic is thought to be a result of swirling interaction mechanisms as for example the phenomenological picture of vortex breakdown and reconnection [77] leads to believe. For this reason, a different mathematical approach which highlights the vortical behaviour of turbulent flows could be useful to understand the physics of turbulence.

In this section an alternative approach for the study of the nonlinear processes, described by the Navier-Stokes equations and responsible for the inertial energy fluxes will be suggested. The nonlinear dynamics of turbulent flows will be adressed with a single quantity which follows from the Helmotz decomposition of the Lamb vector as proposed in [75]. In this view the turbulent generation mechanisms and the turbulence displacement among scales and physical locations will be described with a single quantity, the solenoidal component of the Lamb vector. This quantity is closely related to the stretching and convection of vortex lines. Hence, the resulting approach allows to incorporate in a single framework both dynamical processes of swirling motion and the resulting statistical properties.

C.0.2 Solenoidal Lamb vector and nonlinear velocity effects

Let us consider the incompressible turbulent flow of a viscous fluid governed by the Navier-Stokes equations and the continuity equation

$$\frac{\partial \mathbf{u}}{\partial t} + \mathbf{u} \cdot \nabla \mathbf{u} = -\frac{1}{\rho}\nabla p + \nu \nabla^2 \mathbf{u} \tag{C.1}$$

$$\nabla \cdot \mathbf{u} = 0 \tag{C.2}$$

The acceleration on the left-hand side of equation C.1 can be written in an alternative form,

$$\frac{\partial \mathbf{u}}{\partial t} + \mathbf{u} \cdot \nabla \mathbf{u} = \frac{\partial \mathbf{u}}{\partial t} + \boldsymbol{\omega} \times \mathbf{u} + \frac{1}{2}\nabla |\mathbf{u}|^2 \tag{C.3}$$

where

$$\boldsymbol{\omega} = \nabla \times \mathbf{u} \tag{C.4}$$

is the vorticity vector and $\mathbf{l} = \boldsymbol{\omega} \times \mathbf{u}$ is usually referred to as the Lamb vector. This give rise to an alternative form of the Navier-Stokes equation which was first derived by Lamb (1878),

$$\frac{\partial \mathbf{u}}{\partial t} + \boldsymbol{\omega} \times \mathbf{u} = -\nabla \left(\frac{p}{\rho} + \frac{1}{2}|\mathbf{u}|^2 \right) + \nu \nabla^2 \mathbf{u} \tag{C.5}$$

Since, the inertial energy transfer is a nonlinear velocity effect, it is clear that it must emanate from the Lamb vector $\boldsymbol{\omega} \times \mathbf{u}$. Furthermore, since the vector identity

$$(\mathbf{u} \cdot \boldsymbol{\omega})^2 + |\mathbf{u} \times \boldsymbol{\omega}|^2 = |\mathbf{u}|^2 |\boldsymbol{\omega}|^2 \tag{C.6}$$

holds, it has been argued that regions of high helicity density

$$h = \mathbf{u} \cdot \boldsymbol{\omega}$$

are associated with small Lamb vector, motivating the conjecture that regions of high helicity have an associated low dissipation due to a reduction in the energy cascade. Such conjectures have led to the hypothesis that helical structures are coherent and endure for relatively long times. But these speculations are not supported by the Navier-Stokes equations. Indeed, as done in Speziale [75], the Lamb vector can be decomposed into irrotational and solenoidal parts as follows

$$\boldsymbol{\omega} \times \mathbf{u} = \nabla \alpha + \nabla \times \boldsymbol{\beta} \tag{C.7}$$

where α is a scalar field and $\boldsymbol{\beta}$ is a vector field which can be made solenoidal ($\nabla \cdot \boldsymbol{\beta} = 0$) with no loss of generality. After using this Helmotz decomposition, equation C.5 can be written in the form

$$\frac{\partial \mathbf{u}}{\partial t} + \nabla \times \boldsymbol{\beta} = -\nabla \left(\frac{p}{\rho} + \frac{1}{2}|\mathbf{u}|^2 + \alpha \right) + \nu \nabla^2 \mathbf{u} \tag{C.8}$$

The scalar potential α is absorbed by the pressure and has no effect on the evolution of the velocity field $\mathbf{u}$ which determines the energy cascade. It is thus clear that the energy cascade arises only from the solenoidal part of the Lamb vector $\nabla \times \boldsymbol{\beta}$. For this reason, consistent with equation C.6, small magnitude of the solenoidal part of $\boldsymbol{\omega} \times \mathbf{u}$ need not be associated with large values of $\mathbf{u} \cdot \boldsymbol{\omega}$.

For flow in an infinite domain,

$$\boldsymbol{\beta} = \frac{1}{4\pi} \int \frac{\nabla' \times (\boldsymbol{\omega}' \times \mathbf{u}')}{|\mathbf{x}' - \mathbf{x}|} d^3\mathbf{x}' \tag{C.9}$$

which follows from a direct application of the vector identity $\nabla \times (\nabla \times \boldsymbol{\beta}) = \nabla (\nabla \cdot \boldsymbol{\beta}) - \nabla^2 \boldsymbol{\beta} = -\nabla^2 \boldsymbol{\beta}$, where it is used the fact that $\boldsymbol{\beta}$ is solenoidal. Since,

$$\nabla \times (\boldsymbol{\omega} \times \mathbf{u}) = \mathbf{u} \cdot \nabla \boldsymbol{\omega} - \boldsymbol{\omega} \cdot \nabla \mathbf{u} \tag{C.10}$$

it follows that

$$\nabla \times \boldsymbol{\beta} = \frac{1}{4\pi} \nabla \times \int \frac{1}{|\mathbf{x}' - \mathbf{x}|} \left(\mathbf{u}' \cdot \nabla' \boldsymbol{\omega}' - \boldsymbol{\omega}' \cdot \nabla' \mathbf{u}' \right) d^3\mathbf{x}' \tag{C.11}$$

Phisically, the vector field $\mathbf{u} \cdot \nabla \boldsymbol{\omega} - \boldsymbol{\omega} \cdot \nabla \mathbf{u}$ accounts for the convection and stretching of vortex lines in the fluid. Hence, it is obvious that the energy cascade results from the nonlocal convection and stretching of vortex lines. It should be noted that the vorticity stretching term, $\boldsymbol{\omega} \cdot \nabla \mathbf{u}$, gives rise to the usual energy cascade from large to small scales, whereas, the convective vorticity term $\mathbf{u} \cdot \nabla \boldsymbol{\omega}$ can give rise to a reverse energy cascade from small to large scales (this has been rigorously proven for two dimensional turbulence).

As done in [68], an alternative expression for the irrotational and solenoidal part of the Lamb vector can be obtained. Starting from the Navier-Stokes equations C.5, a set of hydrodynamic Maxwell equations can be achieved which takes the form,

$$\begin{aligned} \nabla \cdot \boldsymbol{\omega} &= 0 \text{ or } \boldsymbol{\omega} = \nabla \times \mathbf{u} \\ \frac{\partial \boldsymbol{\omega}}{\partial t} &= -\nabla \times \mathbf{l} - \nu \nabla \times \nabla \times \boldsymbol{\omega} \end{aligned}$$

$$\begin{aligned} \mathbf{l} &= -\frac{\partial \mathbf{u}}{\partial t} - \nabla\left(\frac{p}{\rho} + \frac{1}{2}|\mathbf{u}|^2\right) - \nu\nabla\times\boldsymbol{\omega} \\ \nabla\cdot\mathbf{l} &= -\nabla^2\left(\frac{p}{\rho} + \frac{1}{2}|\mathbf{u}|^2\right) \end{aligned} \tag{C.12}$$

where $q_h = \nabla\cdot\mathbf{l}$ is the so-called hydrodynamic charge density. Decomposing the Lamb vector into two part according to the Helmotz decomposition, $\mathbf{l} = \nabla\alpha + \nabla\times\boldsymbol{\beta}$, one can infers that the hydrodynamic charge is a function only of the irrotational part of $\mathbf{l}$ and the scalar α is completely determined by the incompressibility constraint,

$$\nabla\cdot\mathbf{l} = \nabla^2\alpha = -\nabla^2\left(\frac{p}{\rho} + \frac{1}{2}|\mathbf{u}|^2\right) \tag{C.13}$$

where

$$\alpha = -\left(\frac{p}{\rho} + \frac{1}{2}|\mathbf{u}|^2\right) \tag{C.14}$$

and decomposing now the Navier-Stokes equations, can be obtained that,

$$\nabla\alpha = -\nabla\left(\frac{p}{\rho} + \frac{1}{2}|\mathbf{u}|^2\right) \text{ and } \nabla\times\boldsymbol{\beta} = -\frac{\partial\mathbf{u}}{\partial t} - \nu\nabla\times\boldsymbol{\omega} \tag{C.15}$$

C.0.3 Solenoidal Lamb vector fluctuations and turbulent energy transfer

Since the solenoidal part of the Lamb vector is responsible of the nonlinear velocity effects and, therefore, of the energy cascade in turbulent flows, it is interesting to analyse the role of such term in the turbulent kinetic energy budget, see [82]. To obtain the equation for the turbulent kinetic energy with the explicitly dependence with the Lamb vector, we have to start from the Navier-stokes equations in rotation form for the velocity fluctuations,

$$\begin{aligned} &\frac{\partial\mathbf{u}}{\partial t} + (\boldsymbol{\omega}\times\mathbf{u} + \boldsymbol{\omega}\times\mathbf{U} + \boldsymbol{\Omega}\times\mathbf{u} - \langle\boldsymbol{\omega}\times\mathbf{u}\rangle) = \\ &-\nabla\left[\frac{p}{\rho} + \frac{1}{2}\left(|\mathbf{u}|^2 - \langle|\mathbf{u}|^2\rangle + 2|\mathbf{u}\mathbf{U}|\right)\right] - \nu\nabla\times\boldsymbol{\omega} \end{aligned} \tag{C.16}$$

Note that the capitol letters stand for mean variables and the lowercase letters stand for fluctuating variables. Considering an extended fluctuating Lamb vector (that is usually applied to the term $\boldsymbol{\omega}\times\mathbf{u}$),

$$\mathbf{l}' = (\boldsymbol{\omega}\times\mathbf{u} + \boldsymbol{\omega}\times\mathbf{U} + \boldsymbol{\Omega}\times\mathbf{u}) = \nabla\alpha + \nabla\times\boldsymbol{\beta} \tag{C.17}$$

and an extended fluctuating enthalpy (that is usually applied to the term $\left(\frac{p}{\rho}+\frac{1}{2}|\mathbf{u}|^2\right)$,

$$h' = \frac{p}{\rho} + \frac{1}{2}\left(|\mathbf{u}|^2 - \langle|\mathbf{u}|^2\rangle + 2|\mathbf{u}\mathbf{U}|\right) \tag{C.18}$$

equation C.16 can be rewritten as,

$$\frac{\partial \mathbf{u}}{\partial t} + \mathbf{l}' - \langle \boldsymbol{\omega} \times \mathbf{u}\rangle = -\nabla\left(h'\right) - \nu\nabla\times\boldsymbol{\omega} \tag{C.19}$$

Under the incompressibility constraint and taking the divergence operator of equation C.19, one finds that

$$\nabla\cdot\mathbf{l}' = \nabla^2\alpha = -\nabla^2 h' \text{ and } \nabla\alpha = -\nabla h' \tag{C.20}$$

and, therefore, equation C.19 reduces to

$$\frac{\partial \mathbf{u}}{\partial t} + \nabla\times\boldsymbol{\beta} - \langle\boldsymbol{\omega}\times\mathbf{u}\rangle = -\nu\nabla\times\boldsymbol{\omega} \tag{C.21}$$

showing the main role of the fluctuating solenoidal Lamb vector on the evolution of turbulence. Such term can be expressed as

$$\begin{aligned}\boldsymbol{\beta} = \frac{1}{4\pi}\int \frac{1}{|\mathbf{x}'-\mathbf{x}|}\left[\left(\mathbf{u}'\cdot\nabla'\boldsymbol{\omega}' + \mathbf{U}'\cdot\nabla'\boldsymbol{\omega}' + \mathbf{u}'\cdot\nabla'\Omega'\right)\right.\\ \left.-\left(\boldsymbol{\omega}'\cdot\nabla'\mathbf{u}' + \boldsymbol{\omega}'\cdot\nabla'\mathbf{U}' + \Omega'\cdot\nabla'\mathbf{u}'\right)\right] d^3\mathbf{x}'\end{aligned} \tag{C.22}$$

where appears the fundamental physical role of the convective transport of mean and fluctuating velocity field of the fluctuating vorticity and of the fluctuating vortex stretching due to mean and fluctuating velocity gradients. Now, from equation C.21, we are able to obtain the turbulent kinetic energy in a novel form. Taking the scalar product of equation C.21 with the velocity fluctuation,

$$\frac{\partial\langle|\mathbf{u}|^2\rangle}{\partial t} = -\langle\mathbf{u}\cdot(\nabla\times\boldsymbol{\beta})\rangle - \nu\langle\mathbf{u}\cdot(\nabla\times\boldsymbol{\omega})\rangle \tag{C.23}$$

where

$$\nu\langle\mathbf{u}\cdot(\nabla\times\boldsymbol{\omega})\rangle = \nu\langle\nabla\cdot l'\rangle = \left(\frac{1}{2}\nabla^2\langle|\mathbf{u}|^2\rangle - \langle 2S_{ij}S_{ij}\rangle + \langle|\boldsymbol{\omega}|^2\rangle\right) \tag{C.24}$$

and

$$S_{ij}S_{ij} + \frac{1}{2}|\boldsymbol{\omega}|^2 = \epsilon \tag{C.25}$$

we can obtain

$$\frac{\partial\langle|\mathbf{u}|^2\rangle}{\partial t} = -\langle\mathbf{u}\cdot(\nabla\times\boldsymbol{\beta})\rangle + \frac{1}{2}\nabla^2\langle|\mathbf{u}|^2\rangle - 2\langle\epsilon\rangle \tag{C.26}$$

Thus it is clear that the nonlinear energy processes such as spatial energy transfer and production are all involved in the same process of transport and stretching of vorticity tubes.

For a better comprehension of the role of the fluctuating solenoidal Lamb vector, i.e. of the vortex stretching and convection of vorticity, it is interesting to show the role of such term into the equation for the velocity correlation. This equation allows to analyse simutaneously energy processes which occur in physical space and which take place in the space of scale. Therefore, we can account also for the energy cascade. To achieve this task, we start from the equation C.21 for the istantaneous fluctuations in rotation form and referencing it to the point $\mathbf{x}$ and $\mathbf{x}'$ and multiplying it for the velocity fluctuations referred to the other point as

$$\mathbf{u}'\cdot\frac{\partial\mathbf{u}}{\partial t} + \mathbf{u}'\cdot(\nabla\times\boldsymbol{\beta}) - \mathbf{u}'\cdot\langle\boldsymbol{\omega}\times\mathbf{u}\rangle = -\nu\mathbf{u}'\cdot(\nabla\times\boldsymbol{\omega}) \tag{C.27}$$

$$\mathbf{u}\cdot\frac{\partial\mathbf{u}'}{\partial t} + \mathbf{u}\cdot(\nabla\times\boldsymbol{\beta}') - \mathbf{u}\cdot\langle\boldsymbol{\omega}'\times\mathbf{u}'\rangle = -\nu\mathbf{u}\cdot(\nabla\times\boldsymbol{\omega}') \tag{C.28}$$

then, adding equations C.27 and C.28 and averaging we obtain,

$$\frac{\partial\langle\mathbf{u}\mathbf{u}'\rangle}{\partial t} + \langle\mathbf{u}'\cdot(\nabla\times\boldsymbol{\beta})\rangle + \langle\mathbf{u}\cdot(\nabla\times\boldsymbol{\beta}')\rangle = -\nu\left[\langle\mathbf{u}'\cdot(\nabla\times\boldsymbol{\omega})\rangle + \langle\mathbf{u}\cdot(\nabla\times\boldsymbol{\omega}')\rangle\right] \tag{C.29}$$

Finally, considering the index form and applying some differential operator we obtain

$$\frac{\partial\langle u_i u_i'\rangle}{\partial t} + \epsilon_{ijk}\left[\frac{1}{2}\frac{\partial}{\partial X_j}\left(\langle u_k'\beta_i + \langle u_k\beta_i'\right) + \frac{\partial}{\partial r_j}\left(\langle u_k'\beta_i - \langle u_k\beta_i'\right)\right] =$$

$$\frac{\nu}{2}\frac{\partial^2}{\partial X_j^2}\langle u_i u_i'\rangle + 2\nu\frac{\partial^2}{\partial r_j^2}\langle u_i u_i'\rangle \tag{C.30}$$

Thus, it is clear that the solenoidal part of the Lamb vector and its dynamical counterpart concerning the physics of the stretching and convection of vortex lines, can be used as basic element to describe the nonlinear energy transfer phenomena of turbulence in both physical and scale space. As a confirmation, Kerr et al. [36] found a direct connection between the properties of the turbulent energy transfer and some components of the Lamb vector

decomposed through a filtering operation. In particular, they found large forward and reverse cascade phenomena in correlation with strong Lamb vector evaluated with velocity at large scales and vorticity at small ones. These observations have been used in [18] to develop an LES model based on the Lamb vector which has been found able to predict both forward and reverse subgrid energy transfer.

Acknowledgements

First and foremost I want to thank my supervisor Prof. E. De Angelis. Her encouragement, guidance and support made this thesis possible. Thanks to her way of doing scientific research, I found my passion in the field of turbulence.

I am grateful to Prof. A. Talamelli who first introduced me into the field of fluid mechanics. He always believed in me and supported my scientific career.

I would like to show my gratitude to Prof. C.M. Casciola and his research group from whom I learned the approach to the study of turbulence and the methodologies used in this thesis.

I would also like to thank all my colleagues in the faculty and in particular Ivan, Gianluca, Paolo, Angela, Stefano, Federico and Davide. In them I found a great help but also a good friendship that I will always carry with me in the future. Thanks for bearing up with me.

A special thank goes to Jean. In these years I shared with him most of the time. He has made available his support in a number of ways. Above all, he taught me many things in both science and life. He will be forever an example for me. Thanks!

Many thanks also to the guys of "Via Pizzardi", Kasia, Stefano, Silvia and Gabriele. Their friendship, warmth and vivacity have been a source of great joy for me and I am thankful for that.

I take the opportunity to thank also my friends, the old ones, those with whom I have shared these years, those lost and those found along the way.

My eternal gratitude goes to my parents Claudio and Nadia, and to my sisters Laura and Chiara. I am grateful for all they have done for me, for the love they have given me and the education I have received.

A big thank goes to Silvia. Her proximity and her joy have been of great help for my work. But, above all, thanks for being the only certainty in my life.

Finally, I offer my thanks to all of those who have had the patience to read also this last line.

Bibliography

[1] R.A. Antonia, L. Djenidi and P.R. Spalart, "Anisotropy of the dissipation tensor in a turbulent boundary layer", *Phys. Fluids*, **6**:2475-2479 (1994).

[2] J.S. Baggett, J. Jimenez and A.G. Kravchenko, "Resolution requirements in large-eddy simulations of shear flows", *CTR, Annual Research Briefs*, 51-66 (1997).

[3] J. Bardina, J.H. Ferziger and W.C. Reynolds, "Improved subgrid scale models for large-eddy simulation", *Am. Inst. Aeronaut. Asronaut. Pap.*, 80-1357 (1980).

[4] R. Benzi, S. Ciliberto, C. Baudet, C. Massaioli and S. Succi, "Extended self-similarity in turbulent flows", *Phys. Rev. E*, **48**:R29-R32 (1993).

[5] C. Brun, R. Friedrich and C.B. da Silva, "A non-linear SGS model based on the spatial velocity increment", *Theor. Comput. Fluid Dyn.*, **20**:1-21 (2006).

[6] C.M. Casciola, P. Gualtieri, R. Benzi and R. Piva, "Scale-by-scale budget and similarity laws for shear turbulence", *J. Fluid Mech.*, **476**:105-114 (2003).

[7] C.M. Casciola, P. Gualtieri, B. Jacob and R. Piva, "Scaling Properties in the Production Range of Shear Dominated Flows", *Phys. Rev. Lett.*, **95**:024503 (2005).

[8] C.M. Casciola, P. Gualtieri, B. Jacob and R. Piva, "The residual anisotropy at small scales in high shear turbulence", *Phys. Fluids* **19**, (2007).

[9] S. Cerutti and C. Meneveau, "Intermittency and relative scaling of subgrid-scale energy dissipation in isotropic turbulence", *Phys. Fluids*, **10**:928-937 (1998).

[10] A. Cimarelli and E. De Angelis, "Analysis of the Kolmogorov equation for filtered wall-turbulent flows", accepted for publication in *J. Fluid Mech.*, (2011).

[11] A. Cimarelli, E. De Angelis and C.M. Casciola, "Scale-energy fluxes in wall-turbulent flows", *iTi* conference, (2010).

[12] A. Cimarelli and E. De Angelis, "Anisotropic dynamics in filtered wall-turbulent flows", *DLES 8* conference, (2010).

[13] A. Cimarelli and E. De Angelis, "Energy cascade and spatial fluxes of filtered wall-turbulent flows", *QLES II* conference, (2009).

[14] L. Danaila, F. Anselmet, T. Zhou and R. Antonia, "Turbulent energy scale budget equations in a fully developed channel flow", *J. Fluid Mech.*, **430**: 87-109 (2001).

[15] P.A. Davidson, *"Turbulence: an introduction for scientists and engineers"*, Oxford Univ. Press, (2004).

[16] E. De Angelis, C.M. Casciola and R. Piva, "DNS of wall turbulence: dilute polymers and self-sustaining mechanisms", *Computer & Fluids*, **31**:495-507 (2002).

[17] J.A. Domaradzki, W. Liu, C. Härtel and L. Kleiser, "Energy transfer in numerically simulated wall-bounded turbulent flows", *Phys. Fluids*, **6**:1583-1599 (1994).

[18] J.A. Domaradzki and E.M. Saiki, "Backscatter models for Large-Eddy Simulations", *Theoret. Comput. Fluid Dynamics*, **9**:75-83 (1997).

[19] L. Fang, L. Shao, J.P. Bertoglio, G.X. Cui, C.X. Xu and Z.S. Zhang, "An improved velocity increment model based on Kolmogorov equation of filtered velocity", *Phys. Fluids*, **21**:065108 (2009).

[20] U. Frisch, *"Turbulence"*, Cambridge Univ. Press, (1995).

[21] P. Gualtieri, C.M Casciola, R. Benzi and R. Piva, "Preservation of statistical properties in large-eddy simulation of shear turbulence", *J. Fluid Mech.*, **592**:471-494 (2007).

[22] M. Germano, U. Piomelli, P. Moin and W.H. Cabot, "A dynamic subgrid-scale eddy viscosity model", *Phys. Fluids A*, **3**:1760-1765 (1991).

[23] J.M. Hamilton, J. Kim, and F. Waleffe, "Regeneration mechanisms of near-wall turbulence structures", *J. Fluid Mech.*, **287**:317-348 (1995).

[24] C. Härtel, L. Kleiser, F. Unger and R. Friedrich, "Subgrid-scale energy transfer in the near-wall region of turbulent flows", *Phys. Fluids*, **6**:3130-3143 (1994).

[25] S. Hoyas and J. Jimenez, "Scaling of the velocity fluctuations in turbulent channels up to $Re_\tau = 2003$", *Phys. Fluids*, **18**:011702 (2006).

[26] R.J. Hill, "Exact second-order structure-function relationship", *J. Fluid Mech.*, **468**:317-326 (2002).

[27] M.Y. Hussaini and T.A. Zang, "Spectral methods in fluid dynamics", *Annu. Rev. Fluid Mech.*, **19**:339-367 (1987).

[28] N. Hutchins and I. Marusic, "Large-scale influences in near-wall turbulence", *Phil. Trans. R.Soc. Lond. A*, **365**:647-664 (2007).

[29] Y. Hwang and C. Cossu, "Self-sustained process at large scales in turbulent channel flow", *Phys. Rev. Lett.*, **105**:04405 (2010).

[30] B. Jacob, C.M. Casciola, A. Talamelli and H.P. Alfredsson, "Scaling of mixed structure functions in turbulent boundary layers", *Phys. Fluids*, **20**:045101 (2008).

[31] J. Jeong and F. Hussain, "On the identification of a vortex", *J. Fluid Mech.*, **285**:69-94 (1995).

[32] J. Jimenez, "The physics of wall turbulence", *Physica A*, **263**:262-262 (1999).

[33] J. Jimenez and A. Pinelli, "The autonomous cycle of near-wall turbulence", *J. Fluid Mech.*, **389**:335-359 (1999).

[34] J. Jimenez and S. Hoyas, "Turbulent fluctuations above the buffer layer of wall-bounded flows", *J. Fluid Mech.*, **611**:215-236 (2008).

[35] T. von Kármán and L. Howarth, "On the statistical theory of isotropic turbulence", *Proc. R. Soc. Lond. A*, **164** (1938).

[36] R.M. Kerr, J.A. Domaradzki and G. Barbier, "Small-scales properties of nonlinear interactions and subgrid-scale energy transfer in isotropic turbulence", *Phys. Fluids*, **8**:197 (1996).

[37] J. Kim, P. Moin and R.D. Moser, "Turbulence statistics in fully developed channel flow at low Reynolds number", *J. Fluid Mech.*, **177**:133-166 (1987).

[38] A. N. Kolmogorov, "The local structure of turbulence in incompressible viscous fluid at very large Rynolds numbers", *Dokl. Akad. Nauk. SSSR*, **30** (1941).

[39] A. N. Kolmogorov, "On degeneration (decay) of isotropic turbulence in an incompressible viscous liquid", *Dokl. Akad. Nauk. SSSR*, **31** (1941).

[40] A. N. Kolmogorov, "Dissipation of energy in the locally isotropic turbulence", *Dokl. Akad. SSSR*, **32** (1941).

[41] A. N. Kolmogorov, "A refinement of previous hypotheses concerning the local structure of turbulence in a viscous incompressible fluid at high Reynolds number", *J. Fluid Mech.*, **13**:82-85 (1962).

[42] R.H. Kraichnan, "The structures of isotropic turbulence at very high Reynolds number", *J. Fluid Mech.*, **5**:497-543 (1959).

[43] R.H. Kraichnan, "Intermittency in the very small scales of turbulence", *Phys. Fluids*, **10**:2080-2082 (1967).

[44] R.H. Kraichnan, "On Kolmogorov's inertial-range theories", *J. Fluid Mech.*, **62**:305-330 (1974).

[45] R.H. Kraichnan, "On Kolmogorov's inertial range theories", *J. Fluid Mech.*, **62**:305-330 (1974).

[46] R.H. Kraichnan, "Eddy viscosity in two and three dimensions", *J. Atmos. Sci.*, **33**:1521-1536 (1976).

[47] E. Lévêque, F. Toschi, L. Shao and J.P. Bertoglio, "Shear-improved Smagorinsky model for large-eddy simulation of wall-bounded turbulent flows", *J. Fluid Mech.*, **570**:491-502 (2007).

[48] I.D. Landau and E.M. Lifshitz, *"Fluid Mechanics"*, 2nd edition Pergamon Press, Oxford (1987).

[49] D.C. Leslie and G.L. Quarini, "The application of turbulence theory to the formulation of subgrid modelling procedures", *J. Fluid Mech. A*, **91**:65 (1979).

[50] D.K. Lilly, "A proposed modification of the Germano subgrid-scale closure method", *Phys. Fluids A*, **4**:633-635 (1992).

[51] D.K. Lilly, "The representation of small scale turbulence in numerical simulation experiments", *Proc. IBM Scientific Computing Symp. Environ. Sci*, (1967).

[52] J.L. Lumley, "Interpretation of time spectra measured in high-intensity shear flows", *Phys. Fluids*, **8**:1056 (1965).

[53] A. Lundbladh, D.S. Henningson and A.V. Johansson, "An efficient spectral integration method for the solution of the Navier-Stokes equations", *Aeronautical research institute of Sweden - Department of mechanics KTH*, FFA-TN-28 (1992).

[54] N. Marati, C.M. Casciola and R. Piva, "Energy cascade and spatial fluxes in wall turbulence", *J. Fluid Mech.*, **521**:191-215 (2004).

[55] N. Marati, *"A scale by scale budget in wall turbulence"*, PhD thesis, (2004).

[56] I. Marusic, B.J. McKeon, P.A. Monkewitz, H.M. Nagib, A.J. Smits and K.R. Sreenivasan, "Wall-bounded turbulent flows at high Reynolds numbers: recent advances and key issues", *Phys. Fluids*, **22**:065103 (2010).

[57] C. Meneveau, "Statistics of turbulence subgrid-scales stresses: necessary conditions and experimental tests", *Phys. Fluids*, **6**:815-833 (1994).

[58] A.S. Monin and A.N. Yaglom, *"Statistical Fluid Mechanics"*, MIT Press, (1975).

[59] R.D. Moser, J. Kim and N.N. Mansour, "Direct numerical simulation of turbulent channel flow up to $Re_\tau = 590$", *Phys. Fluids*, **11**:943-94 (1999).

[60] Q. Nie and S. Tanveer, "A note on third-order structure functions in turbulence", *Proc. R. Soc. Lond. A* **455**, (1999).

[61] C. Pantano, D.I. Pullin, P.E. Dimotakis and G. Matheou, "LES approach for high Reynolds number wall-bounded flows with application to turbulent channel flow", *Jour. of Comp. Physics* **227**:9271-9291 (2008).

[62] U. Piomelli, Y. Yu and R.J. Adrian, "Subgrid-scale energy transfer and near-wall turbulence structure", *Phys. Fluids*, **8**:215-224 (1996).

[63] S.B. Pope, *"Turbulent flows"*, Cambridge Univ. Press, (2000).

[64] M. Quadrio and P. Ricco, "Critical assessment of turbulent drag reduction through spanwise wall oscillation", *J. Fluid Mech.*, **521**:251-271 (2004).

[65] L. Richardson, *"Weather prediction by numerical process"*, Cambridge Univ. Press, (1922).

[66] S.K. Robinson, "Coherent motions in the turbulent boundary layer", *Annu. Rev. Fluid Mech.*, **23**:601-639 (1991).

[67] R.S. Rogallo and P. Moin, "Numerical simulation of turbulent flows", *Annu. Rev. Fluid Mech.*, **16**:99-137 (1984).

[68] G. Rousseaux, S. Seifer, V. Steinberg and A. Wiebel, "On the Lamb vector and the hydrodynamic charge", *Exp. Fluids*, **42**:291-299 (2007).

[69] P. Sagaut, *"Large-eddy simulation for incompressible flows - An introduction"*, Springer-Verlag, (2001).

[70] N. Saikrishnan, E.K. Longmire and I. Marusic, "Analysis of scale energy budgets in wall turbulence using dual plane PIV", *16th Australasian Fluid Mechanics Conference*, (2007).

[71] N. Saikrishnan, E.K. Longmire, E. De Angelis, I. Marusic, C.M. Casciola and R. Piva, "Reynolds number effects on scale energy balance in wall turbulence", *submitted to Phys. Fluids*, (2010).

[72] P. Schlatter and R. Örlü, "Assessment of direct numerical simulation data of turbulent boundary layers", *J. Fluid Mech.*, **659**:116-126 (2010).

[73] A. Segalini, A. Cimarelli, J.D. Rüedi, E. De Angelis and A. Talamelli, "Effect of the spatial filtering and misalignment error of hot-wire probes in a wall-bounded turbulent flow", submitted to *Meas. Sci. and Techn. Journal*, (2011).

[74] J. Smagorinsky, "General circulation experiments with the primitive equations. 1. The basic experiment", *Mon. Weather Rev.*, **61**:99-164 (1963).

[75] C.G. Speziale, "On helicity fluctuations and the energy cascade in turbulence", *ICASE report*, **87-69** (1987).

[76] K.R. Sreenivasan, "On the scaling of turbulent energy dissipation rate", *Phys. Fluids*, **27**:1048-1051 (1984).

[77] K.R. Sreenivasan and R.A. Antonia, "The phenomenology of small-scale turbulence", *Ann. Rev. Fluid Mech.*, **29**:435-472 (1997).

[78] A. Talamelli, F. Persiani, J.H.M. Fransson, P.H. Alfredsson, A.V. Johansson, H.M. Nagib, J.D. Rüedi, K.R. Sreenivasan and P.A. Monkewitz, "CICLoPE-a response to the need for high Reynolds number experiments", *Fluid Dyn. Res.*, **41**:021407 (2009).

[79] A. Townsend, *"The structure of turbulent shear flows"*, Cambridge Univ. Press, (1976).

[80] E.R. Van Driest, "On turbulent flow near a wall", *J. Aero. Sci.*, **23**:1007-1011 (1956).

[81] F. Waleffe, "Exact coherent structures in channel flow", *J. Fluid Mech.*, **435**:93-102 (2001).

[82] J.Z. Wu, Y. Zhou and M. Fan, "A note on kinetic energy, dissipation and enstrophy", *ICASE report*, **98-43** (1998).

[83] V. Yakhot, "Mean-field approximation and small parameter in turbulence theory", *Phys. Rev. E* **63**, 2 (2001).